A FRAMEWORK TO QUANTIFY NEUROMECHANICAL CONTRIBUTIONS TO STABLE STANDING BALANCE: MODELING PREDICTIONS AND EXPERIMENTAL OBSERVATIONS

A Thesis
Presented to
The Academic Faculty

by

Jeffrey T. Bingham

In Partial Fulfillment
of the Requirements for the Degree
Doctor of Philosophy in the
Woodruff School of Mechanical Engineering

Georgia Institute of Technology
August 2013

A FRAMEWORK TO QUANTIFY NEUROMECHANICAL CONTRIBUTIONS TO STABLE STANDING BALANCE: MODELING PREDICTIONS AND EXPERIMENTAL OBSERVATIONS

Approved by:

Andres Garcia, Committee Chair
Woodruff School of Mechanical Engineering
Georgia Institute of Technology

Daniel Goldman
School of Physics
Georgia Institute of Technology

Lena H. Ting, Advisor
Wallace H. Coulter Dept. of Biomedical Engineering
Emory University and Georgia Institute of Technology

C. Karen Liu
School of Interactive Computing
Georgia Institute of Technology

Thomas Burkholder
School of Applied Physiology
Georgia Institute of Technology

Randy Trumbower
School of Medicine
Emory University

Date Approved: May 14, 2013

Veritas. Caritas. Vita.

ACKNOWLEDGEMENTS

In many ways I feel this may be the most important section of my thesis. The work that follows in this document is built on the advice, encouragement, knowledge, help and love of many, many incredible people. Simply put, without them this humble document would not have come to pass.

First, and foremost, I acknowledge my parents. I am truly blessed to have been raised by brilliant people who loved me dearly, forced me to be better and cajoled me onto the right path. I am proud of who I am, and it is because of my dear parents that I-yam-wat-I-yam. In similar fashion, my delightful sister has inspired me to be better. My grandparents and my Uncle Jeff have also been instrumental in my growing up to be an engineer-type scientist.

My academic career has been guided by some very impressive humans, and it is largely their fault that I have continued in school for this long! I will forever be indebted to Marco Schoen, who set me on a path to higher education. I also thank my Masters thesis adviser Guoan Li for making me think that graduate school was always a fun place for everyone. I must also blame Neville Hogan for sparking the idea to pursue research in neuromechanics.

I would also like to make a special acknowledgement here for my thesis committee, who has been absolutely delightful. Tom has been a veritable sounding board for virtually all of my crazy ideas and has ensured that I always check the biomechanics. Without Tom, I probably wouldn't be at GA Tech, so I thank him very much for meeting with me those many years ago. Karen is a genius and her work has inspired my pursuit of hierarchical control, which I believe will one day see the light of day. Randy has given me awesome advice and experimental insight that I believe significantly strengthened this work. Dan, despite always being incredibly busy, has repeatedly set me back on track several times when I thought that all was lost. Finally, I can't imagine what my PhD would have been like without Lena. I lucked out to have a truly great adviser, who gave me enough rope to hang myself, but kept watch to make sure that I never actually broke my neck. I could gush, but really it boils down

to Lena is awesome.

If there is a foundation for the healthy development of a life-long career as a student it is one's friends. I've had a bunch of great ones. Shaobai, Ali, Lu, Ram, Lou, Dan and Jeremy really made things awesome during a time I needed reminding that life is fun. Kris and Lee are two of the craziest guys in the world and I respect them immensely. I have an inordinately high number of friends named Nate and they are all unbelievably cool. A special shout out to Nate Bunderson for hours of awesome technical and philosophical discourse. My labmates Lucas, Stacie, Seyed, Hongchul, Harrison and Julia made it possible to do some pretty nifty things at GT. They will go on to do truly amazing things and I will be inspired. Sam, Sean and Adam are probably the coolest blokes at GT and have kept me insane, which is a good thing.

As both friend and mentor, I am honored to have had the advice and guidance of Mr. Walker. Probably the finest engineer I have met, he has inspired me always, grounded me repeatedly and kept me smiling. He is a constant reminder of what a good engineer should be and what I aspire to be.

I have also been blessed to have the support and love of a truly wonderful woman. My dear Melissa has kept me fed and in clean clothes, while keeping me from thinking the world is collapsing. She is truly a fundamental part of my ability to have written this work. I love her a lot.

This collection of words is, if anything, a journal entry and commemoration of many years spent having an absolutely wonderful time researching and playing at Georgia Tech. I want to thank everyone who has made it "the best" and I look forward to our continued adventures. I'm sure they will be even better.

TABLE OF CONTENTS

ACKNOWLEDGEMENTS . . . . . **iv**

LIST OF TABLES . . . . . **ix**

LIST OF FIGURES . . . . . **x**

SUMMARY . . . . . **xii**

I INTRODUCTION **1**

1.1 Background 3

1.1.1 How can neuromechanical interactions be modeled? 3

1.1.2 Why is standing balance a good paradigm for studying neuromechanical interactions? 5

1.1.3 Why is delay in feedback a significant variable to investigate? 5

1.1.4 Is lumped neuromuscular control a useful approximation? 6

1.1.5 What is stability and how can we measure it? 7

1.1.6 Why is studying frontal plane motion important? 9

1.2 A four-bar linkage as a model of frontal-plane standing 10

1.2.1 Symbols 11

1.2.2 Kinematics 12

1.2.3 Kinetics 16

1.2.4 Dynamics 17

1.3 Organization and summary of work 21

II NEUROMECHANICAL FACTORS THAT AFFECT THE STABILITY OF STANDING BALANCE **25**

2.1 Introduction 25

2.2 Methods 27

2.2.1 Frontal plane model of balance 27

2.2.2 Biomechanical stability analysis 29

2.2.3 Delayed feedback stability analysis 31

2.2.4 Experimental comparisons 32

2.3 Results 33

2.3.1 Mechanical stability decreased with increasing stance width 33

2.3.2 Stable feedback gain boundaries decreased with increasing stance width 35
2.3.3 Ground contact reduced set of stable feedback gains 36
2.4 Discussion 41
2.4.1 Implications of delayed feedback, stance width and foot lift-off for balance control 41
2.4.2 Modeling assumptions and limitations 43
2.4.3 Model-based interpretation of stance width adaptation 46
2.4.4 Is wide stance more stable? 48
III NEUROMECHANICAL FACTORS THAT AFFECT THE TIMING OF BALANCE RESPONSES 49
3.1 Introduction 49
3.2 Methods 50
3.2.1 Model predictions 50
3.2.2 Pilot data and model fits 51
3.3 Results 52
3.3.1 Model predictions 52
3.3.2 Experimental observations 54
3.4 Discussion 57
IV STABILITY RADIUS AS A METHOD TO COMPARE NEUROMECHANICAL SYSTEMS 60
4.1 Introduction 60
4.2 Theory 62
4.2.1 Characteristic equation 62
4.2.2 System stability 63
4.2.3 ϵ-pseudospectra 64
4.2.4 Stability radius 67
4.3 Application 68
4.3.1 Model 68
4.3.2 Analysis 69
4.4 Results 71
4.5 Discussion 73

V THE EFFECTS OF ALTERED BODY INERTIA ON NEURAL CONTROL . . 78

5.1 Introduction 78

5.2 Methods 81

5.2.1 Frontal plane model of balance 81

5.2.2 Experimental design 83

5.2.3 Data analysis 85

5.3 Results 87

5.3.1 Model predictions 87

5.3.2 Anthropometrics and summary statistics of experimental groups 90

5.3.3 Changes in CoM kinematics were more similar within a stance width than across stance widths 91

5.4 Discussion 96

VI CONCLUSION 102

6.1 Stable covariation of biomechanical and neural factors are necessary for healthy standing balance 102

6.2 Clinical relevance 103

6.3 Future work 106

APPENDIX A — FOUR-BAR LINKAGE MODEL 109

APPENDIX B — MODEL FITS TO EXPERIMENTAL DATA AND PRELIMINARY STABILITY RADIUS RESULTS 114

REFERENCES 120

LIST OF TABLES

3.1 Summary of parameter effects on time to peak torque. 58

5.1 Three hypotheses of changes in neural control in response to increased body mass and their predicted effects on CoM kinematics 90

5.2 Average CoM excursion and velocity from the B group across all possible conditions. 91

5.3 Average CoM excursion and velocity from all subjects at selected time points of 100, 250 and 500 ms. 93

A.1 Anthropometric data for four-bar linkage model of human standing 110

B.1 Average feedback gain and stability results from fitting the fourbar model to experimental trials 118

LIST OF FIGURES

1.1 Neuromechanics is the study of the three sub-systems needed to produce movement in humans. . . . 2

1.2 Specification of dimensions and angles of four-bar linkage used to model frontal-plane standing balance. . . . 11

1.3 Free-body diagram for the four-bar linkage. . . . 17

1.4 Generalized inertia changes most over stance width. . . . 21

2.1 Frontal-plane model of human balance control. . . . 28

2.2 Changes in biomechanical properties of the body as stance width increased. . . . 34

2.3 Regions of stable feedback gains across stance widths. . . . 36

2.4 Boundaries on physiological feedback gains due to foot lift-off criterion and damped center-of-mass dynamics for a nominal human. . . . 37

2.5 Comparison of simulated stepping boundaries and analytic measures of relative stability. . . . 38

2.6 Comparison of model trajectories fit to experimentally measured center-of-mass kinematics. . . . 39

2.7 Changes in subject feedback gains with stance width. . . . 40

2.8 Subject feedback gains overlaid on simulated stepping boundaries and gain margin. . . . 40

2.9 Effect of non-delayed position and velocity feedback on stable sets of delayed feedback for a nominal human. . . . 44

3.1 Increased feedback delay increase increased the time to peak torque. . . . 53

3.2 Decreased stance width increased the time to peak torque. . . . 54

3.3 Increased position feedback gain increased the time to peak torque. . . . 55

3.4 Decreased velocity feedback gain increased the time to peak torque. . . . 56

3.5 Stance width and time to peak torque change with age. . . . 56

3.6 Fit feedback gains increased with age. . . . 57

3.7 Stance width was associated with changes in time to peak torque and feedback gains. . . . 58

4.1 Application for a frontal-plane model of human mediolateral balance control. . . . 69

4.2 Eigenvalues and pseudospectra for a single feedback gain pair at the nominal stance width. . . . 71

4.3 Stability radius across all stable feedback gains at the nominal stance width. . . . 72

4.4 Stable feedback gains across stance width. 72

4.5 Simulated center-of-mass position across stance widths using feedback gains that produce the same stability radius. 73

5.1 Location of CoM data points analyzed. 86

5.2 Changes to simulated CoM trajectories with changes in biomechanical parameters. 87

5.3 Changes to simulated CoM trajectories with changes in neural feedback parameters. 88

5.4 Predicted changes in CoM based on differences in feedback gain when inertia was matched. 89

5.5 Perturbation direction resulted in responses that suggested possible limb dominance. 92

5.6 Increased perturbation magnitude caused increased CoM excursion across conditions. 93

5.7 Increased stance width resulted in decreased CoM excursion. 94

5.8 Increased mass did not significantly affect CoM excursion. 94

5.9 Responses from matched inertia scaled with stance width and not mass. 95

B.1 Stability radius predicts decreased stability with increased body mass. 118

B.2 Stability radius varies across subjects. 119

SUMMARY

Interactions between the neural and musculoskeletal systems are a prerequisite for the production of robust movement. In spite of this, the neural control and musculoskeletal structure underlying biological movements are typically studied independently, with little attention paid to how changes in one may affect the other. Understanding these interactions may be critical to improving current rehabilitation technologies and therapy methods. As an example, balance disorders are multifactorial in nature and identifying whether biomechanical or neural changes are the source of instability remains an unanswered question.

This thesis presents a combined experimental and modeling approach to understand neural and biomechanical interactions governing human balance control. A simple four-bar linkage model with delayed feedback was developed to investigate frontal-plane standing balance. Using methods from time-delay systems, evidence from this model suggests that biomechanical structure is important for behavioral function and shows that neural control and biomechanical structure co-vary for stable human balance. Predictions from the model were tested experimentally to dissociate the effects of inertia and postural configuration on balance. In addition, stability radius, a robust control method, was applied to solve the difficult problem of comparing the relative performance between neuromechanical systems that differ in parameter values and predicted a common mechanism to explain changes in neural control across biomechanical contexts.

In the future, the analytical tools and simulation methods developed herein can be generalized to investigate changes in neuromechanical interactions of various deficits in biomechanics (ACL rupture, amputation) and neural control (Parkinson's disease, stroke). Furthermore, this approach can be used to explain how neural control and biomechanical structure relate to the diversity of animal form and function, as well as suggest biomimetic control policies for robotics.

CHAPTER I

INTRODUCTION

In order to move and balance in every-day life requires stable interaction between the neural, muscular and skeletal systems of our bodies. However, little is known about how these systems interact to stabilize the body in the presence of perturbations. A goal of this thesis was to quantify the changes in stability under different neuromechanical interactions. Thus, in the context of this thesis, stability is defined as the ability to maintain desired motion and balance after a disturbance and the study of the combined neural, muscular, and skeletal systems will be defined as neuromechanics (Figure 1.1).

Neuromechanical interactions offer a potentially vast number of redundant strategies for stable behavior; however, the inherent constraints of muscle properties, skeletal geometry and neural conduction delays likely impose trade-offs in selecting a particular neural strategy or postural configuration to achieve stability. Experimental evidence suggests that the relative contribution of each system is adjusted depending on the task and environment. For example, observations of human reaching tasks show that the nervous system selects arm postures tuned to stabilize in the direction of the perturbations presented [135]. Also, the nervous system likely adjusts neural feedback to stabilize imposed changes in configuration, as muscle responses to translational perturbations in standing balance are observed to decrease as stance width increases [39]. While current models have contributed much to our understanding of sagittal plane stability, they do not allow for an integrative analysis of the relative contributions of body configuration, feedback gains and neural delay on postural stability. The goal of this thesis was to ***develop a simple predictive model of human balance***

and test predictions experimentally to investigate the changes required in the nervous and musculoskeletal systems to compensate for postural reconfiguration and neural delay.

To better understand both healthy and neurologically-impaired subjects, this research developed a model validated by experimental data to quantify the interactions and contributions of nervous and musculoskeletal systems to the stability of human standing balance. These results may be useful in developing quantitative measures of standing stability and help to explain the consequences of various neuromusculoskeletal deficits. The combined use of modeling, experimentation, and analysis provide a framework that could be used to diagnose motor control deficits, develop improved prostheses and aid in the engineering of legged robots.

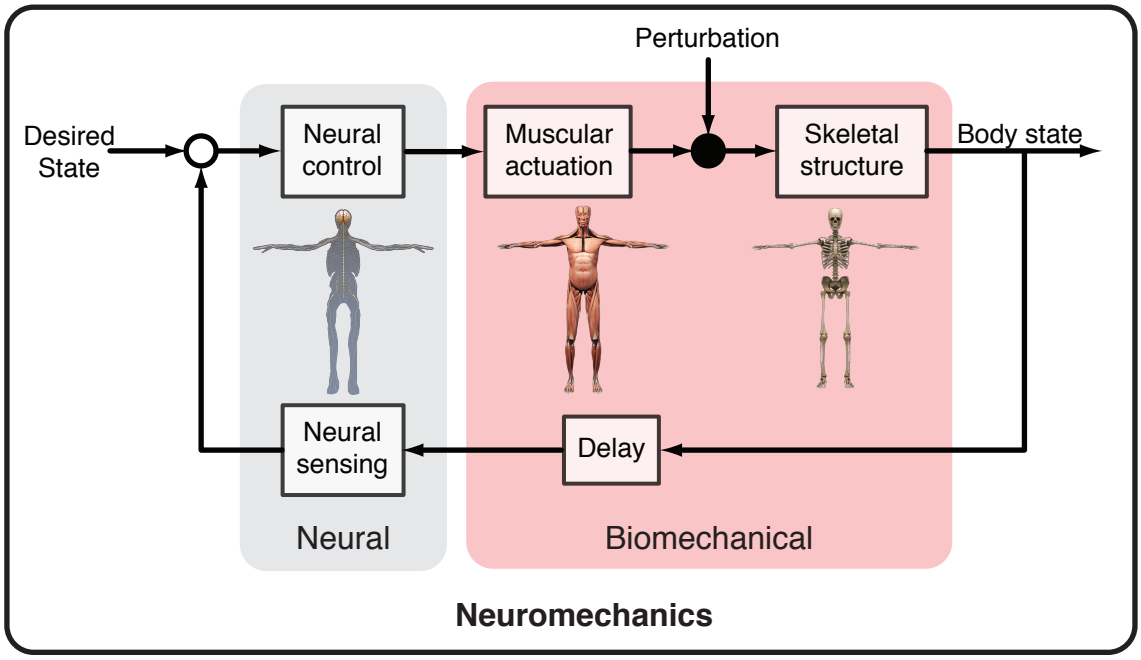

Figure 1.1: Neuromechanics is the study of the three sub-systems needed to produce movement in humans. The skeleton – to provide structure, Musculature – to provide actuation of the skeleton, and the nervous system – to provide sensing and control of the muscles. Biomechanics is the field of study pertaining to the musculoskeletal systems and study of the neural components (motor, sensory, perception, etc.) are the purview of neuroscience. Neuromechanics is the term used to describe the integrated study of biomechanics and neural control.

1.1 Background

To understand the movements people make, how they walk, hold a toothbrush or hit a home-run, requires an understanding of the underlying biomechanics and neural control. Knowledge of how these systems interact could offer insight into how to improve performance for a particular movement or how to compensate for deficiencies in muscular, skeletal or neural areas. However, neural control and biomechanics are unavoidably intertwined, making it difficult to identify the contributions of each system to a particular motion by external observation alone. It is not well understood what relative contributions the musculoskeletal and neural systems make to standing balance or how these systems interact to produce stable behavior. The goal of this research is to separate the contributions of the biomechanics and neural control to human movement by using both computational models and experiments with carefully designed protocols.

1.1.1 How can neuromechanical interactions be modeled?

To begin, we may consider the interaction of the neuromechanics contributing to a behavior as a feedback loop (Figure 1.1). This suggests a classical control scheme that divides the neuromechanical dynamics into components that are to be controlled (plant) and those that are added to achieve a desired behavior (controller). In this simplified model, we describe the biomechanics (muscles and skeleton) as the plant, which is regulated by neural elements (neural control and sensation) that define the control. Here we specify *neural feedback* defined as the components of body state (joint kinematics, body orientation, etc.) that are possible to be sensed through proprioceptive, visual, vestibular, etc. sensory modalities [56]. Through integration along the neural axis this information is transformed into appropriate motor commands [48, 99]. This is represented in Figure 1.1 as a comparison with a desired neural state and the error is scaled with *neural gains*, which is ultimately the input into the muscular dynamics that actuate the skeleton to produce an output behavior [114, 101].

However, in neuromechanical systems both the plant and control can potentially change independently and concurrently in order to achieve a desired behavior. For example, subjects have been observed to choose arm configurations that increase stability along directions of

environmental instability [135] and the center-of-mass has been observed to be tightly regulated in standing under a variety of postures [39, 132] and perturbations [49] as well as in locomotion over different surface conditions [28] where changes in posture were accompanied with changes in muscle activity that likely reflected changes in neural control [49, 39, 132]. Furthermore, neuromechanical systems tend to leverage the intrinsic biomechanical characteristics suitable for a desired behavior. Evidence of the importance of biomechanics in neural control is exemplified by passive dynamic walkers [79], resonance of feeding apparatus in aplysia [154] and multi-leg interaction in cockroaches running over rough terrain [118]. Therefore, the instantaneous state of the neuromechanical system can be set (posture, muscle state, neural sensitivity) in a feedforward manner to alter the dynamics, which in balance the neural component is termed *postural set* [49, 101]. The ability to change the dynamics of the neuromechanics *a priori* is especially important when considering that all neural signals are accompanied with non-negligible delay [48, 56]. Thus, the sensorimotor transformation (the round trip of neural sensation to motor command) is limited in how it may be able to actively correct the system in response to a perturbation.

Therefore, for the purposes of this thesis, it will be assumed that feedforward mechanisms that set the configuration of the skeleton, sensitivity of the neural sensorimotor transformation and muscle state are slow relative to perturbed responses. This assumption is extended such that each neuromechanical component may be updated prior to a perturbation, but then held constant during a response. Neural feedback is then the ideal information about the body state and neural feedback gain is the scaled response of the sensorimotor transformation that produces muscle activation. Changes in muscle properties and skeletal configuration are then part of the postural set. This type of modeling allows for predictive modeling of sensorimotor integration [138, 99, 35], postural control [59, 65, 69] and learning [113, 130]. More complex modeling schemes may be required when feedforward control mechanisms must be modeled concurrently with feedback control, such as in understanding reaching tasks[131, 129].

1.1.2 Why is standing balance a good paradigm for studying neuromechanical interactions?

The biomechanical and neural mechanisms required for standing balance are likely the fundamental prerequisites for all locomotor behavior [82]. Furthermore, understanding standing balance has significant clinical impact, as the leading cause of injury and death in the US elderly is complications resulting from falls [15]. Increased morbidity caused from falls in the elderly is likely due, in part, to deterioration of standing balance. Since standing balance is a relatively steady-state behavior it is the best paradigm for observing responses to perturbations as a method for probing the underlying mechanisms of balance [128, 82]. Due to the inherent delay of neural feedback, it is possible to apply discrete translational perturbations that result in an initial response solely due to biomechanics followed by a reflexive response and an automatic postural response (APR) [48]. This allows a temporal separation to observe responses first from solely biomechanics and then the whole body.

1.1.3 Why is delay in feedback a significant variable to investigate?

Physiological delays are significant during postural control and can limit the range of feedback gains that generate stability. Active responses in muscles that restore the body center-of-mass occur at a latency of about 100 ms, and the resulting musculoskeletal forces are further delayed by 50 ms due to the time course associated with muscle force production and transmission [48]. As a result of this delay, the maximum magnitude of sensorimotor feedback gain is limited, with longer latencies reducing the set of feasible gains [75, 100]. Delayed feedback models of posture have been used to identify the complex stable boundaries of anterior-posterior balance [75, 99, 138, 87, 82]. Furthermore, delayed feedback models have been used to describe the entire time-course of muscle activity during sagittal plane postural responses in both cats and humans [69, 145]. However, how changes in delay affect stability and interact with stance width is unknown.

Modeling dynamic systems with delay impose additional technical challenges for analysis and computation of resulting behavior. Introducing a delay into an ordinary differential

equation results in a class of equations termed *delay differential equations* (DDE) [117]. Classification of DDEs is done based on whether the delay occurs in derivatives less than the order of the system (retarded system) or in derivatives equal to (neutral) or higher (advanced) than the highest non-delayed derivative [86]. Further classification of DDEs may be defined based on whether the delay is itself state-dependent, distributed across states or lumped into a single value [142]. Within the scope of this thesis, a single lumped delay in a retarded form will be explored. The technical challenges that this will introduce are the requirement of specifying a delay history in addition to traditional initial conditions. Furthermore, dynamical analysis of the system will show that an infinite number of eigenvalues exist for this class of DDE. Luckily, this is not insurmountable for retarded DDEs, as only a finite number of eigenvalues will exist to the right of any vertical cut of the complex plane [86]. These eigenvalues can also be readily solved for numerically using a variety of techniques [27, 152].

1.1.4 Is lumped neuromuscular control a useful approximation?

Lumped neuromuscular control trades attribution of components of neural control to physiological structures for qualitative insight and analytical simplicity. To develop a neuromechanical model that can be derived analytically requires vast simplifications of the neuromuscular control. Muscle physiology and its relationship to the nervous and skeletal systems is complex [156]. Muscle force is considered to be dependent on the level of neural activation, length of the muscle and the rate of contraction [40]. Even simple muscle models, such as the Hill-type [148], rely on nonlinear functions to specify the resultant output force of the muscle based on its biomechanical and neural state. However, some of the nonlinear behavior of muscle as an isolated force actuator may be offset by short-latency neural pathways that result in "linearized" behavior [90]. Therefore, the most rudimentary assumption of muscular force output may be to assume a linearized form from a Taylor series expansion of a nonlinear function, $F(x,\dot{x},u)$ that is dependent on muscle length, x, contraction velocity, $\dot{x}$, and neural activation, u:

$$F(x,\dot{x},u) \approx F(x_o,\dot{x}_o,u_o) + \frac{\partial F}{\partial x}\Delta x + \frac{\partial F}{\partial \dot{x}}\Delta \dot{x} + \frac{\partial F}{\partial u}\Delta u \tag{1.1}$$

Next, an assumption must be made on the form of the neural control that activates the muscle. The evidence of long-latency feedback responses in postural control suggest delay, τ is important and previous modeling efforts have had success with phenomenological neural control models that are based on proportional (k_p), derivative (k_v) feedback of body position information [35, 66, 83, 99, 139]. This does not suggest that this is the underlying form of neural control, rather it is merely a good fit that qualitatively gives insight into changes in control. Another assumption may be made that moment-arms, R, for muscles are roughly constant for a particular posture; this appears to be the case for ad/abduction of large muscles spanning the hip [108]. With these assumptions a model of joint torque can be stated:

$$T((x(t),\dot{x}(t)) \approx R\left(\underbrace{kx(t)+b\dot{x}(t)}_{muscular}+\underbrace{k_p x(t-\tau)+k_v\dot{x}(t-\tau)}_{neural}\right) \tag{1.2}$$

While drastically simplified from the actual physiology, this model of the neuromuscular system provides model parameters that can be varied independently of inertial and geometric parameters that may be more directly measured from subject anthropometrics. Finally, this simplification of neuromuscular control has proven to be very useful to understand changes in sensorimotor control [138, 99, 35]. While this does not give insight into the individual components of neuromuscular control that might change (muscle spindle sensitivity, synaptic weighting, etc) changes in lumped parameters are useful for identifying and predicting changes in overall behavior. For example, changes in this form of control have been used to predict deficiencies in various sensory modalities in standing balance [138, 99]. These qualitative changes can then be used to inform finer grained, complex models using the template-anchor philosophy [31].

1.1.5 What is stability and how can we measure it?

Behaviorally, stable standing balance is a complicated set of behaviors that result in maintaining the center-of-mass roughly above the base of support (stable) as opposed to behaviors resulting in steps or falls (unstable). Clinical measures of balance such as the Berg Balance Scale, Brunel Balance Assessment and Romberg Test use a mixture of self-reporting and clinician graded performance of specific motor tasks. These clinical tests are largely qualitative

and more precise measures of balance are needed to quantify progress of treatments. More accurate quantification of stability may be found by linking behavioral stability to mathematical models that have precise definitions of stability.

Ordinary differential equations can be assembled that approximate neuromechanical systems using rigid body dynamics for skeletal and environmental physics with state-dependent differential equations for muscle force and neural sensing and actuation. Behavioral stability is then connected to the mathematical description of the physics by relating the consistency of the behavior to mathematical "attractors" that model maintaining, or returning to, the original behavior in response to some perturbation. If the model is unable to return to the initial behavior after perturbation, the model is considered destabilized. If the model is predictive, this mathematical instability will also be observed as a change in behavior of the subject being modeled. As an example, a shove to a standing person might initiate a transition from standing to stepping (behavioral instability), which may be observed in a model as a system departing from an equilibrium (mathematical instability).

Mathematical models of human behavior that result in complex nonlinear equations can be analyzed using an array of tools from dynamical systems theory that allow characterization of system behavior based on local information. In the case that these equations are linear, the classical method for determining stability is to use the eigenvalues of the characteristic equation[123]. The eigenvalues are the exponential constants that define the time evolution of the system behavior. Eigenvalues with positive real part are considered unstable, because as time advances the eventual behavior of the system will tend to depart from equilibrium. Thus, asymptotic stability of a linear system is defined by all eigenvalues having strictly negative real part. Similarly, this definition of asymptotic stability may be extended to the class of non-linear ODEs with Lyapunov's Indirect Method, which states that the eigenvalues of the linearized system about an equilibrium point describe the system's stability if the eigenvalues are not identically zero [58]. Many more techniques exist. Some attempt to solve for a general region (region of attraction) where the dynamical system is bounded based on some input [32, 58, 77, 125, 73], others for special cases of dynamical systems [33, 85, 117, 142] and still others based on a measure of system sensitivity [44, 74, 102].

Application of these techniques to neuromechanical systems have produced useful results that connect observed behavior to mathematical modeling [14, 7, 141, 121, 25].

However, a common definition of stability has not been agreed upon. Models of human balance have been used to quantify the limits of stability through measures of joint torque [95], relative motion between center-of-mass and center-of-pressure kinematics [93, 94], time series trajectories [121, 25] and feedback gain [100, 75, 82, 138]. In order to interpret the stability of measured dynamics of human standing balance requires a model and a metric, to investigate the effects of neural and biomechanical changes, such as neural delay and stance width. Unfortunately, classical stability analysis tools, such as gain margin [26], cannot be used to compare behavior across neuromechanical conditions where both biomechanics (plant) and neural control (controller) change during a task. Therefore, to overcome these challenges and quantify the stability of standing balance across different conditions we introduce the technique of stability radius [44, 102], an approach that builds upon eigenvalue analysis as a compact representation of dynamical behavior.

1.1.6 Why is studying frontal plane motion important?

Examining stance width in the frontal plane offers a tractable way to control for changes in postural configuration in order to examine the effects of postural configuration on standing balance. Changes in postural configuration affect the dynamics of the body and likely necessitate changes in neural control to perform a movement. The nervous system may select specific postural configurations to reduce the neural demand for a task. For example, subjects have been observed to choose arm configurations that increase stability along directions of environmental instability [135]. The selection of a postural configuration may also reduce energy expenditure or sensitivity to noise [111]. Although this evidence demonstrates the importance of neuromechanical interactions in understanding motor control, little is known about the individual contributions and interplay between biomechanical and neural components that are required for stable posture. Furthermore, few models exist to explore the influence of postural configuration and feedback delay on stable balance in the frontal plane [109, 36].

Consistent with our intuitions about standing balance control, wider stance widths are often considered to provide increased mechanical stability [148], but little quantitative evidence exists to support these suppositions. The preferred stance width in healthy individuals is approximately equal to hip width [110, 80]. However, in uncertain conditions, like riding on a moving train, we often adopt a wider stance. In healthy subjects, muscle activation decreases in response to the same external perturbation when standing with wider stance, while center-of-mass displacement stays roughly the same [132, 39]. This has been suggested to be due to increased reliance on passive stability mechanisms and a reduction in neural control [39]. However, these observations cannot be used to dissociate the contributions of biomechanical and neural systems to stability during these behaviors.

Focusing on frontal plane is of particular interest as stability in the medial-lateral direction is markedly decreased in the elderly [72, 81], cerebellar ataxia [4] and Parkinson's disease [24]. Evidence from patients with neural deficits suggests that increasing stance width alone may not be stabilizing. Patients with Parkinson's disease who suffer from high postural instability exhibit deficits in appropriate scaling of postural feedback gains [60] and tend to choose a narrower stance – roughly half as wide as matched healthy controls [47]. To better understand both healthy and neurologically-impaired subjects, a frontal plane model with delayed feedback is necessary to quantify the neuromechanical interactions underlying stable balance control across postural configurations.

1.2 A four-bar linkage as a model of frontal-plane standing

Standing upright in the frontal-plane naturally lends itself to being modeled by a closed chain mechanism fondly referred to as the four-bar linkage. The ad/abduction movement of the behavior is accomplished primarily by hip and ankle joints; the knee remains practically locked. Furthermore, it is the next level of sophistication over inverted pendulum models [149] and allows for an intuitive way to account for changes in stance width. The four-bar linkage is the simplest possible planar mechanism with a single-degree-of-freedom that employs only pinned joints. However, this reduced simplicity has limitations; perhaps most importantly

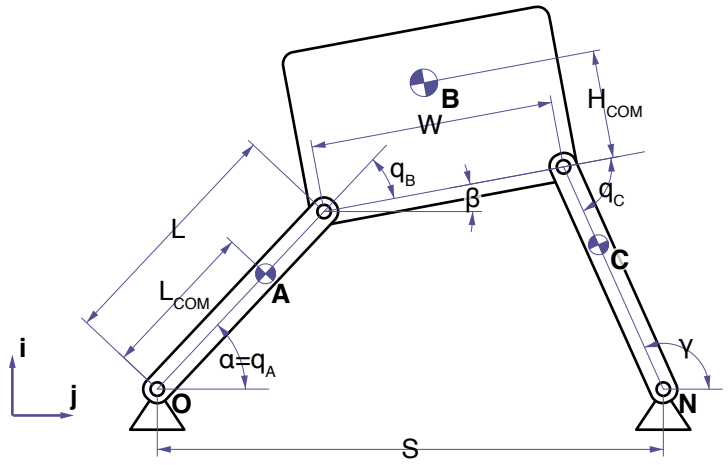

Figure 1.2: Specification of dimensions and angles of four-bar linkage used to model frontal-plane standing balance. O marks the origin for the inertial frame. A and C mark the center-of-mass of the leg links and B is the COM of the torso link. The ground (distance S) defines the fourth link.

that it does not account for independent movement of the upper-body. This may be unacceptable if modeling responses to rotational perturbations [36]. To orient the reader to this model of frontal-plane standing balance the basic kinematics and kinetics are presented for the special case of the parallelogram four-bar linkage where two-links are of equal length (Figure 1.2). This section should be used to familiarize the reader with the dynamics of the system, but care should be taken if the reader wishes to implement these equations in simulation as small typographical errors (read incorrect signs, etc.) can lead to catastrophically incorrect results. Therefore, the reader is encouraged to pursue other texts for detailed analyses [92] and it is suggested to leverage existing software packages (AutoLev, Maple, Matlab, etc) to aid in developing the equations of motion.

1.2.1 Symbols

The equations that follow utilize the dot notation to symbolize differentiation with respect to time, $\dot{q_A} = \frac{d}{dt} q_A(t)$, and the explicit dependence on time is omitted, e.g. $q_A(t)$ is written as just q_A. Parameters are designated primarily as upper-case roman characters. Time-varying coordinates and variables are primarily designated as lower-case roman and greek characters. Bold-face is used to designate vectors and for simplicity these are assumed to be

defined in $\mathbb{R}^2$. Moments and inertia dyads are written as scalar quantities with the implicit assumption that they are defined in coordinates perpendicular to the plane of motion, i.e $\mathbf{i} \times \mathbf{j}$.

COM	center-of-mass
S	stance width
W	hip width
L	leg length
L_{COM}	length from ankle to center-of-mass of leg
H_{COM}	vertical distance from hip center to center-of-mass of torso segment
q_A	relative ankle angle
q_B	relative hip angle
q_C	relative hip angle
α	absolute leg angle
β	absolute torso angle
γ	absolute leg angle
$\mathbf{r}_A$	position vector from origin to COM of link A (leg)
$\mathbf{r}_B$	position vector from origin to COM of link B (torso)
$\mathbf{r}_C$	position vector from origin to COM of link C (leg)
M_{leg}	mass of leg about its COM (links A and C)
M_{trunk}	mass of trunk about its COM (link B)
I_{leg}	inertia of leg about its COM (links A and C)
I_{trunk}	inertia of trunk about its COM (link B)
$T(q, \dot{q})$	total kinetic energy of the system
$V(q)$	total potential energy of the system
$L(q, \dot{q})$	Lagrangian or difference in kinetic and potential energy
$I(q)$	generalized system inertia of linkage
$Q(q, \dot{q})$	generalized centripetal and coriolis forces
$G(q)$	generalized conservative and gravitational forces

1.2.2 Kinematics

1.2.2.1 Position

The absolute angles, those with reference to the inertial frame, can be found by solving a vector loop equation, which are written in exponential form for compactness with aid of Euler's identity ($e^{j\theta} = \cos\theta + j\sin\theta$):

$$Le^{j\alpha} + We^{j\beta} = S + Le^{j\gamma} \tag{1.3}$$

Solving the vector loop equation in terms of angle α gives trigonometric relations for the remaining absolute angles:

$$\beta = 2\arctan\left[\frac{-c_B \pm \sqrt{c_B^2 - 4c_D c_F}}{2c_D}\right] \tag{1.4}$$

$$\gamma = 2\arctan\left[\frac{-c_B \pm \sqrt{c_B^2 - 4c_A c_C}}{2c_A}\right] \tag{1.5}$$

The simplifying terms for Eqs. 1.4 and 1.5 are provided below with common terms collected and reduced:

$$c_1 = \frac{S}{L} \tag{1.6a}$$

$$c_2 = \frac{2L^2 + S^2 - W^2}{2L^2} \tag{1.6b}$$

$$c_3 = \frac{S}{W} \tag{1.6c}$$

$$c_4 = \frac{-S^2 - W^2}{2LW} \tag{1.6d}$$

$$c_A = c_2 + (1 - c_1)\cos\alpha - c_1 \tag{1.6e}$$

$$c_B = -2\sin\alpha \tag{1.6f}$$

$$c_C = c_2 - (1 + c_1)\cos\alpha + c_1 \tag{1.6g}$$

$$c_D = c_4 + (1 + c_3)\cos\alpha - c_1 \tag{1.6h}$$

$$c_E = c_4 - (1 - c_3)\cos\alpha + c_1 \tag{1.6i}$$

It is important to note that the arctangent function has singular points and is often numerically implemented only over $-\pi/2$ to $\pi/2$. Adequate evaluation may require interjecting numerical noise or heuristic checks to avoid the singularities if using these equations directly.

The relative angles, those with respect to the previous link, can be written in terms of the

absolute angles:

$$q_A = \alpha \tag{1.7a}$$

$$q_B = \beta - \alpha \tag{1.7b}$$

$$q_C = \gamma - \beta \tag{1.7c}$$

Next, the positions to the COM of each link are given in the inertial frame using the definitions specified from the absolute angles:

$$\begin{aligned} \mathbf{r}_A = \quad & L_{COM}\cos\alpha\mathbf{i} + \\ & L_{COM}\sin\alpha\mathbf{j} \end{aligned} \tag{1.8}$$

$$\begin{aligned} \mathbf{r}_B = \quad & \left(L\cos\alpha + \tfrac{W}{2}\cos\beta - H_{COM}\sin\beta\right)\mathbf{i} + \\ & \left(L\sin\alpha + \tfrac{W}{2}\sin\beta + H_{COM}\cos\beta\right)\mathbf{j} \end{aligned} \tag{1.9}$$

$$\begin{aligned} \mathbf{r}_C = \quad & \left(L_{COM}\cos\gamma + S\right)\mathbf{i} + \\ & \left(L_{COM}\sin\gamma\right)\mathbf{j} \end{aligned} \tag{1.10}$$

1.2.2.2 Velocity

The angular velocities with respect to the inertial frame can also be solved by taking the derivative of Eq. 1.3 and in a similar fashion the angular velocity for the driven angles can be found by solving the vector velocity loop equation:

$$jL\dot{\alpha}e^{j\alpha} + jW\dot{\beta}e^{j\beta} = jL\dot{\gamma}e^{j\gamma} \tag{1.11}$$

The driven angular velocities are then given below in terms of the driving angle, $\dot{\alpha}$, which must be solved using Eqs. 1.4 and 1.5 from above.

$$\dot{\beta} = \frac{L}{W}\frac{\sin\left(\gamma - \alpha\right)}{\sin\left(\beta - \gamma\right)}\dot{\alpha} \tag{1.12}$$

$$\dot{\gamma} = \frac{\sin\left(\beta - \alpha\right)}{\sin\left(\beta - \gamma\right)}\dot{\alpha} \tag{1.13}$$

The relative velocities are then just the derivatives of the relative angular positions (Eq. 1.7c) and can be written in terms of the absolute angular velocities as:

$$\dot{q}_A = \dot{\alpha} \tag{1.14a}$$

$$\dot{q}_B = \dot{\beta} - \dot{\alpha} \tag{1.14b}$$

$$\dot{q}_C = \dot{\gamma} - \dot{\beta} \tag{1.14c}$$

The velocities of the COM for each link are given in the inertial frame by taking the derivatives of the position vectors (Eq. 1.8):

$$\begin{aligned} \dot{\mathbf{r}}_A = \quad & -L_{COM}\dot{\alpha}\sin\alpha\mathbf{i} + \\ & L_{COM}\dot{\alpha}\cos\alpha\mathbf{j} \end{aligned} \tag{1.15}$$

$$\begin{aligned} \dot{\mathbf{r}}_B = \quad & \left(-L\dot{\alpha}\sin\alpha - \left(\tfrac{W}{2}\sin\beta + H_{COM}\cos\beta\right)\dot{\beta}\right)\mathbf{i} + \\ & \left(L\dot{\alpha}\cos\alpha + \left(\tfrac{W}{2}\cos\beta - H_{COM}\sin\beta\right)\dot{\beta}\right)\mathbf{j} \end{aligned} \tag{1.16}$$

$$\begin{aligned} \dot{\mathbf{r}}_C = \quad & -\left(L_{COM}\dot{\gamma}\sin\gamma\right)\mathbf{i} + \\ & \left(L_{COM}\dot{\gamma}\cos\gamma\right)\mathbf{j} \end{aligned} \tag{1.17}$$

1.2.2.3 Acceleration

Finally, the angular acceleration of the driven angles can be solved for using the solutions from the angular position (Eqs. 1.4 and 1.5) and velocity (Eqs. 1.12 and 1.13) from above and writing the final loop equation as the derivative of the velocity loop equation (Eq. 1.11):

$$\left(j\ddot{\alpha} - \dot{\alpha}^2\right)Le^{j\alpha} + \left(j\ddot{\beta} - \dot{\beta}^2\right)We^{j\beta} = \left(j\ddot{\gamma} - \dot{\gamma}^2\right)Le^{j\gamma} \tag{1.18}$$

The angular accelerations are given below in terms of simplified variables:

$$\ddot{\beta} = \frac{c_W c_X - c_U c_Z}{c_U c_Y - c_V c_X} \tag{1.19}$$

$$\ddot{\gamma} = \frac{c_W c_Y - c_V c_Z}{c_U c_Y - c_V c_X} \tag{1.20}$$

The simplified terms used in the equations above are given below:

$$c_U = L\sin\gamma \tag{1.21a}$$

$$c_V = W\sin\beta \tag{1.21b}$$

$$c_W = L\ddot{\alpha}\sin\alpha + L\dot{\alpha}^2\cos\alpha + W\dot{\beta}^2\cos\beta - L\dot{\gamma}^2\cos\gamma \tag{1.21c}$$

$$c_X = L\cos\gamma \tag{1.21d}$$

$$c_Y = W\cos\beta \tag{1.21e}$$

$$c_Z = L\ddot{\alpha}\cos\alpha - L\dot{\alpha}^2\sin\alpha - W\dot{\beta}^2\sin\beta + L\dot{\gamma}^2\sin\gamma \tag{1.21f}$$

For completeness, the accelerations of the COM for each link are given in the inertial frame by taking the derivatives of the velocity vectors (Eq. 1.15):

$$\begin{aligned}\ddot{\mathbf{r}}_A = \quad & -L_{COM}\left(\ddot{\alpha}\sin\alpha + \dot{\alpha}^2\cos\alpha\right)\mathbf{i} + \\ & L_{COM}\left(\ddot{\alpha}\cos\alpha - \dot{\alpha}^2\sin\alpha\right)\mathbf{j}\end{aligned} \tag{1.22}$$

$$\begin{aligned}\ddot{\mathbf{r}}_B = \quad & \left(-L\left(\ddot{\alpha}\sin\alpha + \dot{\alpha}^2\cos\alpha\right) - \left(\tfrac{W}{2}\sin\beta + H_{COM}\cos\beta\right)\ddot{\beta} - \left(\tfrac{W}{2}\cos\beta - H_{COM}\sin\beta\right)\dot{\beta}^2\right)\mathbf{i} + \\ & \left(L\left(\ddot{\alpha}\cos\alpha - \dot{\alpha}^2\sin\alpha\right) + \left(\tfrac{W}{2}\cos\beta - H_{COM}\sin\beta\right)\ddot{\beta} - \left(\tfrac{W}{2}\sin\beta + H_{COM}\cos\beta\right)\dot{\beta}^2\right)\mathbf{j} +\end{aligned} \tag{1.23}$$

$$\begin{aligned}\ddot{\mathbf{r}}_C = \quad & -L_{COM}\left(\ddot{\gamma}\sin\gamma + \dot{\gamma}^2\cos\gamma\right)\mathbf{i} + \\ & L_{COM}\left(\ddot{\gamma}\cos\gamma - \dot{\gamma}^2\sin\gamma\right)\mathbf{j}\end{aligned} \tag{1.24}$$

1.2.3 Kinetics

It may be useful to investigate joint reactions in order to determine the validity of the model for approximating standing balance. Since the model is pinned at the feet, it is helpful to monitor the pinned reactions. In reality, a human subject will take a step or at least lift up their feet, so if these reactions switch sign, or *pull up*, then the model is no longer approximating the physics of the behavior. Using conservation of linear momentum (Newton's equations) and angular momentum (Euler's equations), we can formulate a series of equations that will reveal the joint reactions for the linkage (Figure 1.3). With the assumption

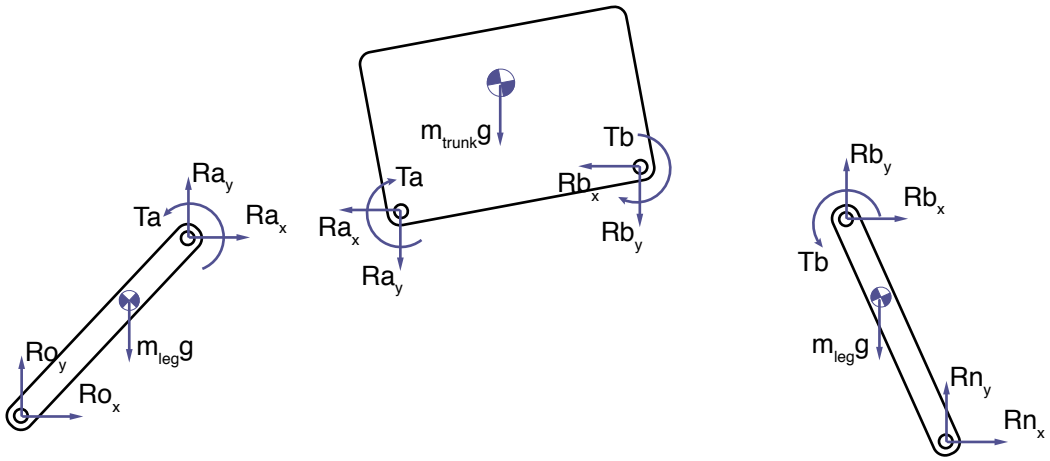

Figure 1.3: Free-body diagram for the four-bar linkage. Torques, Ta and Tb, are shown as the internal joint torques generated by neuromuscular control.

that all kinematics are known as well as the joint torques, the 8 equations below (3 vector linear momentum equations, 2 scalar angular momentum equations) can be rearranged as desired to solve for any of the 8 unknown joint reactions:

$$M_{leg}\ddot{\mathbf{r}}_A = (Ro_x + Ra_x)\mathbf{i} + \left(Ro_y + Ra_y - m_{leg}g\right)\mathbf{j} \tag{1.25a}$$

$$M_{trunk}\ddot{\mathbf{r}}_B = (-Ra_x - Rb_x)\mathbf{i} + \left(-Ra_y - Rb_y - m_{trunk}g\right)\mathbf{j} \tag{1.25b}$$

$$M_{leg}\ddot{\mathbf{r}}_C = (Rb_x + Rn_x)\mathbf{i} + \left(Rb_y + Rn_y - m_{leg}g\right)\mathbf{j} \tag{1.25c}$$

$$I_{leg}\ddot{\alpha} = (Ro_x L_{COM} - Ra_x(L - L_{COM}))\sin\alpha + \left(Ra_y(L - L_{COM}) - Ro_y L_{COM}\right)\cos\alpha + Ta \tag{1.25d}$$

$$I_{leg}\ddot{\gamma} = (Rn_x L_{COM} - Rb_x(L - L_{COM}))\sin\gamma + \left(Rb_y(L - L_{COM}) - Rn_y L_{COM}\right)\cos\gamma + Tb \tag{1.25e}$$

1.2.4 Dynamics

The unforced equations of motion for the four-bar linkage can be determined using the kinematics (Section 1.2.2), the free-body diagram (Figure 1.3), and principles of linear and angular momentum or work and energy. The model was originally formulated using Kane's method [57]. In this primer the equations of motion are derived using an Euler-Lagrange formulation for clarity without any loss in usefulness or functional changes.

As a point of clarification, it is important to reiterate that the four-bar linkage has only a single degree-of-freedom. Therefore, for the sake of this derivation the generalized coordinate will be assumed to be q_A. Also, for convenience of notation the time dependence of this coordinate will be assumed implicit, $q_A = q_A(t)$. Furthermore, it is important to note that $\alpha = q_A$ and that the absolute angles β and γ are to be interpreted as functions of q_A, e.g. $\beta = \beta(q_A)$.

1.2.4.1 Potential energy

In this section, the potential energy is quantified for each individual source and summed. Without any additional energy-storage elements, such as springs, or additional conservative body forces, gravity is the only source of potential energy. Therefore, the potential energy may be written as the sum of gravitational potential energy from each of the separate links. Using the form Mgh, where the height, h, can be determined from the position to the COM (Eq. 1.8), the total potential energy can be written as a function in terms of q_A:

$$V(q_A) = M_{leg} g \mathbf{r}_A \cdot \mathbf{j} + M_{trunk} g \mathbf{r}_B \cdot \mathbf{j} + M_{leg} g \mathbf{r}_C \cdot \mathbf{j} \tag{1.26}$$

1.2.4.2 Kinetic energy

In this section, the kinetic energy is quantified for each individual source and summed. The total kinetic energy for each link is a sum of the translational, $\frac{1}{2} M |\dot{\mathbf{r}}|^2$, and angular, $\frac{1}{2} I \dot{q}^2$, kinetic energy. Using the definitions of linear and angular velocity (Section 1.2.2) the sum of the kinetic energy from each link can be written as a function in terms of q_A and $\dot{q}_A$:

$$T(q_A, \dot{q}_A) = \frac{1}{2} \left(M_{leg} |\mathbf{r}_A|^2 + I_{leg} \dot{q}_A^2 + M_{trunk} |\mathbf{r}_B|^2 + I_{trunk} \dot{q}_B^2 + M_{leg} |\mathbf{r}_C|^2 + I_{leg} \dot{q}_C^2 \right) \tag{1.27}$$

1.2.4.3 Euler-Lagrange and the equations of motion

Having identified sources of potential and kinetic energy it is now possible to formulate the Lagrangian (Eq. 1.28), which gives a nice form to insert into the Euler equation (Eq. 1.29) and solve to apply the "least-action principle" to generate equations of motion.

$$L(q_A, \dot{q}_A) = T(q_A, \dot{q}_A) - V(q_A) \tag{1.28}$$

$$\frac{d}{dt}\left(\frac{\partial L(q_A,\dot{q}_A)}{\partial \dot{q}_A}\right)-\frac{\partial L(q_A,\dot{q}_A)}{\partial q_A}=0 \tag{1.29}$$

I digress for a moment to point out how very impressive the Euler-Lagrange result is; if you have a second, check out its derivation from variational calculus principles. This gives an elegant statement that within a conservative system the trajectories that result in an extremum for the Lagrangian are the solutions of the Euler equation. This is mechanics formulated as an optimization problem!

The potential and kinetic energy can be readily dropped into these equations and a single scalar equation for the equation of motion can be solved by performing the necessary derivatives.

1.2.4.4 Components of the equation of motion and their meaning

Individual components of the Euler-Lagrange equation can be uncovered that are useful for understanding how changes in parameters might affect behavior. The first expansion of the Euler-Lagrange equation (Eq. 1.29) is achieved by using the chain-rule on the time derivative. Below are the steps to expand the leading term of the Euler-Lagrange equation, where for compactness $L = L(q_A,\dot{q}_A)$:

$$\frac{d}{dt}\left(\frac{\partial L}{\partial \dot{q}_A}\right)=\frac{\partial}{\partial q_A}\frac{\partial q_A}{\partial t}\left(\frac{\partial L}{\partial \dot{q}_A}\right)+\frac{\partial}{\partial \dot{q}_A}\frac{\partial \dot{q}_A}{\partial t}\left(\frac{\partial L}{\partial \dot{q}_A}\right)+\frac{\partial}{\partial t}\left(\frac{\partial L}{\partial \dot{q}_A}\right) \tag{1.30a}$$

$$=\frac{\partial}{\partial q_A}\left(\frac{\partial L}{\partial \dot{q}_A}\right)\dot{q}_A+\frac{\partial}{\partial \dot{q}_A}\left(\frac{\partial L}{\partial \dot{q}_A}\right)\ddot{q}_A+0 \tag{1.30b}$$

Then equation 1.29 is rewritten in a form that allows for identifying components that can be attributed to inertial, coriolis/centripetal, and gravitational forces:

$$\left(\frac{\partial^2 L(q_A,\dot{q}_A)}{\partial \dot{q}_A \partial \dot{q}_A}\right)\ddot{q}_A+\left(\frac{\partial^2 L(q_A,\dot{q}_A)}{\partial q_A \partial \dot{q}_A}\right)\dot{q}_A-\frac{\partial L(q_A,\dot{q}_A)}{\partial q_A}=0 \tag{1.31}$$

With one last step the Euler-Lagrangian is expanded again by inserting Eq. 1.28 into Eq. 1.31 and some components are removed due to their partial derivatives vanishing and the remainder results in the final set of components:

$$\left(\frac{\partial^2 T(q_A,\dot{q}_A)}{\partial \dot{q}_A \partial \dot{q}_A}\right)\ddot{q}_A+\left(\frac{\partial^2 T(q_A,\dot{q}_A)}{\partial q_A \partial \dot{q}_A}\right)\dot{q}_A-\frac{\partial T(q_A,\dot{q}_A)}{\partial q_A}+\frac{\partial V(q_A)}{\partial q_A}=0 \tag{1.32}$$

This equation can be compared to the form of equations of motion that have inertial, $I(q)$, coriolis/centripetal, $Q(q,\dot{q})$, and gravitational forces, $G(q)$.

$$I(q)\ddot{q} + Q(q,\dot{q}) + G(q) = 0 \tag{1.33}$$

From this final expansion (Eq. 1.32) the linear term with respect to the generalized acceleration, $\ddot{q}_A$, is isolated and named as the generalized inertia of the system:

$$I(q_A) = \left(\frac{\partial^2 T(q_A,\dot{q}_A)}{\partial\dot{q}_A\partial\dot{q}_A}\right) \tag{1.34}$$

The generalized inertia gives a measure of the distribution of the mass of the linkage and gives some intuition as to how readily the linkage will move when acted upon by an external force. Generalized inertia is closely related to traditional methods of determining second-moments of inertia when computing angular momentum; however, instead of computing moments of distribution of mass about a point the generalized inertia is derived from the momenta directly. In the case of a purely rotational system with a fixed axis of rotation the second-moment of inertia about that point will be identical to the generalized inertia. Intuition of how generalized inertia changes with four-bar configuration and motion is not necessarily intuitive. Figure 1.4) illustrates that for four-bar linkage parameters that approximate human subjects the majority of the change occurs as stance width changes, but within a stance width inertia is relatively constant across physiologically observed motion.

Next, terms having quadratic generalized velocity are identified and are lumped together as the generalized centripetal and coriolis forces:

$$Q(q_A,\dot{q}_A) = \left(\frac{\partial^2 T(q_A,\dot{q}_A)}{\partial q_A\partial\dot{q}_A}\right)\dot{q}_A - \frac{\partial T(q_A,\dot{q}_A)}{\partial q_A} \tag{1.35}$$

These components are complex and can have significant effects when velocities are large; conversely, when velocities are small these terms are negligible and will vanish altogether if the equations of motion are linearized.

Finally, the remaining term associated only with the potential energy is defined as the generalized conservative or gravitational force:

$$G(q_A) = \frac{\partial V(q_A)}{\partial q_A} \tag{1.36}$$

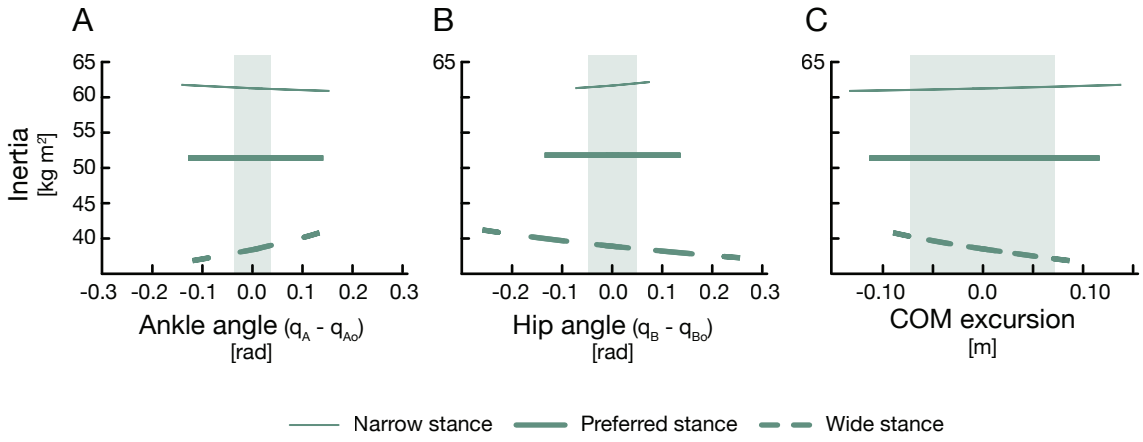

Figure 1.4: Generalized inertia changes most over stance width and less with changes in kinematics. The plots give the change in inertia over a range of linkage motion for a human sized four-bar (mass = 70 kg, height = 1.8 m). Shaded area marks the largest observed changes for that variable. Kinematic variables are zeroed with respect to their starting value for each particular stance width in the symmetric configuration.

This component is particularly useful for analysis of stability of the system and if the partial of this quantity with respect to the generalized coordinate is positive the conservative field are known to be destabilizing.

Linearization of all three of these components was performed and the results can be found in Appendix A.

1.3 Organization and summary of work

The organization of this thesis was built around three areas of neuromechical interaction in human standing balance: stance width, neural delay and neural feedback. The primary goal of the chapters herein was to provide evidence of how changes in biomechanics and/or neural control can affect balance responses and to lay the framework for quantifying how these interactions may affect stability. The secondary goal was to develop an analytic model of frontal plane standing balance (Appendix A) and develop procedures to quantify stability of neuromechanical systems (Chapter 4).

Each chapter, for the most part, is capable of standing alone; however, if a primer is needed it may be worthwhile to investigate the methods described in chapter 2 and the corresponding appendix A, which provide the explanation of the four-bar linkage model with

delayed feedback that is referenced throughout the rest of the work. The scope of the work pertains to three basic aims, which are described below with how pertinent chapters support the respective aim:

- **Aim 1** Predict changes to stability due to changes in stance width, feedback gains, and delays. The central hypothesis was that a constant level of stability could be maintained by either changes in stance width or neural feedback to compensate for altered biomechanical or neural parameters.
  - *Chapter 2* Model results predict that delayed feedback gain must increase as stance width decreases in order to maintain stability.
  - *Chapter 3* As a corollary, simulations predicted that changes in neural control could be compensated by changes in stance width to produce similar torque responses.
  - *Chapter 5* Model predictions of center-of-mass motion show that both postural set and delayed neural feedback change with altered stance width.
- **Aim 2** Quantify trade-offs in stability of standing balance from changes in neuromechanical interactions. This aim's hypothesis was that the responses from balance behaviors are the result of neuromechanical factors that coordinate to produce a similar level of stability across a variety of biomechanical contexts.
  - *Chapter 2* Analytic measures of gain margin were predictive of feedback gains within a stance width that correlated with perturbation magnitude that induced experimentally observed stepping behavior.
  - *Chapter 4* Stability radius allowed quantifying stability in a model across biomechanical contexts and showed similar stability could be achieved across stance widths by decreasing feedback gain as stance width increased.
  - *Chapter 5* Simulated center-of-mass motion with feedback gains selected with similar stability across stance width matched experimental observations.

- **Aim 3** Compare neuromechanical interactions across biomechanical contexts. Similar to the hypothesis of Aim 2, here it was hypothesized that changes in neural feedback accompany differences in biomechanical context in order to maintain similar CoM behavior.
  - *Chapter 3* Stance width decreased with age, but performance in time to peak torque was similar, which required increased feedback gain in the older subjects.
  - *Chapter 4* Feedback gains selected with similar stability radius resulted in similar performance across stance widths.
  - *Chapter 5* Using different conditions of body mass it was shown that similarity in CoM motion required delayed neural feedback to scale with both body mass and stance width, or inertia of the subject.

The thesis also has components of modeling, experimentation, and analysis that are spread throughout the various chapters. If the reader is more interested in the modeling aspects chapter 2 and the appendix A develop the four-bar linkage model of frontal plane balance. The model is probed in detail for how parameters of stance width, feedback gain and feedback delay effect torque generation in chapter 3. The effects of these parameters on center-of-mass motion of the model are explored in chapter 5.

Experimental study tie-ins are found in most of the chapters. Most of the populations consist of healthy, college-aged volunteers, but the protocols are different. Thus, a particular chapter may be of more interest based on the experiments performed. Chapter 2 utilized a subset of trials collected by Julia Choi from healthy college-aged students where the stance widths were specified at 10, 19, and 32 cm with perturbations specified at 12 cm, 35 cm/s, and 0.45 g. Chapter 3 used data collected in part by Kyla Ross for a Tai Chi study that included individuals across a range of ages, 23-62 years, with subjects selecting their own preferred stance width and perturbations specified at 12 cm, 35 cm/s, and 0.5 g. The final chapter 5 used data specifically collected for the study from healthy, college-aged volunteers that included a variety of stance widths (10 cm, 30 cm, self-selected), perturbations (high and low relative to 24 cm, 15 cm/s, 0.1 g), and weight conditions (unweighted and +20% body

mass).

Analysis and development of tools for quantifying stability of neuromechanical systems was also a large part of this thesis. Chapter 2 and the corresponding appendix A review how boundaries of stability can be found using Nyquist stability criteria for delayed systems. This chapter also shows how gain and phase margin can be calculated for the delayed feedback four-bar linkage system. Chapter 4 is the most critical chapter for quantifying stability of neuromechanical systems and gives a review of the stability radius technique, which gives a robust measure of relative stability. This chapter also provides a basic primer for applying the stability radius to delay systems. Application of the stability radius method for quantifying the parameters of frontal plane standing balance is provided as a proof of concept in appendix B.

In short, the message of the following chapters is that biomechanics and neural control covary to produce stable behavior. These chapters were written with the bias that neither neural control nor biomechanics alone are capable of explaining motor behavior. Therefore, I hope that this thesis provides some evidence that even the simple maneuver of increasing one's stance width is accompanied with sophisticated changes in neural control along with the obvious change in skeletal geometry and changes in muscle operating properties. This thought is expanded and future directions are suggested in the concluding chapter.

CHAPTER II

NEUROMECHANICAL FACTORS THAT AFFECT THE STABILITY OF STANDING BALANCE

2.1 Introduction

If you are standing do you feel more stable with your feet close together or spread apart? Changes in postural configuration affect the dynamics of the body and likely necessitate changes in neural control to perform a movement. Changes in stance width in a simple robotic model of standing balance control were found to be destabilizing without coordinated adjustments in physiologically-inspired delayed feedback control gains for moderate perturbations [109]. The nervous system likely selects specific postural configurations to reduce the neural demand for a task. For example, subjects have been observed to choose arm configurations that increase stability along directions of environmental instability [135]. The selection of a postural configuration may also reduce energy expenditure or sensitivity to noise [111]. Although this evidence demonstrates the importance of neuromechanical interactions in understanding motor control, little is known about the individual contributions and interplay between biomechanical and neural components that are required for stable posture and movement.

Consistent with our intuitions about standing balance control, wider stance widths are often considered to provide increased mechanical stability (Winter 1995), but little quantitative evidence exists to support these suppositions. The preferred stance width in healthy individuals is approximately equal to hip width [110, 80]. However, in uncertain conditions, like riding on a moving train, we often adopt a wider stance. In healthy subjects, muscle activation decreases in response to the same external perturbation when standing with wider stance,

while the body's center-of-mass displacement stays roughly the same across different stance widths [39, 132]. This has been suggested to be due to increased reliance on passive stability mechanisms and a reduction in neural control [39]. However, these observations cannot be used to dissociate the contributions of biomechanical and neural systems to stability during these behaviors. Evidence from patients with neural deficits suggests that increasing stance width alone may not be stabilizing. Patients with Parkinson's disease who suffer from high postural instability exhibit deficits in appropriate scaling of postural feedback gains [60] and tend to choose a narrower stance - roughly half as wide as matched healthy controls [47]. To better understand both healthy and neurologically-impaired subjects, a frontal plane model with delayed feedback is necessary to quantify the neuromechanical interactions underlying stable balance control across postural configurations.

Physiological delays are significant during postural control and can limit the range of feedback gains that generate stability; however, the consequences for how balance is controlled in the frontal plane is not known. Active responses in muscles that restore the body center-of-mass occur at a latency of about 100 ms, and the resulting musculoskeletal forces are further delayed by 50 ms due to the time course associated with muscle force production and transmission [48]. As a result of this delay, the maximum magnitude of sensorimotor feedback gain is limited, with longer latencies reducing the set of feasible gains [75, 100]. Delayed feedback models of posture have been used to identify the complex stable boundaries of anterior-posterior balance [75, 99, 138, 87, 83]. Furthermore, delayed feedback models have been used to describe the entire time-course of muscle activity during sagittal plane postural responses in both cats and humans [69, 145]. However, feedback control of frontal plane balance has received little attention, and may be more dramatically influenced by postural configuration [36, 109].

We hypothesized that changing stance width during standing balance control alters the neuromechanical interactions, necessitating appropriate adjustments of neural feedback gains to maintain stability. We performed analytic and computational analysis on a simple frontal-plane model to examine how delayed feedback control of standing balance must change as a function of stance width. In our model, we examined the mechanical stability of the body

alone, and as stabilized by delayed feedback control. We also considered foot lift-off constraints and the effect of perturbation size on the robustness of stability during balance control. Our results showed that many different feedback gains produce stable behavior for each stance width. However, stable balance was not possible with a single feedback gain across all stance widths. This suggests that reduction of muscle activity in wide stance is not due to increased biomechanical stability in wide stance. Rather, increased sensitivity of body motion to joint torque production may necessitate that the nervous system appropriately tune feedback gains according to the biomechanical context.

2.2 Methods

We developed a model of frontal plane balance to investigate the effects of postural configuration and delayed feedback control on stability to perturbations as stance width changed. We first quantified biomechanical properties and the stability of the model in the absence of feedback control as stance width changed. To investigate how postural configuration influenced the effect of feedback information during perturbations, we identified a relationship between hip angle and center-of-mass motion to a generalized coordinate (ankle angle). Next, the stability of the model under delayed feedback control was analyzed subject to different combinations of configuration, feedback gains and delay. Further, we determined how foot lift-off constraints and perturbation magnitude further reduced the feasible range of delayed feedback gains. Finally, we compared model predictions with recorded frontal plane motion in human experiments. Details about the model are provided in Appendix A and summarized here.

2.2.1 Frontal plane model of balance

In order to simulate and analyze frontal plane motion of an adult human we modeled the body segments as a four-bar linkage and the neural control as delayed position and velocity feedback. The linkage consisted of four segments corresponding to the ground, two legs and the torso connected by pin joints in a closed chain (Figure 2.1). Inertial and geometric properties were based on average anthropometric data for an adult male of height 1.8 m and weight 70 kg (Appendix A: Table A.1) (Winter 2003). The leg segments were a lumped

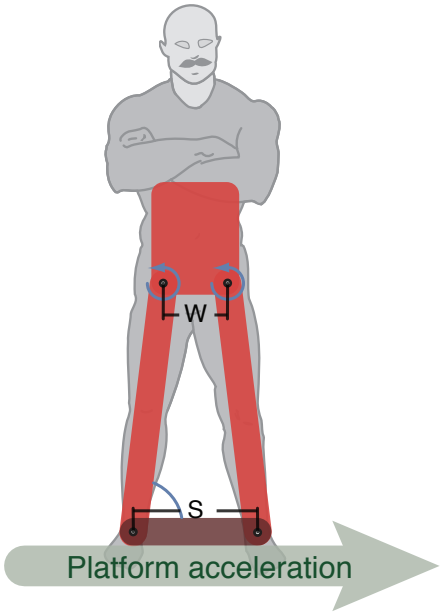

Figure 2.1: Frontal plane model of human balance control. Frontal plane motion of the body was modeled as a four-bar linkage. Two bars represent the legs, the third the torso and the fourth bar is the ground. Perturbations are applied as ground translations. Important parameters of the model are the hip width, W; stance width, S; hip torque, T_H; and the ankle angle, q_A.

representation of the shank and thigh with a locked knee and pin joints for the ankle and hip. The torso segment included head, arms (folded across the chest), trunk, and pelvis and was attached to the leg segments by pin joints at the hips. The ground segment was considered immobile and its length was used to specify the stance width of the model.

The equations of motion for the four-bar linkage were derived using a symbolic dynamics package (AutoLev 4.1, OnLine Dynamics, Inc) and matched those found in engineering texts [92]. The nonlinear equations of motion had one mechanical degree-of-freedom, which was specified by a generalized coordinate defined by the angle between the ground and the left leg, i.e. the ankle angle. Muscular force was modeled as a lumped term and applied with constant moment arms as torque about each hip joint. Perturbations to the model were included in the equations of motion as a time-varying acceleration to the inertial frame.

Hip torque was generated as delayed feedback with fixed gains on position and velocity. Feedback was dependent on either hip joint or center-of-mass horizontal excursion. Analysis of the model was done using hip joint feedback unless stated otherwise. The delay was

selected to be a single lumped value of 150 ms to account for neural transmission from sensation to actuation (100 ms) and mechanical actuation (50 ms) as observed from the automatic postural response [48].

The perturbation applied to the four-bar linkage was applied as an inertial acceleration of the ground that matched platform translations from experimental ramp-and-hold protocols. The acceleration profile consisted of two Gaussian pulses with opposite directions, each 40 ms wide, spaced 500 ms apart and having amplitudes ranging from 0.1-0.5 times earth gravity (g). This perturbation resulted in a zero starting velocity, a constant velocity movement phase and finally ending at rest.

In addition we performed numerical simulation of the equations of motion in Matlab. Integration was performed with the explicit trapezoidal rule with a step size of 1 ms and a total simulation time of 6 s. Initial conditions and state history were assumed to be zero. The perturbation was introduced as previously described. Center-of-mass trajectories and ground reaction forces were then recorded.

2.2.2 Biomechanical stability analysis

We identified stance width dependent changes in the biomechanical properties of the model as quantified by the inertia, gravitational moment, sensitivity of the center-of-mass motion to joint torque, and the stability of the model, as defined by the eventual return of the model to an equilibrium position after a perturbation. The equilibrium position of the model was defined by the symmetrical configuration (Figure 2.1) where all external forces were statically balanced, the center-of-mass was mid-way between the ankle joints and the hip angles were equal. Inertia, gravitational moment and joint torque was determined by linearizing the uncontrolled equations of motion with respect to the generalized coordinate and plotting them as functions of stance ratio (stance width divided by hip width). The anthropometric properties of an average adult male human were used for the plots (Appendix A: Table A.1) [148].

Inertia is a measure of an object's resistance to a change in motion, and was used as

an indicator of whether acceleration of the body would result in large motions (small inertia) or small motions (large inertia). Linearized inertia was calculated from the non-linear equations of motion resulting in a configuration dependent term (see Appendix A: Eq. A.7). The linearized inertia was used to quantify the magnitude of center-of-mass motion from accelerations induced by perturbations and joint torques.

Although gravity is constant, it presents a destabilizing perturbation that is configuration dependent and is mathematically equivalent to a negative, or destabilizing, stiffness. A large magnitude of the linearized gravitational stiffness would result in a large destabilizing perturbation for a small deviation from the equilibrium configuration. The linearized gravitational stiffness was also represented as a configuration dependent lumped parameter (see Appendix A: Eq. A.8).

The sensitivity of the joint torque quantified the efficiency of transmitting torque at the hip to motion of the center-of-mass. This relationship was calculated by employing the law of power continuity, which states that the product of torque and angular velocity must be conserved throughout a linkage (Norton 2001). The amplification or attenuation of the effective torque due to changes in stance width was used to determine the efficiency of that configuration. Effective torque on the center-of-mass due to torque applied at the hip joints was written as a configuration dependent term for the entire four-bar linkage (see Appendix A: Eq. A.9).

To investigate differences between center-of-mass and joint angle as possible feedback variables, linear relations were calculated between hip angle, center-of-mass horizontal excursion and the generalized coordinate (ankle angle). Ratios from the linearized equations of motion were calculated that transformed a small increment in either hip angle or center-of-mass horizontal excursion into an increment in the generalized coordinate. These ratios were plotted as functions of stance ratio (stance width-to-hip width) using average anthropometric values (Appendix A: Table A.1).

2.2.3 Delayed feedback stability analysis

To determine the stability of delayed feedback on the biomechanical system the hip joint feedback gains were compared across different delays, stance widths and perturbations. The stability of the hip joint feedback gains was found by solving the non-linear equations of motion for the critically stable boundaries. These boundaries were defined mathematically by the feedback gain values that resulted in solutions to the characteristic equation having zero real part. Behaviorally, this boundary divided gains resulting in falls (unstable) from those that returned the center-of-mass to the equilibrium position (stable). Since the characteristic equation for the delayed system resulted in an infinite number of solutions, numerical techniques were utilized to solve for a finite number of eigenvalues and to check the analytic stability boundaries using custom Matlab routines and the DDE-BIFTOOL delayed-differential equation toolbox [27].

To quantify the relative stability between different stable feedback gain values, a frequency domain analysis of the linearized equations of motion was performed. The measures of gain margin and phase margin were used to identify robustness and system performance to perturbation magnitude. Gain margin is defined as the loop gain measured when the excitation frequency causes a -180° phase difference between input and output. This was used to quantify the perturbation magnitude the model could withstand, where a large gain margin inferred the model was stable against a large perturbation. Phase margin is defined as the phase difference from -180° measured when the excitation frequency results in a loop gain of 1. Similarly, a large phase margin was inferred to mean the model was stable for a large perturbation.

To model physiological boundaries of stability, numerical simulations were used to identify hip joint feedback gains that produced feet-on-ground behavior. Simulations were performed in a grid-wise manner across stance-ratios 0.5-2.0, all stable feedback gains and perturbation magnitude 0.1-0.5 g. The ground reaction forces were calculated for each simulation and used to determine if foot lift-off could occur. If ground reaction forces changed in sign during simulation, the associated parameters were classified as producing foot lift-off behavior. For each perturbation magnitude and stance width the hip joint feedback gains producing

feet-on-ground behavior were identified, and the boundary of these gains was plotted.

2.2.4 Experimental comparisons

In order to compare simulated and experimental results, body segment kinematics and ground reaction forces were collected from healthy human subjects during platform perturbations. All protocols were approved by the Georgia Tech and Emory University Institutional Review Boards and conformed to the Declaration of Helsinki. Five subjects (3 male, 2 female, 20.6 $\pm$ 1.8 years of age) were recruited. Subjects stood with arms crossed and their feet spaced at three fixed distances of 10, 19 and 32 cm. Each foot was located on an individual calibrated force plate (AMTI, Watertown, MA) that recorded all six reaction forces and moments. Subjects were instructed to stand upright and to maintain balance during perturbations, but were not given information about time of perturbation onset. Perturbations were administered with a custom platform (Factory Automation Systems, Atlanta, GA) with position and acceleration of the platform recorded. At each stance width, subjects received 10 ramp-and-hold platform perturbations in the medial-lateral direction with the platform moving to the subject's left. The perturbations had an overall movement distance of 12 cm, a plateau velocity of 35 cm/s and a peak acceleration of 0.45 g. Subjects could not predict perturbation onsets because inter-trial intervals were varied between 5-15 s.

Subject kinematics were captured with a custom 26-marker set that included head-arms-trunk, thigh, shank, and foot segments using a motion capture system (Vicon, Oxford, UK) utilizing 8 cameras. Motion capture was sampled at 120 Hz and platform kinematics at 1080 Hz. Platform kinematics were low-pass filtered at 30 Hz (third-order zero-lag Butterworth filter) and combined with motion capture kinematics to produce relative position, velocity and acceleration of the markers with respect to the platform. The relative motion of the markers and a proportional model of human mass were used to calculate center-of-mass position, velocity and acceleration for each subject [148].

Simulated center-of-mass position was fit to experimental data through optimization of the feedback gains for the non-linear equations-of-motion. Fits were calculated for two feedback rules, one using hip angle and the other center-of-mass excursion. Each experimental

trial was fit using the subject's measured mass, height, stance width and perturbation acceleration profile. For a given subject and stance width, model parameters were fixed and only feedback gain values were allowed to vary. This resulted in a total of 300 fits: 2 feedback rules by 10 perturbations by 3 stance widths by 5 subjects. Optimization to solve for the feedback gains utilized a cost function defined by the difference between simulated and experimental center-of-mass trajectories with penalties on absolute (weight of 1) and sum-squared error (weight of 10).

2.3 Results

2.3.1 Mechanical stability decreased with increasing stance width

2.3.1.1 Inertia decreased with increasing stance width

The linearized inertia about the equilibrium configuration was found to decrease as stance width increased within the physiological range (Figure 2.2A). The combined inertia of the body and legs was configuration dependent, changing with stance width and joint angle. Changes to stance width had the most effect on the apparent inertia of the body segment. Increasing stance width resulted in decreased inertia. Therefore, the same amount of applied torque produced at wide stance resulted in greater center-of-mass motion then when applied at narrow stance.

2.3.1.2 Gravitational stiffness remained constant with changing stance width

The destabilizing effect of gravity remained nearly constant across the physiological range of stance (Figure 2.2B). In general the gravitational stiffness was found to have a minimum near the stance ratio of 1 and increased to a maximum as stance width approached the singular configuration. The destabilizing effect of gravity therefore remained nearly constant for physiological stance ratios of 0.8-2.0.

2.3.1.3 Hip torque was more effective at wider stance

For constant torque at the hip, the effective torque on the center-of-mass increased as stance width increased. The amplification of the hip joint torque was found to quadratically increase with stance width. As stance width increased the same input torque produced a greater total

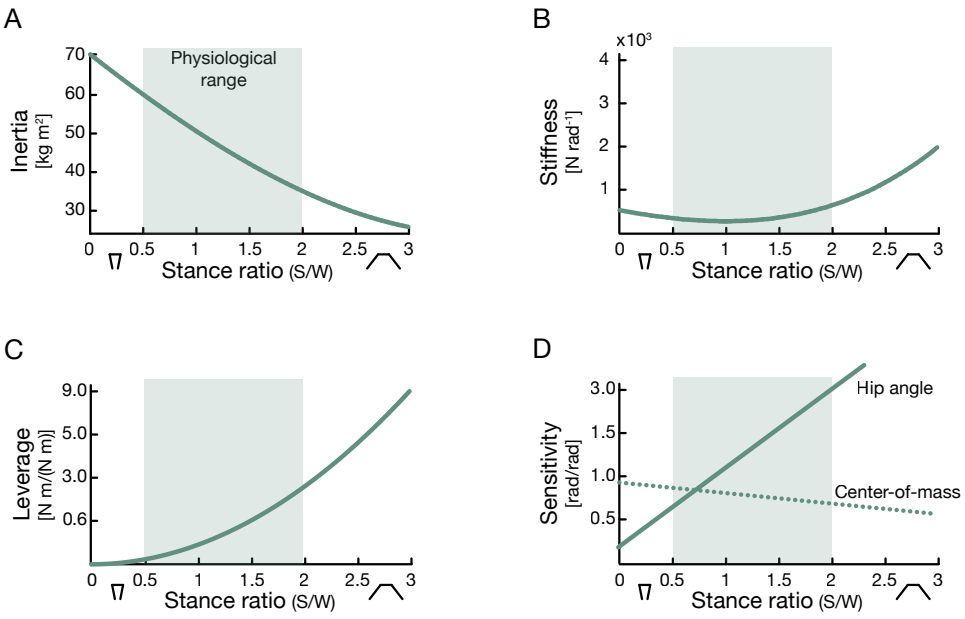

Figure 2.2: Changes in biomechanical properties of the body as stance width increased. For a nominal human (70 kg, 1.8 m) as stance width increased A) inertia decreased B) gravitational "stiffness" stayed roughly the same C) hip torque leverage increased and D) hip angle sensitivity to ankle angle changes increased (center-of-mass sensitivity decreased slightly), which all resulted in decreased biomechanical stability. Shaded regions mark physiological stance ratios.

torque on the motion of the four-bar linkage (Figure 2.2C). In other words, torque applied at the hip had more leverage on the center of mass at wider stances.

2.3.1.4 Model without delayed feedback was unstable across stance widths

The four-bar linkage without torque feedback was found to be unstable for all physiological stance widths. Stability decreased as stance width increased due to decreasing inertia while the destabilizing gravitational stiffness remained constant. In order to stabilize the mechanical system with delayed feedback both position and velocity were required. Position feedback was required to counteract destabilizing gravitational stiffness and velocity feedback was required to produce a damped response.

2.3.1.5 Center-of-mass and joint angle feedback scale linearly across stance widths

The effect of a small change in the generalized coordinate (ankle angle) on the hip angle or center-of-mass excursion changed proportionally with different stance widths (Figure 2.2D).

The hip angle became more sensitive to changes in ankle angle as stance width increased. Conversely, the center-of-mass excursion decreased in sensitivity to changes in ankle angle with increasing stance width. Center-of-mass excursion was more sensitive to changes in ankle angle than hip angle for stance ratios (S/W) less than 0.8 and hip angle was more sensitive to changes in ankle angle at wider stances. Furthermore, sensitivity to changes in ankle angle varied much less for center-of-mass excursion compared to hip angle over the physiological range. A small perturbation to the overall body angle resulted in larger excursion of the hip angle at wide stances. The linear relationships to the generalized coordinate predicted the non-linear feedback gains on center-of-mass excursion from hip joint angle feedback gains very closely.

2.3.2 Stable feedback gain boundaries decreased with increasing stance width

2.3.2.1 Stable delayed feedback gains have upper and lower bounds

The stable limits for the delayed feedback gains produced D-shaped boundaries associated with functional instabilities (Figure 2.3A). The boundaries were determined as a parametric solution to the characteristic equation (Appendix A: Eq. A.12). The left-hand boundary (Appendix A: Eq. A.13) represented a lower limit on delayed position feedback gain, k_p. The functional consequence of this limit corresponded to the delayed position feedback gain (k_p) being unable to counteract the destabilizing gravitational stiffness. The right-hand boundary (Appendix A: Eq. A.14) restricted both position and velocity feedback gains. This upper boundary was a consequence of the feedback delay and functionally represented instability due to over-correction. Finally, an upper limit on the length of delay was found, 429 ms for an average human at preferred stance, for which there were no feedback gain values that were stable (Appendix A: Eq. A.15).

2.3.2.2 Stable gain space decreased with increasing stance width

The set of stable delayed position and velocity hip joint feedback gains was found to decrease as stance width increased (Figure 2.3A). The maximum and minimum values of stable feedback gain were found to decrease as stance width increased. Specifically, narrow stance width (S/W=0.8) was found to have 98% more gain space area than the wide stance width (S/W=2.0).

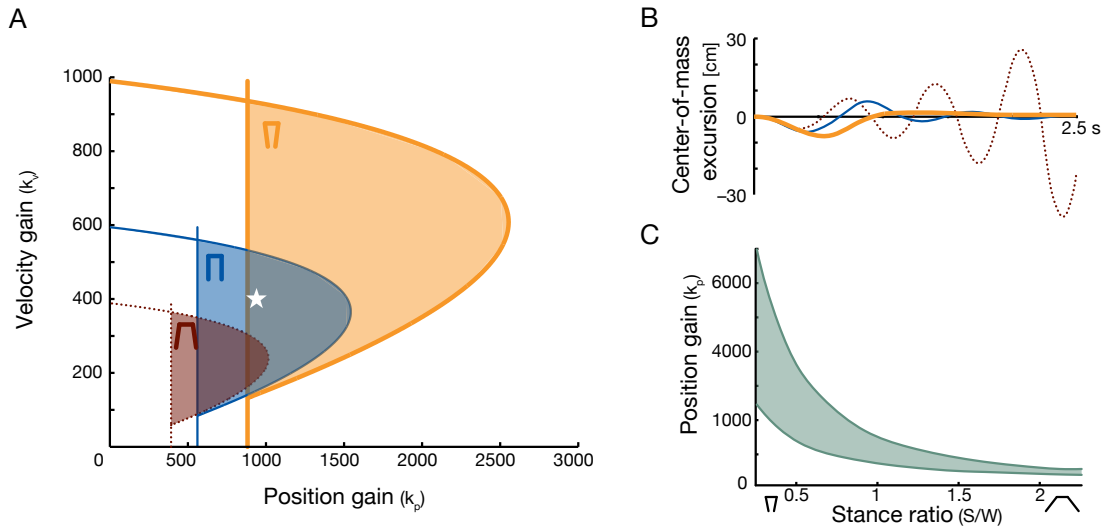

Figure 2.3: Regions of stable feedback gains across stance widths demonstrated that a fixed set of gains was not stable across different stance widths. A) Shaded areas represent stable position and velocity feedback gain values for a nominal human (70 kg, 1.8 m) with stance ratios of 0.8 (dotted), 1.0 (thin) and 1.2 (thick). B) Center-of-mass trajectories resulting from a 0.4 g perturbation for each stance-ratio using the same gain value, marked as a white star in gain space. C) Stable position feedback gain values across all physiological stance widths.

High gain values that were stable for narrow stance were unstable for wide stance. Stable gain regions did not completely overlap for different stance widths. However, even when overlap did occur, the simulated center-of-mass trajectories for the same gain across stance widths varied considerably (Figure 2.3B). Similar results were found when center-of-mass excursion feedback was used; however, more overlap was observed in the stable gain regions across stance widths.

2.3.3 Ground contact reduced set of stable feedback gains

2.3.3.1 Ground contact constraint produced more physiological center-of-mass trajectories

Center-of-mass trajectories associated with hip joint feedback gains limited by the feet-on-ground condition matched more closely with experimentally observed trajectories. High stable feedback gains produced center-of-mass trajectories that were highly oscillatory in the model (Figure 2.4). These did not match experimental observations of human motion that show near critically damped center-of-mass trajectories when subjected to a platform perturbation. Limiting stable feedback gains to those that produced feet-on-ground behavior

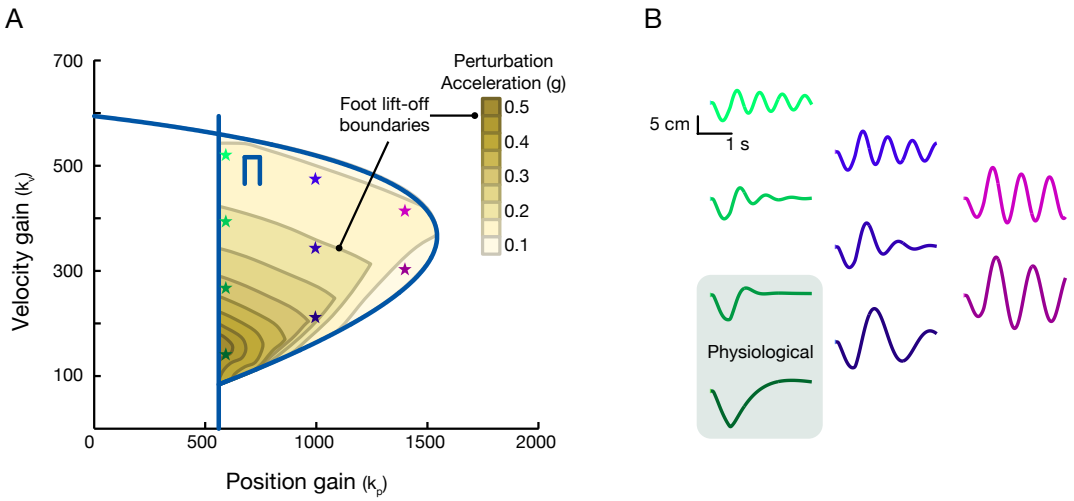

Figure 2.4: Boundaries on physiological feedback gains due to foot lift-off criterion and damped center-of-mass dynamics for a nominal human (70 kg, 1.8m) with a stance ratio of 1.0. A) The thick outer line is the stability boundary without considering foot lift-off. The thin lines and shaded areas correspond to the boundaries for foot lift-off at different perturbation magnitudes. B) Center-of-mass trajectories for 0.5 g perturbation. Each trajectory corresponds to the shaded starred gain pair. Gains outside of the stability region due to foot lift-off produce non-physiological, oscillatory motion of the center-of-mass, which require the feet to pull up on the ground. Physiological trajectories shown in the gray shaded region were close to critically-damped and did not violate foot lift-off constraints.

resulted in more physiological looking trajectories and removed highly oscillatory center-of-mass responses.

2.3.3.2 Stable gain space decreased as perturbation magnitude increased

Restricting stable hip joint feedback gains to those that produced simulations with feet-on-ground behavior when the model was subjected to a finite perturbation resulted in a reduction in the stable boundaries. Infinitesimally small perturbations resulted in feet-on-ground behavior for all feedback gain values determined from the analytic stable boundaries. However, as perturbation acceleration magnitude increased the set of stable gains associated with feet-on-ground behavior was reduced (Figure 2.4A). The gain space area of feet-on-ground behavior for a perturbation acceleration of 0.45 g and S/W=1.0 was reduced by 96%.

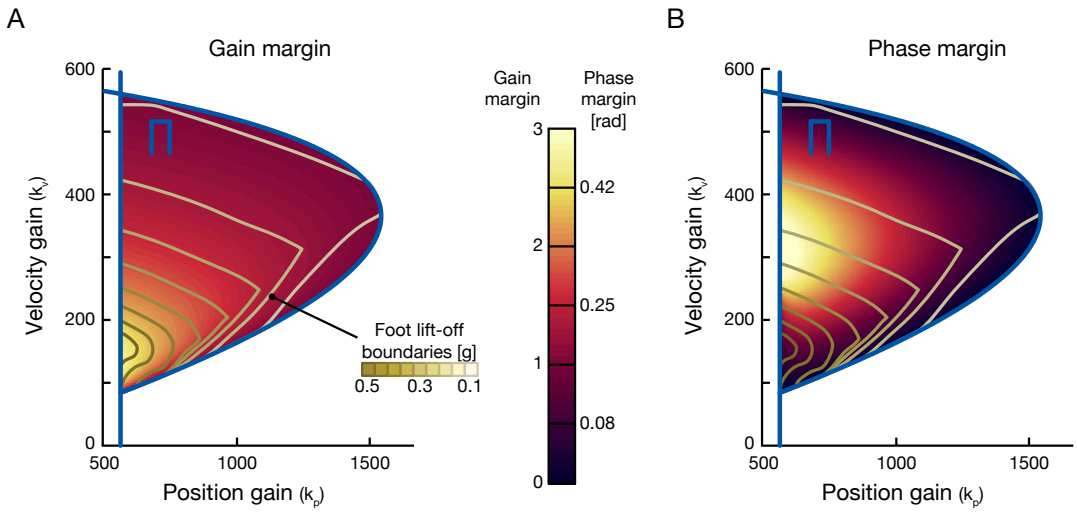

Figure 2.5: Comparison of simulated stepping boundaries and analytic measures of relative stability. For a nominal human (70 kg, 1.8m) with a stance ratio of 1.0, heavy outer lines are stability boundaries, light lines delineate non-stepping boundaries for different perturbations derived from simulations (see Figure 2.4). Shaded gradient represents the magnitude of the analytic measures A) gain margin and B) phase margin.

2.3.3.3 Gain margin predicted simulated foot lift-off threshold

Similar foot lift-off thresholds were predicted from full nonlinear simulations as well as from the gain margin of the linearized system (Figure 2.5A). From simulations, the right-hand stability boundary associated with delayed feedback and feet-on-ground behavior decreased in size as perturbation magnitude increased, while the left-hand boundary remained constant. As perturbation magnitude increased, this boundary decreased until no feedback gains were stable. The analytic measure of gain margin was found to increase as feedback gain decreased to the lower limits of position and velocity (Figure 2.5A). A gain margin greater than 6 times the perturbation magnitude was capable of predicting stable feet-on-ground responses. The phase margin increased as position feedback decreased and velocity feedback was near the middle of its range (Figure 2.5B). Gain and phase margin were found to be identical for both hip joint and center-of-mass excursion feedback.

2.3.3.4 *Experimental feedback gain decreased as stance width increased*

The full nonlinear simulated center-of-mass trajectories fit using hip feedback gains matched the experimental trajectories with an average root-mean-square error of 8.00± 2.82 mm (r^2 = 0.97± 0.02) across all subjects and trials (Figure 2.6). The position and velocity feedback gains necessary to fit the center-of-mass trajectories were found to both decrease as stance width increased (Figure 2.7A and 2.7B). The fits using center-of-mass excursion feedback resulted in nearly identical fits to those calculated using hip joint feedback, and these gains were related closely by a fixed configuration dependent ratio. Feedback gains were found to scale proportionally together with stance width at a ratio where position gain was approximately 3.6 times velocity gain, see slope of line in Figure 2.7C. Finally, the fitted feedback gains were found to have a gain margin larger than 1.5 (Figure 2.8).

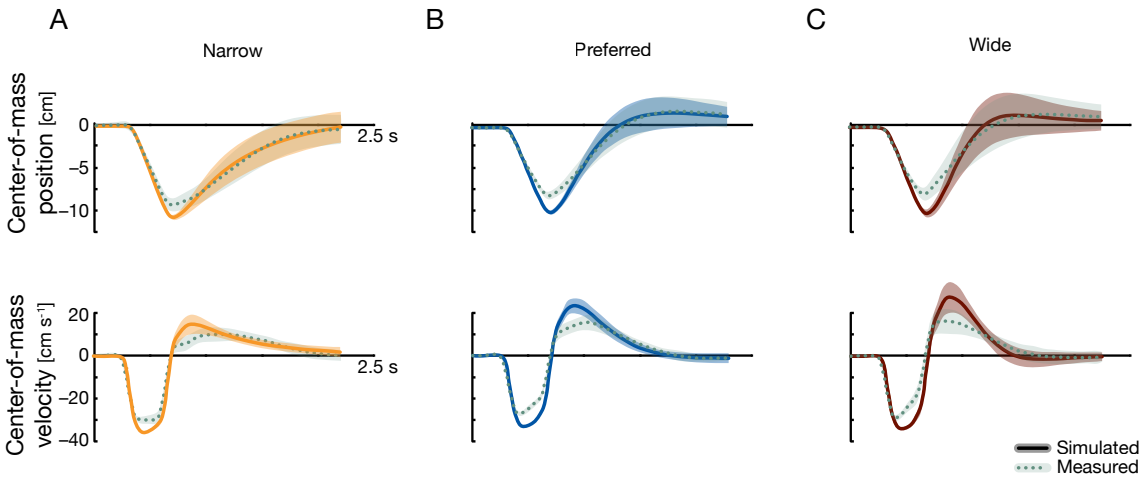

Figure 2.6: Comparison of model trajectories fit to experimentally measured center-of-mass kinematics with respect to subjects' feet across stance widths. Lines represent average behavior across all subject trials and shaded regions the standard deviation. Solid lines are simulation and dotted lines are experiments. Center-of-mass kinematics are similar in shape and maximum excursion across A) narrow (stance width = 10 cm) B) preferred (19 cm) and C) wide (32 cm).

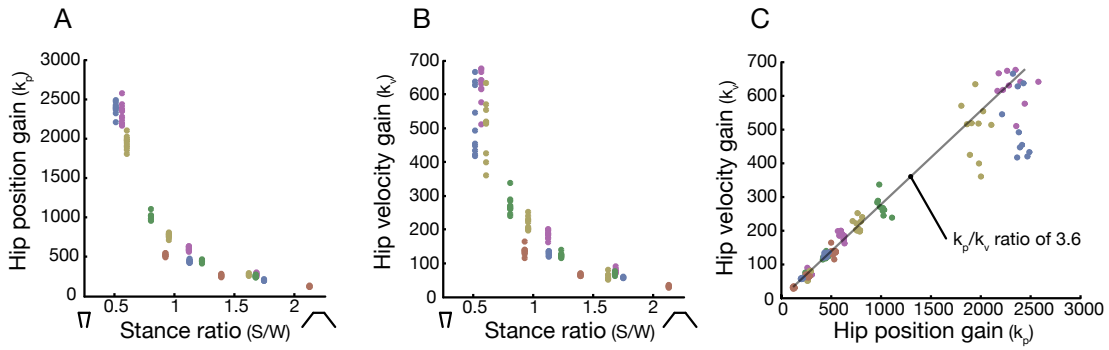

Figure 2.7: Changes in subject feedback gains with stance width. Trial by trial variation in the position and velocity feedback gains of the model matched the measured center-of-mass trajectories across subjects. Feedback gains for A) position and B) velocity were similar across subjects and variability decreased as stance width increased. C) The ratio of position to velocity feedback gain (k_p/k_v=3.6) was consistent across subjects and stance widths.

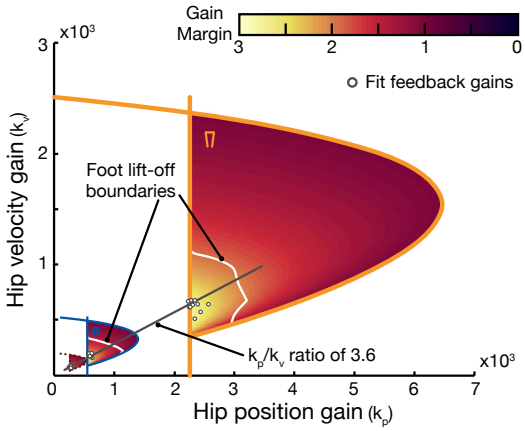

Figure 2.8: Subject feedback gains overlaid on simulated stepping boundaries and gain margin. For a representative subject the stability boundaries for narrow (thick), preferred (thin) and wide (dotted) are plotted with a gradient representing gain margin. The simulated foot lift-off boundary (white line) closely matched a lower bound on gain margin of 1.85. The white dots show the location of fitted feedback gains that lie within the stable boundaries.

2.4 Discussion

The seemingly simple act of increasing one's stance width requires that the nervous system appropriately alter delayed sensorimotor feedback gains due to the reduced torque required for stability at wider stance widths. Contrary to intuition, biomechanical stability decreases at wider stances due to the reduction in rotational inertia, while the destabilizing gravitational moment remains nearly constant. Without neuromuscular involvement, a wide stance is less stable than a narrow stance. The changes in the biomechanical properties of the body result in increased leverage and sensitivity of center-of-mass motion to changes in hip torque at wide stance. Maintaining the same center-of-mass motion in response to perturbations requires less hip torque at wide stance than at narrow stance. This prediction is consistent with observations that muscle activity from postural responses decreases with increasing stance width [132, 39]. However, in order to achieve appropriate levels of stabilizing torque with delayed sensorimotor feedback, a decrease in gain is required as stance width increases. Therefore, feedback gains that are stable for a narrow stance width are unstable for a wide stance width (Figure 2.3A). Thus, to maintain postural stability, the nervous system must rapidly adjust the magnitude of feedback gains appropriate for a selected postural configuration.

2.4.1 Implications of delayed feedback, stance width and foot lift-off for balance control

Our model demonstrates that neural strategies for human postural control are constrained by physiological delays associated with the transmission of sensory and motor signals. Neuromechanical delays in healthy humans are relatively long, typically 150 ms for postural responses, which constrain the rapidity that neural feedback systems can affect body dynamics [48]. Delays result in upper bounds for feedback gains, as large gain magnitudes lead to instability [120]. Furthermore, as delays increase, the upper boundary and the set of stable feedback gains decreases [116, 109, 100, 75]. The inclusion of delay in postural control models is thus necessary to appropriately predict the set of stable feedback gains for standing balance control [99, 82, 75, 138]. In contrast, feedback models that omit physiological time

delays [95, 65] would not identify the upper limits for feedback gains. The lack of an upper limit on allowable feedback gains could lead to the incorrect conclusion that a single set of gains would be sufficient for stability across different stance widths. Furthermore, H.S. Black's original concept of high-gain negative feedback may produce the unintended consequence that the control completely masks the underlying system dynamics [8]. In contrast, biological systems tend to leverage the intrinsic biomechanical characteristics suitable for a desired behavior. Evidence of the importance of biomechanics in neural control is exemplified by passive dynamic walkers [79], resonance of feeding apparatus in aplysia [154] and multi-leg interaction in cockroaches running over rough terrain [118]. Neglecting neural delay allows the application of high gain feedback that is likely non-physiological and may result in incorrect interpretations of closed loop stability.

The set of feasible feedback gains are further constrained by the functional limits of foot lift-off. Utilizing a foot lift-off criterion is important when identifying functional limits of stability. Many studies utilize an inverted pendulum to model postural control, as the second order dynamics and gravitational instability capture the characteristics of observed center-of-mass motion [150, 99, 94, 82, 75, 70, 69]. However, the simplicity of the inverted pendulum lacks straightforward methods for implementing realistic ground contact and determining the effects of configuration. Pendulum models alone may overestimate stability boundaries for a specific perturbation magnitude. Pai and Patton have addressed foot lift-off in sagittal plane models by imposing limitations on the amount of allowable torque at the base joint [93, 94]. Foot lift-off in our four-bar linkage model utilizes the dynamics of the body and the nonlinear ground contact force, regardless of a subject's strength. Using the four-bar linkage model may allow decoupling of muscle strength and skeletal dynamics effects for both sagittal and frontal plane studies. The four-bar linkage model could be readily adapted to sagittal plane analyses by setting the hip and stance width to the length of the foot.

Foot lift-off for a specified perturbation to the model can be estimated by an analytic measure of relative stability, gain margin. Relative stability allows for comparing stability under different conditions, which has been accomplished with numerical methods in previous research [97]. Calculation of the gain margin does not require computationally costly

simulations to quantify relative stability. Gain margin is a distance from the critically stable gain. For symmetric initial conditions, the gain margin for a set of feedback gains matches favorably with the stepping boundaries found through forward simulations of the four-bar linkage. Feedback gains with a higher gain margin can withstand larger perturbations. Feedback gains with common gain margin across stance widths lie on a line (Figure 2.8). This suggests that position and velocity feedback gains can be scaled by a single parameter as stance width changes to maintain similar body dynamics. This may be a general principle of neural control for balance, as sagittal plane models also show proportional scaling of position and velocity feedback gains due to sensory re-weighting [99]. Furthermore, feedback gains fit to experimental data show that, despite changes in feedback gain magnitudes, individuals utilize feedback gains with a common gain margin across stance widths. Common gain margin across stance widths suggests neural feedback control is modulated to maintain a consistent level of stability, which may explain the consistency of center-of-mass trajectories across stance widths [39].

2.4.2 Modeling assumptions and limitations

The relative stability of feedback gains would increase with the addition of passive, non-delayed stiffness and damping, but would not alter the primary result that delayed feedback gains must decrease as stance width increases. Without explicit intrinsic stiffness elements, our model is unable to identify stability conferred by muscle co-contraction when fit to experimental data [30]. Since non-delayed stiffness and damping produce a stabilizing effect [46], our model may result in a conservative estimate of delayed feedback gains. However, the relative contribution of non-delayed components to the stability of standing balance is likely small. Seminal work on ankle stiffness in seated subjects performing dorsi-plantar flexion reported values of 1.75 N-m/deg (100 N-m/rad) during passive behavior and up to 17.5 N-m/deg (1000 N-m/rad) during active behavior [144]. The order of magnitude difference between passive and active stiffness has also been reported in postural tasks. Specifically, sagittal plane models of postural control have demonstrated that non-delayed feedback is ten times smaller than delayed feedback during standing: 1.6 N-m/deg (92 N-m/rad) versus 16.9 N-m/deg (968

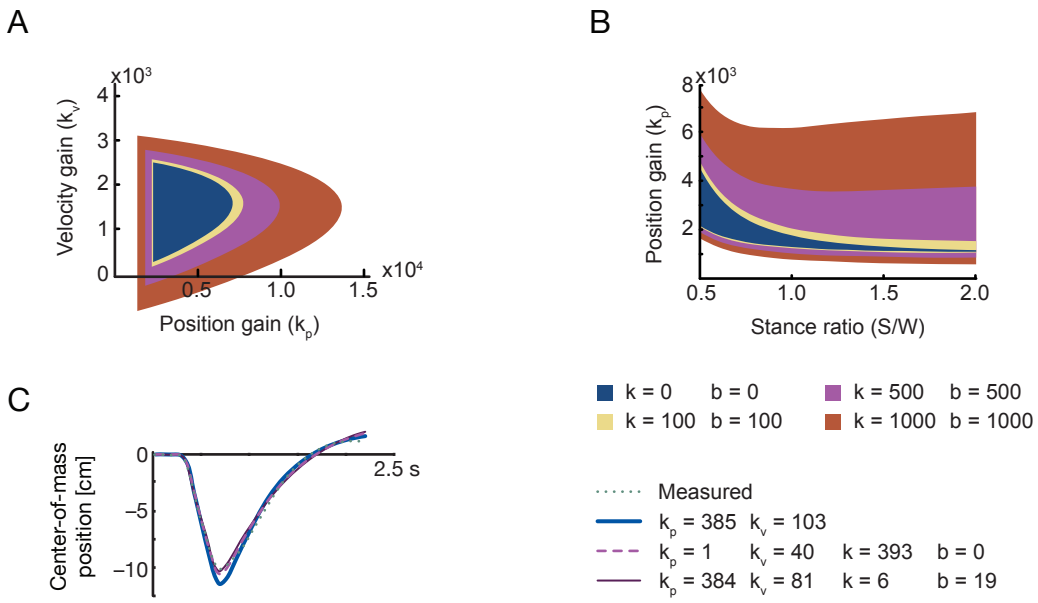

Figure 2.9: Effect of non-delayed position and velocity feedback on stable sets of delayed feedback for a nominal human (70 kg, 1.8 m) with stance ratio of 1.0. A) Assuming physiological levels of non-delayed feedback (k=100, b=100) showed only slight increase in the allowable set of stable non-delayed feedback gains. B) Large values of non-delayed feedback (k=500, b=500) resulted in decreased non-delayed feedback gain as stance width increases. C) If non-delayed feedback is used, multiple combinations of feedback gains (dashed and solid lines) reconstructed experimental kinematics (dotted line), while only one delayed gain pair (thin line) reproduced the trajectory.

N-m/rad), respectively [70, 99]. Adding physiological quantities of non-delayed stiffness and damping to our model only slightly increased the set of possible stable delayed feedback gains (Figure 2.9A, lightest shaded area). Moreover, increasing non-delayed stiffness and damping by 10-fold greater than physiological amounts still resulted in the sets of stable delayed feedback gains decreasing as stance width increased (Figure 2.9B). Therefore, the addition of non-delayed elements does not alter the fundamental finding that delayed feedback gain must decrease as stance width increases, although passive elements may relax the amount of delayed feedback modulation required for stability [128]. Furthermore, the inclusion of non-delayed feedback adds redundancy in the fitting of kinematic trajectories. When fitting two delayed feedback gains to match experimental center-of-mass trajectories only a single solution was found. However, multiple, divergent solutions were found to produce equivalent center-of-mass trajectories when non-delayed feedback components were added

(Figure 2.9C). Thus, it is not possible to distinguish the delayed and non-delayed stiffness components with our current methodologies. Muscle activity or independent measures of non-delayed stiffness and damping may be required to quantify these separate contributions. Non-delayed stiffness and damping are likely important factors to consider when analyzing pathological populations where muscle tone and muscle co-contraction are increased [23], which may emphasize the role of non-delayed feedback and reduce the contribution of delayed feedback for maintaining stability [14].

The single degree-of-freedom nature of the four-bar linkage model leads to the result that torque applied at either of the ankles or hips can be equivalently represented as a torque at the hip. Therefore, the actions of the modeled hip torque could be equally achieved by a distribution of torques at the hip and ankle joints. Our model demonstrates that frontal plane inertia decreases as stance width increases, requiring that the magnitude of torque applied at any joint must also decrease to produce the same center-of-mass motion (Figure 2.9A). Accordingly, activity in muscles producing torque at the hip and ankle is observed to scale with stance width in response to medio-lateral perturbations [39, 132]. It is likely that a large proportion of torque is produced at the hip as frontal plane peak hip torque (90 N-m) [10, 19] is significantly greater than peak ankle torque (25 N-m) [55, 62]. While peak torque is not necessarily representative of the proportion of torque produced at each joint for standing balance in sagittal perturbations [66], hip torque is further favored in frontal plane balance control because leverage effects scale hip torque proportionally with stance width but do not scale ankle torque.

Our model accounts for a majority of the center-of-mass kinematics, and may be improved by including additional degrees of freedom. By adjusting position and velocity feedback gains, center-of-mass kinematics from nonlinear simulations match experimental observations with only slight over-shoot of the maximum center-of-mass excursion (Figure 2.6). This overshoot is more pronounced in wider stances, which may be due to an inability in the model to predict correct phasing between upper and lower body movement [36]. These deviations in center-of-mass kinematics are small and the model corroborates experimental observations of peak center-of-mass excursion remaining constant across stance widths [39]. Previous modeling

studies suggest that feedback control of human muscle activity may rely on an estimate of body center-of-mass motion, rather than local joint feedback [146, 145]. This is consistent with neurophysiological evidence of global variables being encoded by the nervous system [11]. Remarkably, center-of-mass kinematics reproduced with either center-of-mass and joint feedback control were similar even though these two feedback signals are not linearly related. The similarity in kinematic output precludes using system identification to distinguish between these strategies in the four-bar linkage model. We predict that a model with flexible knees and upper-body would allow decoupling of the ankle and hip joints and potentially reveal differences in stability between center-of-mass and joint feedback control.

2.4.3 Model-based interpretation of stance width adaptation

Despite the relative simplicity of our model, it provides new insight into the interdependence between neural and biomechanical stability during balance control. The healthy nervous system may exploit different combinations of feedback gain and posture configurations to flexibly achieve balance. Choosing a wider stance width necessitates reduced torque and may be advantageous when muscle torque generation is a limiting factor. Due to increased leverage, wide stance may reduce the torque requirement during a perturbation response. However, the benefits of wide stance are countered by a reduction in maneuverability and an increase in static metabolic cost, which suggests why healthy individuals only select wide stance in unstable conditions. Further, our model suggests that the increase in sensorimotor delay associated with aging [151] should result in decreased feedback gains [2] and smaller feasible feedback gains for maintaining stability at wide stances. Another possible compensation to increased delay may be to decrease stance width, which has been observed in elderly populations [80, 124].

Changes in postural stability during and following pregnancy may be explained by our model if long-term adaptation of neural feedback to changes is slow compared to biomechanical changes in postural configuration. During pregnancy, stance width increases gradually and frontal plane sway remains consistent. However, shortly after delivery, preferred stance

width returns to pre-pregnancy width and frontal plane sway increases [54]. We hypothesize that the set-point for sensorimotor feedback gains adapt slowly to the increasing stance width over the course of pregnancy. The decrease in stability postpartum may be due to using low feedback gains appropriate for wide stance at the preferred stance width, generating a transient aftereffect [112] of instability while the neural gains must readapt to the preferred configuration.

The adoption of a narrow stance in Parkinson's patients may be a compensatory strategy for the inflexibility in adapting to the biomechanical context of movement. Damage to the basal ganglia may impair the ability to modify postural muscle responses in response to changing postural configurations. Parkinson's subjects can maintain balance to postural perturbation when standing, but persist in activating leg muscle when subsequently seated [50]. Similarly, the muscle activity evoked during standing balance perturbation responses are not modulated with stance width in Parkinson subjects [24]. These observations can be interpreted as an inability to adjust feedback gains associated with changing biomechanical constraints [60]. Moreover, Parkinson subjects have characteristically stiff joint responses to perturbations [47]. Stiffening may be the result of increased feedback gains, which our model suggests are less stable in wide stance. Thus, patients with Parkinson's disease may select narrow stance to compensate for inflexible high gains, even though it may require greater muscle activity.

Predictions from our model should be interpreted as system level phenomena and finer grained analysis should "anchor" our "template" in a more detailed model [31]. Our model does not speak to the physiological location of where sensorimotor feedback gain changes occur. However, others have shown that sensorimotor feedback pathways for balance control involve the brainstem [21, 71] with cortical influences [53]. Intrinsic muscular or neural properties may also contribute to sensorimotor gain changes. For example, muscle torque production can be affected by moment arms [155], muscle length [51] or motoneuron gain [52] due to changes in configuration. Observations of muscle co-contraction in many neurological populations [9, 23] may be explained by expanding our model to include passive stiffness to quantify the contribution of co-contraction to postural balance stability. Predictions from

this model may be used to guide future experimental research about motor variability, motor adaptation, energetic efficiency and functional stability of standing balance.

2.4.4 Is wide stance more stable?

Conventional wisdom suggests that wide stance is more stable, as intuition is to widen one's stance width when situations become more challenging. Our model demonstrates that the increase in stance width allows for larger center-of-mass excursions before a step is necessary. Furthermore, mechanical leverage at the hip is increased, allowing greater torque generation about the center of mass. A wider stance thus lessens the muscular effort required for balance control, improving the stability of the subject in the presence of a perturbation. However, our results demonstrate that this increase in functional stability is only possible when accompanied by appropriately scaled delayed neural feedback. The same mechanical effects that allow for reduced effort and larger responses to perturbations in wide stance also increase the inherent instability of the musculoskeletal system and limit the set of feasible stable feedback gains at wide stance. Thus, an impaired nervous system may not be able to exploit the intuitive benefits of wide stance due to increased neural delay, improper context-dependent modulation or increased sensorimotor noise. The perception of increased stability at wide stance is not simply due to changes in the biomechanics of the body, but predicated on the requisite flexibility of neural mechanisms controlling balance.

CHAPTER III

NEUROMECHANICAL FACTORS THAT AFFECT THE TIMING OF BALANCE RESPONSES

3.1 Introduction

Although medial-lateral stability in balance is reduced with age, the underlying mechanisms of the instability are not well understood. Changes in stability are likely the cause of increased fall risk and this has a drastic effect on quality of life, as the leading cause of morbidity for elderly adults in the USA is from falls [15]. It has been suggested that the mechanisms for decreased stability in the elderly is due to changes in posture and deficits to neural control. Delays associated with muscle responses to perturbations and time to peak joint torque have been shown to increase as individuals age [20, 151, 153]. Furthermore, it is observed that elderly subjects, particularly those prone to fall, stand with stance width decreased by 9% [124, 80]. However, it is unclear how changes in neural delay, feedback gain and stance width are interrelated and contribute to reduced postural stability.

Physiological delays are significant during postural control and can limit the range of feedback gains that generate stability. In healthy young individuals, active responses in muscles that restore the body center-of-mass occur at a latency of about 100 ms, and the resulting musculoskeletal forces are further delayed by 50 ms due to the time course associated with muscle force production and transmission [48]. This substantial delay has been suggested to lengthen in elderly populations during perturbations to anterior/posterior balance where peak torque generation was delayed (up to 20 ms) due to prolonged neural delays that led to increased latency of muscular responses [2, 151, 153]. These subtle changes in

delay may have significant consequences on stability since delay limits the maximum magnitude of sensorimotor feedback gain, with longer latencies reducing the set of feasible gains [75, 100].

Changes in postural configuration may also affect stability, and may be driven by changes in neural feedback gains. Previously, we have shown that covariation between stance width and feedback gains is necessary for stable standing balance [7]. Decreased stance width, as observed in elderly populations, requires increased neural feedback gains. Neural feedback gains from model fits to data from rotation perturbations were greater by 30% in older subject groups, but the time to peak torque was not explored [16]. Also, increased feedback gain may be limited by lengthened neural delays, thus imposing limitations on the generation of joint torque and stability of standing balance.

Therefore, to investigate the possible mechanisms leading to reduced medial-lateral stability from possible effects caused by aging, we tested how neural delay, feedback gains and stance width alter time to peak torque in a frontal-plane model of standing balance [7]. We hypothesized that, in addition to neural delay and feedback gains, stance width can affect time to peak torque. We predicted that feedback delay, stance width, and feedback gains can each affect the time to peak torque and effects of one factor on time to peak torque can be compensated by the remaining factors.

3.2 Methods

3.2.1 Model predictions

A previously developed model of frontal plane stability was used to model the medial-lateral center-of-mass response to step changes in hip torque (see Appendix A) [7]. The dynamics of medial-lateral stance were modeled by a four-bar linkage with delayed feedback having nominal anthropometric parameters based on a human subject with height of 1.8 m and mass of 70 kg. The hip width and stance width were set equal at a distance of 24 cm. The neural feedback control was set with a delay of 120 ms and the feedback gains were set at 673 N-m/rad for position and 224 N-m/rad/s for velocity.

The response to an external perturbation was used to quantify the effects of delay, stance

width and feedback gain on the time to peak torque. The perturbation was applied as a square pulse of external torque applied to the hip (1 kN-m for 5 ms). This perturbation was selected to approximate the CoM acceleration observed from a standard platform translation [7, 145], while providing an analytically simple input for the mode.

The response to the perturbation was quantified by the time between perturbation onset and the time to reach peak hip torque. Responses were simulated for multiple conditions where one parameter was varied while all other parameters of the model were held at their nominal values. Feedback delay was varied over the range of 80 to 160 ms in 2 ms intervals. Stance width was varied over stance ratios (stance width/hip width) of 0.9 to 1.1 in increments of 0.01. Feedback gains for position were varied over the range of 600 to 900 N-m/rad for position and 160 to 280 N-m/rad/s for velocity in increments of 5 N-m/rad and 2 N-m/rad/s, respectively.

3.2.2 Pilot data and model fits

In order to compare simulated and experimental results, body segment kinematics were collected from healthy human subjects during platform perturbations. All protocols were approved by the Georgia Tech and Emory University Institutional Review Boards and conformed to the Declaration of Helsinki. Thirteen subjects (7 male, 6 female, 23-62 years of age) were recruited. Groups were divided into older and younger categories at 40 years of age and narrow and wide categories at a stance ratio of 1.0.

Subjects stood with arms crossed and their feet spaced at the subjects' own self selected distance. Each foot was located on an individual calibrated force plate (AMTI, Watertown, MA) that recorded all six reaction forces and moments. Subjects were instructed to stand upright and to maintain balance during perturbations, but were not given information about time of perturbation onset. Perturbations were administered with a custom platform (Factory Automation Systems, Atlanta, GA) with position and acceleration of the platform recorded. Subjects received 5 ramp-and-hold platform perturbations in the medial-lateral direction with the platform moving to the subject's left or right. The perturbations had an overall movement distance of 12 cm, a plateau velocity of 35 cm/s and a peak acceleration of 0.5 g.

Subject kinematics were captured with a custom 26-marker set that included head-arms-trunk, thigh, shank, and foot segments using a motion capture system (Vicon, Oxford, UK) utilizing 8 cameras. Motion capture was sampled at 120 Hz and platform kinematics at 1080 Hz. Platform kinematics were low-pass filtered at 30 Hz (third-order zero-lag Butterworth filter) and combined with motion capture kinematics to produce relative position, velocity and acceleration of the markers with respect to the platform. The relative motion of the markers and a proportional model of human mass were used to calculate center-of-mass position, velocity and acceleration for each subject [148].

Using the model, simulated center-of-mass position was fit to experimental data through optimization of the feedback gains for the non-linear equations-of-motion. Each experimental trial was fit using the subject's measured mass, height, stance width and perturbation acceleration profile. For a given subject and stance width, model parameters were fixed and only feedback gain values were allowed to vary. Optimization to solve for the feedback gains utilized a cost function defined by the difference between simulated and experimental center-of-mass trajectories with penalties on the sum of absolute (weight of 1) and sum-squared error (weight of 10).

3.3 Results

3.3.1 Model predictions

3.3.1.1 Increased feedback delay lengthens time to peak torque

Increasing the delay in feedback resulted in a multiplicative increase in time to peak torque (Figure 3.1). Increasing feedback delay by 6 ms caused a lengthening of 20 ms in time to peak torque. Increasing delay also caused an increase in the magnitude of peak torque of approximately 2% for each additional 10 ms. Furthermore, increasing the delay limited the maximum feedback gain magnitude and the maximum stance width for stable behavior. The multiplicative increase in time predicted that any increase in feedback delay would result in a two-fold increase in additional time to peak torque.

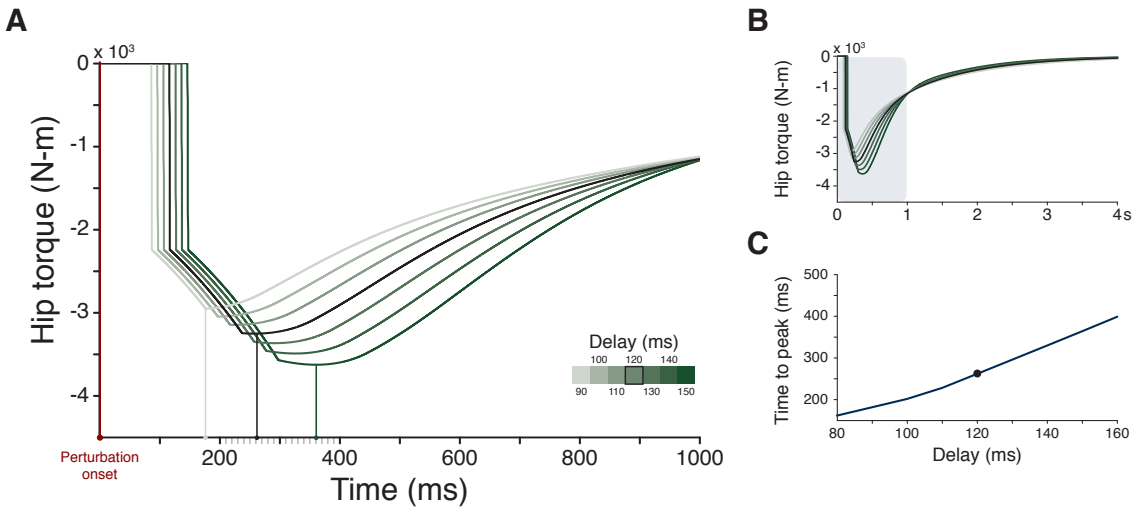

Figure 3.1: Increased feedback delay increase increased the time to peak torque. A) Increased magnitude and time to peak torque are shown in the torque response. B) Shaded region shows range of time course in previous detailed view. C) Time to peak torque scales linearly with increased feedback delay at a ratio of roughly two.

3.3.1.2 Decreased stance width lengthens time to peak torque

Changes in stance width affected both leverage and inertia of the model (chapter 2: Figure 2.2), which caused significant changes to torque responses [7]. Decreasing the stance width by 0.5 cm caused a lengthening of 20 ms in time to peak torque and a decrease in the magnitude of peak torque (Figure 3.2). Conversely, increasing the stance width increased the magnitude of peak torque and decreased the time to peak torque up to a minimum time that was twice the feedback delay. Increasing stance width also limited the maximum feedback gain for stable behavior. It was predicted that the most significant effect to time to peak torque would be caused by a decrease in stance width.

3.3.1.3 Increased position feedback gain lengthens time to peak torque

Increasing delayed position feedback gain by 50 N-m/rad caused a lengthening of 20 ms in time to peak torque and a decrease in the magnitude of peak torque (Figure 3.3). In addition, increasing the delayed position feedback gain resulted in a longer settling time for the torque response. Furthermore, it was found that position feedback gain can only compensate for a feedback delay increase of 30 ms. It was predicted that increases in position feedback gain would result in lengthened time to peak torque with larger magnitude.

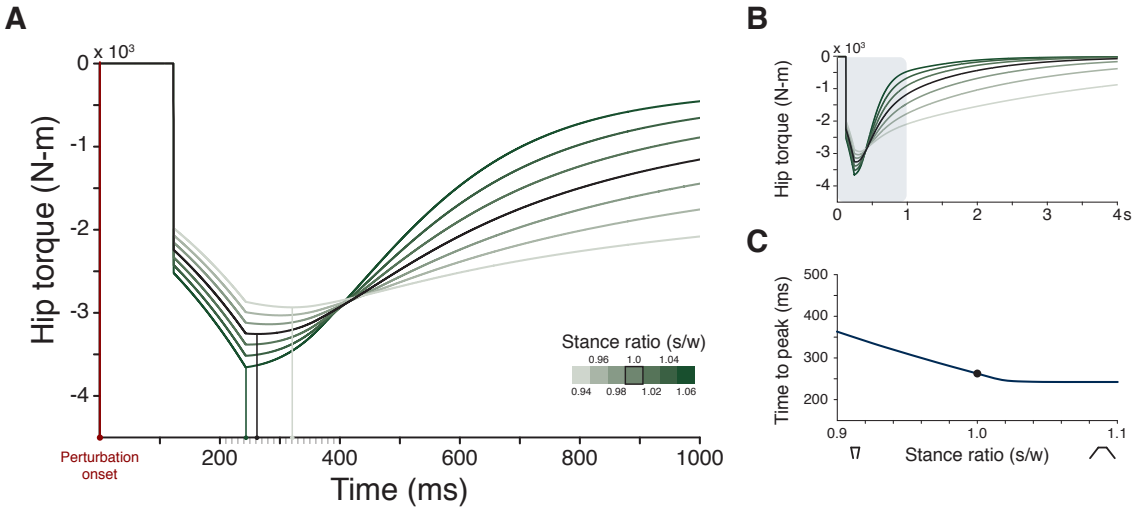

Figure 3.2: Decreased stance width increased the time to peak torque. A) Increased magnitude and time to peak torque are shown in the torque response. B) Shaded region shows range of time course in previous detailed view. C) Decreasing stance width resulted in increased time to peak torque, but increasing stance width had little affect on time to peak torque.

3.3.1.4 Decreased velocity feedback gain lengthens time to peak torque

Decreasing delayed velocity feedback gain by 10 N-m/rad/s caused a lengthening of 20 ms in time to peak torque and a decrease in the magnitude of peak torque (Figure 3.4). Time to peak torque could be decreased by increasing velocity feedback up to a minimum time that was twice the feedback delay. Increasing velocity feedback gain also resulted in much smoother torque responses with greater oscillation and longer settling times. It was predicted that increases in velocity feedback gain would decrease the time to peak torque, but increase the magnitude of the response.

3.3.2 Experimental observations

3.3.2.1 Differences in stance width and time to peak torque were observed across age

Subjects' had a varied range of possible stance widths ranging from less than hip width to slightly wider than shoulder width (Figure 3.5A). On average, older subjects selected a narrower stance width (S/W = 1.05±0.21) in comparison to the younger cohort (S/W = 1.44±0.18). Also, older subjects reached peak torque faster with an average time to peak torque of 459±166 ms in comparison to the younger group that took 687±192 ms (Figure 3.5B).

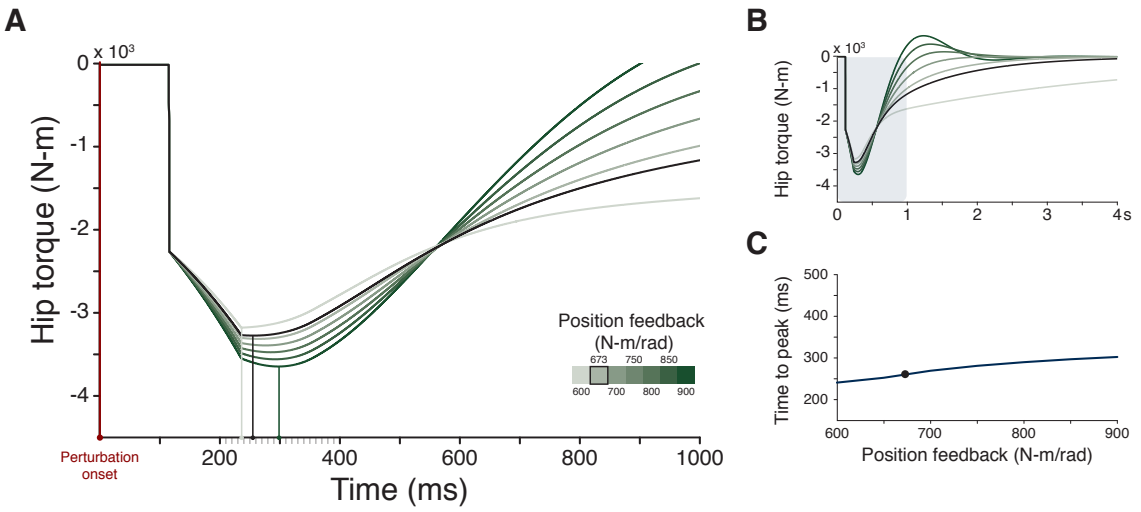

Figure 3.3: Increased position feedback gain increased the time to peak torque. A) Increased magnitude and time to peak torque are shown in the torque response. B) Later response is significantly affected by increasing position feedback gain causing larger oscillation. Shaded region shows range of time course in previous detailed view. C) Time to peak torque scales slightly with increased delayed position feedback gain.

3.3.2.2 Differences in fit feedback gains were observed across age

Corresponding to the variation in stance width, the feedback gains fit to the subjects center-of-mass trajectories were also varied within and across subjects. Feedback gains for the older subjects were found to have larger magnitude where the average position feedback gain 604±215 N-m/rad was greater than 358±146 N-m/rad and the average velocity feedback gain 147±53 N-m/rad/s was greater than 69±33 N-m/rad/s.

3.3.2.3 Time to peak torque was longer for wide stance width subjects

There was a large variation in time to peak torque within and across stance widths indicating stance width was not the sole contribution to changes in time to peak torque. Older subjects had a trend towards shorter time to peak torque (Figure 3.7A). Also, time to peak torque was in general shorter for narrow stance widths (S/W $\leq$ 1.0) at 473±156 ms over wider stance widths (S/W $>$ 1.0) at 565±221 ms. This was the opposite trend predicted from the model (Figure 3.2C).

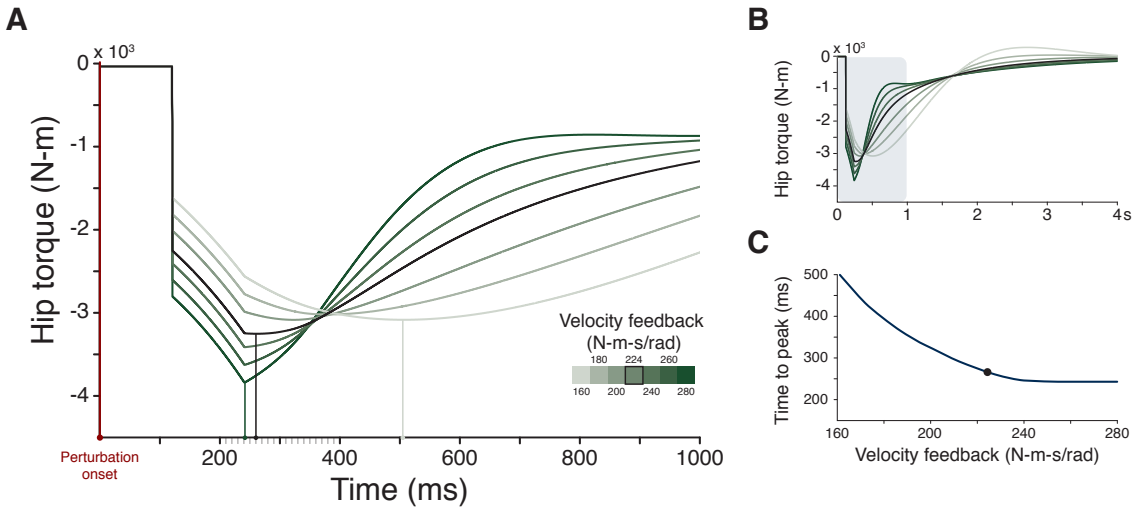

Figure 3.4: Decreased velocity feedback gain increased the time to peak torque. A) Time to peak torque is significantly affected by changes in velocity feedback with more subtle changes to peak magnitude. B) The shape of the torque response is significantly smoothed as velocity feedback increases. Shaded region shows range of time course in previous detailed view. C) Time to peak torque decreases as a power-law up to a minimum time as velocity feedback increases.

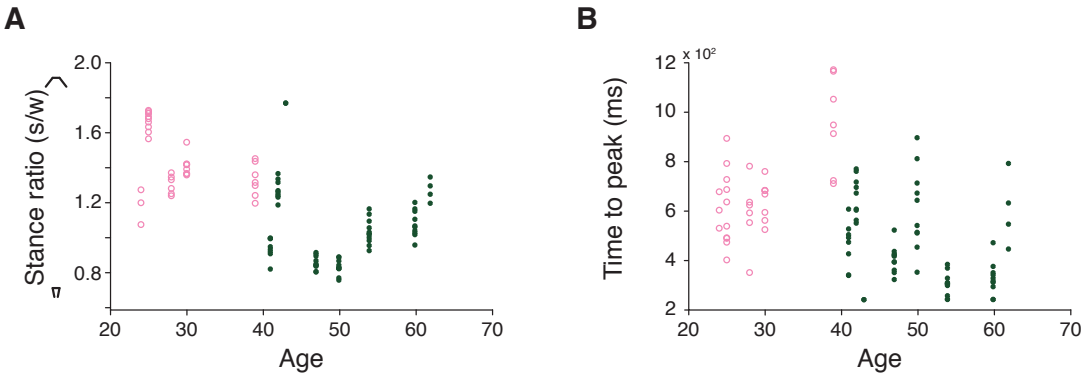

Figure 3.5: Stance width and time to peak torque change with age. A) Subjects greater than 40 years (filled circles) tended to select a narrower stance. B) Time to peak torque was found to be faster in many of the subjects in the older age group.

3.3.2.4 Differences in feedback gain across age were best explained by changes in stance width

Across age, average position feedback gain was higher for narrow (783±161 N-m/rad) than for wide (408±147 N-m/rad) stance widths (Figure 3.7B). The increased position feedback across stance width alone did not explain decreased time to peak torque at narrow stance (Figure 3.7A) based on the model prediction (Figure 3.3C).

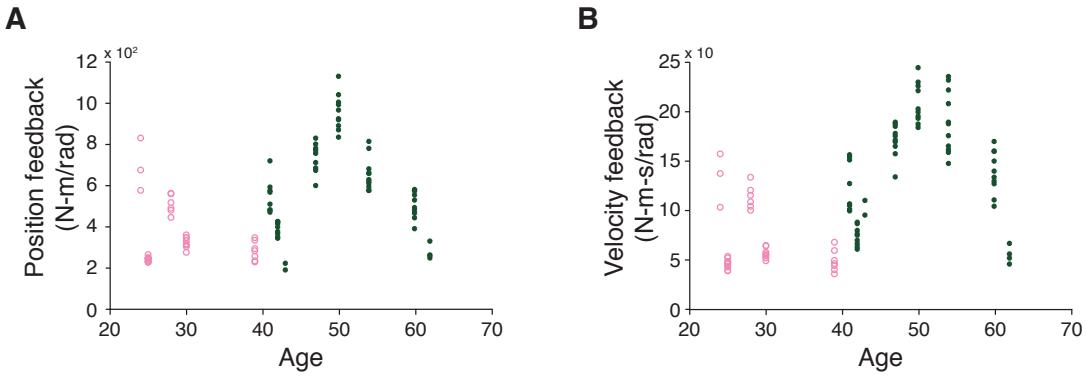

Figure 3.6: Fit feedback gains increased with age. The older age group (filled circles) had larger magnitudes for both A) position and B) velocity delayed feedback gains.

Similarly, average velocity feedback gain was higher across age for narrow (183±35 N-m/rad/s) than for wide (93±47 N-m/rad/s) stance widths (Figure 3.7C). The increased velocity feedback across stance width was consistent with decreased time to peak torque at narrow stance (Figure 3.7A) based on the model prediction (Figure 3.4C).

3.4 Discussion

Our model shows that increases in time to peak torque are not necessarily indicative of increased neural delay. Time to peak torque can be increased through many model parameters: lengthened neural delay, narrowed stance width, increased position feedback, or decreased velocity feedback (Table 3.1). Furthermore, interactions of these parameters may allow for many combinations of parameters to achieve similar time to peak torque. As a case in point, lengthening the neural delay, which has been reported to be destabilizing through over-correction [7, 100, 75], caused both an increase in time to peak torque and an increase in peak torque magnitude, which is reported for elderly subjects [2, 151, 153]. The destabilizing influence of a longer neural delay could be compensated by either increasing velocity feedback without changing stance width, or narrowing stance width without changing feedback gains.

Compensating interaction between biomechanical factors like stance width and neural

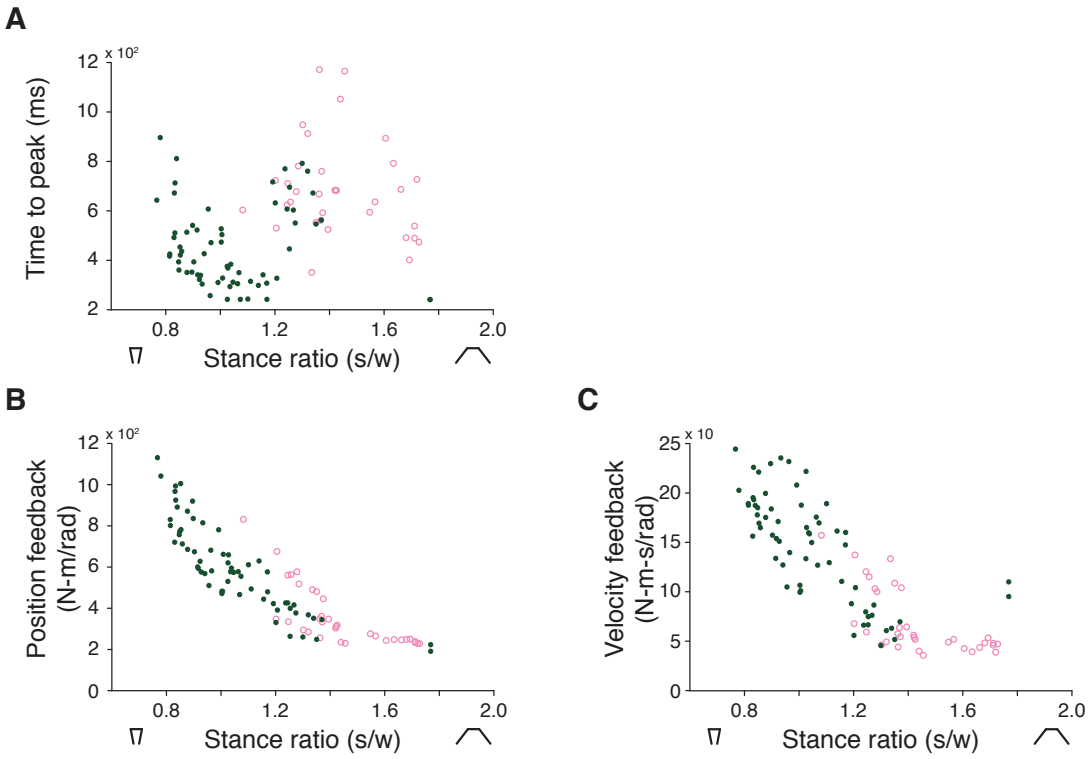

Figure 3.7: Stance width was associated with changes in time to peak torque and feedback gains. A) Older subjects (filled circles) did not necessarily have longer time to peak torque, but subjects with wider stance width did. B) Position and C) velocity feedback decreased as stance width increased across age.

factors like neural feedback control may afford consistent behavior when either the biomechanics or nervous system is compromised. Our pilot data highlighted a perplexing phenomenon, corroborating observations in literature [124, 80], that the average stance width of decreases as subjects age. Why would an individual select narrowed stance width, which was predicted to increase the time to peak torque (Figure 3.1)? Interestingly our pilot experimental data showed that older subjects actually responded with a shorter time to peak torque (Figure 3.5B) despite an observed decrease in stance width; however, this was also

Table 3.1: Summary of parameter effects on time to peak torque.

Increasing parameter	Effect on time to peak torque
Feedback delay	↑ increased
Stance width	↓ decreased
Position feedback	↑ increased
Velocity feedback	↓ decreased

associated with increased velocity feedback (Figure 3.6B). Our previous work has shown that to maintain stability in frontal plane standing balance, stable feedback gain boundaries increase as stance width decreases [7]. Decreasing stance width may allow for larger velocity feedback gains that decrease time to peak torque while maintaining stability. Larger velocity feedback gains that significantly shorten time to peak torque may then justify the delay resulting from decreased stance width. Therefore, to maintain stability in the presence of lengthened neural delay, elderly subjects may reduce stance width and increase feedback gains as a compensatory strategy.

Time to peak torque is likely an important measure of postural performance, but it may be limited by stability considerations. Thus, the variety of stance width and feedback gain combinations observed in our pilot data may be due to trade-offs between performance and stability. Due to the possible complex interaction between neural and biomechanical factors, this raises interesting questions pertaining to previous results that suggest the electromechanical delay is lengthened as we age [20, 151, 153]. The changes in observed lengthening of electromechanical delay may be further confused with contraindications of reduced strength and changes in muscle physiology. These differences are important to isolate as they may suggest directions of rehabilitation for patients who are at risk of falling. In some cases, muscle strengthening may be useful while in others changes in posture may be most useful. Furthermore, training for performance may be at odds with maximizing the stability of a particular individual. This study proposes that performance, time to peak torque, can be attained by compensatory trade-offs in neural and biomechanical factors; however, changes in stability were not addressed. Since the pilot data does not suggest significant differences in performance, but shows trends in differences of biomechanical and neural factors it suggests that it may be important to investigate possible changes in stability introduced by these alterations in neuromechanics with age.

CHAPTER IV

STABILITY RADIUS AS A METHOD TO COMPARE NEUROMECHANICAL SYSTEMS

4.1 Introduction

Biological systems are composed of many complex, interacting components and as Aristotle remarked over two millennia ago *"... the whole is something beside the parts."* Even with sophisticated computational models, behaviors resulting from such interactions are difficult to analyze and compare using tools from classical control theory that divide a system's dynamics into components that are to be controlled (plant) and those that are added to achieve a desired behavior (controller). For example, neuromechanical models of human movement contain redundant biomechanical and inherently delayed neural feedback control components that can change concurrently in order to achieve a desired behavior. Unfortunately, classical stability analysis tools, such as gain margin[26], cannot be used to compare behavior across neuromechanical conditions where both biomechanics (plant) and neural control (controller) change during a task. To overcome these challenges we introduce the technique of stability radius, an approach that builds upon eigenvalue analysis as a compact representation of dynamical behavior.

The technique of stability radius is useful for identifying different sets of parameter values that can produce similar behaviors, or quantifying the sensitivity of a system's stability to parameter changes. The mathematical theory is derived from the fields of pseudospectral analysis [44, 134] and robust control [41, 74]. Initially developed for linear time invariant systems, it has been expanded to systems with feedback delays [142, 84, 85]. Many techniques for stability analysis, such as Lyapunov's indirect method, utilize eigenvalues to classify the

stability of dynamical behavior. However, the eigenvalues by themselves do not indicate sensitivity of stability to perturbations, modeling errors or parameter changes. Furthermore, it may be difficult to calculate eigenvalues for some systems, e.g. delayed systems having an infinite number of eigenvalues. Instead of using eigenvalues directly to characterize stability, the stability radius gives a scalar measure of the smallest change to any system parameter that would result in instability. This provides a single measure to compare stability of one system against itself as parameters change, as well as against entirely different systems. Stability radius can also be used to test the sensitivity of system stability to model parameters. This single number can be used to classify a system's dynamical behavior on a relative scale of stability and to predict system responses across different modeling conditions.

Given these characteristics, stability radius may be well suited to quantify changes in stability due to changes in biomechanical and neural feedback parameters in neuromechanical systems. Neuromechanical systems in different biomechanical contexts can achieve similar motor performance by altering biomechanical configuration, neural strategy, or both [127]. Experiments in the upper extremity suggest that changes in biomechanical configuration and neural control are the result of a neural strategy to maximize stability in the presence of a disturbance [111, 135, 103]. Here, our application of the stability radius to the control of frontal-plane balance control is motivated by the experimental observation that subjects respond to support surface translations in the frontal-plane with nearly identical center-of-mass motion regardless of their stance width [39]; however, muscle activity is observed to decrease as stance width increases, demonstrating a concurrent change in neural control [39, 133, 132]. We propose that the similar behavior observed across stance widths during standing balance may be the result of a neural strategy to select feedback gains that maximize stability for a given stance width. Previously, we developed a model of frontal-plane balance that demonstrated increasing stance width necessitates decreasing delayed feedback gains to maintain stability [7]. However, using classical stability analysis we were not able to compare stability across biomechanical contexts and could not quantify the contribution of neural versus biomechanical parameters in achieving a given behavior. This was because traditional tools to compare stability, such as gain margin, are formulated based on the premise

that the stability of the plant, or musculoskeletal system in our case, is fixed and only alterations to control affect stability.

Here we present the theoretical background and context to introduce the stability radius technique for a linearized system with and without delays. Next, we apply this technique to our frontal-plane model of balance control [7] to illustrate its utility in characterizing changes in stability from different delayed feedback gains (controller parameters) and stance widths (plant parameters). We use stability radius to identify feedback gains that produce either maximum stability or similar performance across stance widths, i.e. postural configurations. We show that model feedback parameters that have the same stability radius across postural configurations also produce similar trajectories in simulations. The stability radius therefore predicts how neural control and biomechanical parameters interact to produce a desired behavior.

4.2 Theory

We introduce stability radius as a robust measure of the sensitivity of a system's asymptotic stability to parameter changes. Starting with the linearized equations of motion we provide a brief overview of how to identify the characteristic equation and the eigenvalues for non-delayed and delayed systems. Next, we introduce ϵ-pseudospectra as a method to analyze the sensitivity of eigenvalues to parameter changes. Finally, we connect the concepts of stability and ϵ-pseudospectra to give a definition of stability radius.

4.2.1 Characteristic equation

Here we show how to generate a characteristic equation for a large class of ordinary differential equations (ODEs) with delays. We start our discussion assuming the dynamic equations are linear and first-order. This can be achieved for nonlinear systems by linearizing the ODE about an equilibrium point using Taylor-series expansion and converting higher-order linear ODEs into a system of first-order ODEs [123]. We first show how to generate the characteristic equation for a linear system of first-order ODEs without delays and then expand this to delayed systems of the retarded type.

A system of linear, constant-coefficient, first-order ODEs can be described with a system

matrix, A, and state vector, $\mathbf{x}$.

$$\frac{d}{dt}\mathbf{x}(t) + \mathsf{A}\mathbf{x}(t) = 0 \tag{4.1}$$

The deterministic solution for this system is a matrix exponential (4.2), which can be evaluated by writing the system as (4.3) where the new matrices are the result of the eigenvalue decomposition, $\mathsf{A} = \mathsf{U}\Lambda\mathsf{U}^{-1}$.

$$\mathbf{x}(t) = e^{\mathsf{A}t}\mathbf{x}_0 \tag{4.2}$$

$$\mathbf{x}(t) = \mathsf{U}e^{\Lambda t}\mathsf{U}^{-1}\mathbf{x}_0 \tag{4.3}$$

The matrix, Λ, is a diagonal matrix whose elements are the eigenvalues of the matrix, A, and are found algebraically by solving for the roots of the characteristic equation (4.4) [123].

$$\det(\mathsf{A} - \lambda\mathsf{I}) = 0 \tag{4.4}$$

A similar method can be applied to linear, constant-coefficient, delayed differential equations (DDE) of the retarded type (4.5) written in the form where the terms collected in matrix, A_k, are associated with the k-th delay, τ_k.

$$\frac{d}{dt}\mathbf{x}(t) + \mathsf{A}_0\mathbf{x}(t) + \sum_{k=1}\mathsf{A}_k\mathbf{x}(t-\tau_k) = 0 \tag{4.5}$$

The characteristic equation for the delayed system (4.6) now includes exponential terms [117]. The addition of transcendental functions results in an infinite number of solutions to this characteristic equation [152]; therefore, DDEs of this form will have an infinite number of eigenvalues.

$$\det\left(\mathsf{A}_0 + \sum_{k=1}\mathsf{A}_k e^{-\tau_k\lambda} - \lambda\mathsf{I}\right) = 0 \tag{4.6}$$

4.2.2 System stability

Eigenvalues are critical descriptors of a dynamical system's stability. We first give an overview of the definition of eigenvalues of a matrix, show how this leads to a characteristic equation and then define asymptotic stability.

The *eigenvalues* of a system are the set of complex values, $\lambda \in \mathbb{C}$, for a matrix, $\mathsf{A} \in \mathbb{C}^{n \times n}$, associated with *eigenvectors*, $\mathbf{v} \in \mathbb{C}^n \neq \mathbf{0}$, that satisfy (4.7).

$$\mathsf{A}\mathbf{v} = \lambda\mathbf{v} \tag{4.7}$$

After rewriting (4.7) we require that solutions for eigenvalues and eigenvectors non-trivially satisfy the following relation.

$$(\mathsf{A} - \lambda\mathsf{I})\mathbf{v} = \mathbf{0} \tag{4.8}$$

For (4.8) to hold and satisfy $\mathbf{v} \neq \mathbf{0}$, then the resulting matrix of $(\mathsf{A} - \lambda\mathsf{I})$ must be singular. In other words, if the inverse existed (i.e. the matrix was non-singular) then $\mathbf{v} = \mathbf{0}$, which violates the definition of the eigenvector. Thus, to ensure that the matrix is singular its determinant must be zero. This leads to the characteristic equation for a matrix, which is identical in form to the characteristic equation of an ODE (4.4).

$$\det(\mathsf{A} - \lambda\mathsf{I}) = 0 \tag{4.9}$$

In linear ODEs, with or without delays, eigenvalues are the exponential constants that define the time evolution of the system behavior. Eigenvalues with positive real part are considered unstable, because as time advances the eventual behavior of the system will tend to depart from equilibrium. Thus, asymptotic stability of a linear system is defined by all eigenvalues having strictly negative real part. Similarly, this definition of asymptotic stability may be extended to the class of non-linear ODEs with Lyapunov's Indirect Method, which states that the eigenvalues of the linearized system about an equilibrium point describe the system's stability if the eigenvalues are not identically zero [58].

4.2.3 ϵ-pseudospectra

Here we define ϵ-pseudospectra and show its relationship to eigenvalues. We give equations for calculating ϵ-pseudospectra and then describe how this gives a measure of sensitivity of eigenvalues to parameter changes.

The sensitivity of an eigenvalue to parameter change can be found by comparing eigenvalues of the original system to new eigenvalues calculated from a system with altered parameters. For a specified magnitude of parameter change there are a set of new eigenvalues,

which are displaced by some amount compared to the eigenvalues of the original system. This set of new eigenvalues (4.10) is the ϵ-pseudospectra for a corresponding set of parameter perturbations, $\mathsf{E} \in \mathbb{C}^{n \times n}$, whose magnitude is less than a specified value, ϵ. Thus, the distribution of ϵ-pseudospectra about the eigenvalue give a measure of sensitivity to a specified amount of parameter change.

$$z \in \text{eig}(\mathsf{A} + \mathsf{E}) \; with \; \|\mathsf{E}\| < \epsilon \tag{4.10}$$

An alternate definition, to avoid calculating eigenvalues directly, is to use the knowledge that the ϵ-pseudospectra are the perturbed eigenvalues, $z = \lambda + \delta$. First, consider the definition of the new eigenvalues, with normalized eigenvectors, $|\mathbf{v}| = 1$.

$$(\mathsf{A} + \mathsf{E})\mathbf{v} = z\mathbf{v} \tag{4.11}$$

Next, the parameter perturbation matrix is defined as, $\mathsf{E} = s\mathbf{u}\mathbf{v}^*$, with $s < \epsilon$ and $|\mathbf{u}| = 1$. Then, we introduce the resolvent (4.12) of the matrix, A, at a value, $z \in \mathbb{C}$ [134].

$$\mathsf{R}(z) = (\mathsf{A} - z\mathsf{I})^{-1} \tag{4.12}$$

Note that the resolvent evaluated at the eigenvalues of A will produce a singular matrix having a norm with infinite magnitude. Furthermore, the norm of the resolvent evaluated away from the eigenvalues will, by definition, be non-singular and finite. Using these definitions equation (4.11) can be rewritten as (4.12) in terms of the resolvent and the definition of the parameter perturbation.

$$z\mathbf{v} - \mathsf{A}\mathbf{v} = \mathsf{E}\mathbf{v} \tag{4.13a}$$

$$-(\mathsf{A} - z\mathsf{I})\mathbf{v} = s\mathbf{u}\mathbf{v}^*\mathbf{v} \tag{4.13b}$$

$$-s^{-1}(\mathsf{A} - z\mathsf{I})^{-1}(\mathsf{A} - z\mathsf{I})\mathbf{v} = s^{-1}(\mathsf{A} - z\mathsf{I})^{-1}s\mathbf{u} \tag{4.13c}$$

$$-s^{-1}\mathbf{v} = (\mathsf{A} - z\mathsf{I})^{-1}\mathbf{u} \tag{4.13d}$$

$$-s^{-1}\mathbf{v} = \mathsf{R}(z)\mathbf{u} \tag{4.13e}$$

Taking the norm of (4.13e) relates the magnitude of the resolvent to the the magnitude of the

parameter change. This is accomplished by using the property of a norm that $\|\mathsf{X}\|\|\mathsf{Y}\| \geq \|\mathsf{XY}\|$.

$$\|\mathsf{R}(z)\mathbf{u}\| = \| - s^{-1}\mathbf{v}\| \tag{4.14a}$$

$$\|\mathsf{R}(z)\|\|\mathbf{u}\| \geq \|\mathsf{R}(z)\mathbf{u}\| = s^{-1}\|\mathbf{v}\| \tag{4.14b}$$

$$\|\mathsf{R}(z)\| \geq s^{-1} > \epsilon^{-1} \tag{4.14c}$$

Finally, the ϵ-pseudospectra are now defined as the values for which the inverse of the resolvent is less than a specified magnitude of parameter perturbation.

$$\|\mathsf{R}(z)\|^{-1} < \epsilon \tag{4.15}$$

This form also allows for a compact extension to ODEs with delays by using the resolvent for delayed differential equations [85].

$$\mathsf{R}(z) = \left(\mathsf{A}_0 + \sum_{k=1} \mathsf{A}_k e^{-\tau_k z} - z\mathsf{I}\right)^{-1} \tag{4.16}$$

Simplified calculation of the ϵ-pseudospectra can be achieved by using the Frobenius norm, or matrix 2-norm, in conjunction with properties of singular value decomposition (SVD). A property of the SVD is that the largest singular value, s_{max}, of a matrix, B, is equivalent to the matrix's Frobenius norm. In addition, the largest singular value, s_{max}, of a matrix's inverse is equal to the inverse of the smallest singular value, s_{min}.

$$\|(\mathsf{B})^{-1}\| = s_{max}\left((\mathsf{B})^{-1}\right) = (s_{min}(\mathsf{B}))^{-1} \tag{4.17}$$

Substituting 4.16 into (4.15) and using the relations of (4.17) results in a compact and stable method to numerically calculate the ϵ-pseudospectra for non-delayed ($k = 0$) and delayed ($k > 0$) systems.

$$s_{min}\left(\mathsf{A}_0 + \sum_{k=1} \mathsf{A}_k e^{-\tau_k z} - z\mathsf{I}\right) < \epsilon \tag{4.18}$$

The ϵ-pseudospectra are the values of z that satisfy (4.18). The value of the resolvent can be computed by evaluating the left-hand side of (4.18) at a desired grid of values over a region of the complex plane. The resulting surface will have valleys with a minimum zero value about the eigenvalues. Narrow valleys suggest eigenvalues that are less sensitive to

parameter change while wide valleys correspond to the eigenvalues that are most sensitive to parameter change. Therefore, the ϵ-pseudospectra correspond to the open subset of the complex plane bounded by the level curve formed by the norm of the resolvent equal to ϵ^{-1}.

4.2.4 Stability radius

We now present the complex stability radius with unstructured parameter perturbation using the concepts of stability and ϵ-pseudospectra. The mathematical definition is extended to the delayed case and presented in a form that is can be implemented numerically.

Stability radius is defined as the smallest change to a system parameter that results in shifting eigenvalues so that the corresponding system is unstable. In terms of the ϵ-pseudospectra this is equivalent to finding the smallest magnitude of parameter change where the pseudospectral set is grown to just contain part of the positive right-half complex plane. When the parameter perturbation is allowed to be a complex value the mathematical definition of stability radius is:

$$\begin{aligned} r = \min & \epsilon \\ \text{s.t. } & \|\mathsf{R}(z)\|^{-1} < \epsilon \\ & \Re(z_0) \geq 0 \end{aligned} \tag{4.19}$$

This can be further simplified by minimizing $\|\mathsf{R}(z)\|^{-1}$ in place of ϵ. In addition, we can restrict the minimization to only pseudospectral values strictly on the boundary of stability, $\Re(z) = 0$.

$$r = \min_{\Re(z)=0} \|\mathsf{R}(z)\|^{-1} \tag{4.20}$$

Finally, using properties of the SVD (4.17) and the extended resolvent (4.16) we can write a compact and stable method to numerically calculate the complex stability radius for non-delayed ($k = 0$) and delayed ($k > 0$) systems. Therefore, minimization can be achieved quickly by evaluating the SVD of the characteristic equation only over values on the imaginary axis.

$$r = \min_{\Re(z)=0} s_{min}\left(\mathsf{A}_0 + \sum_{k=1} \mathsf{A}_k e^{-\tau_k z} - z\mathsf{I}\right) \tag{4.21}$$

4.3 Application

We present an application of stability radius to identify how changes in delayed feedback gains and stance width affect frontal-plane balance control. Subjects during standing balance respond to support surface translations in the frontal-plane with nearly identical center-of-mass motion regardless of their stance width[133]; however, muscle activity is observed to decrease as stance width increases, demonstrating a change in neural control[39]. We used stability radius as a tool to analyze the changes in stability due to different stance widths and delayed feedback gains.

First, we give an overview of a mathematical model of frontal-plane standing balance. Using this model we show the steps necessary to calculate the stability radius for a set of parameters. Then, we use stability radius to identify the feedback gains that produce the maximum stability at nominal stance width and the feedback gains that produce similar stability radius at narrow and wide stance width. Finally, we compare simulated center-of-mass responses at narrow and wide stance width using the feedback gains identified to have the same stability radius.

4.3.1 Model

We examined a delayed second order system that modeled human frontal-plane standing balance as a four-bar linkage (Fig 4.1) with hip angle, q, using scaled anthropometric parameters based on healthy adults.

$$I(q(t))\ddot{q}(t) + Q(q(t), \dot{q}(t)) + G(q(t)) = -C\left(k_p q(t-\tau) + k_v \dot{q}(t-\tau)\right) \tag{4.22}$$

Inertial, I, coriolis, Q, and gravitational, G, terms were included in the closed-chain, nonlinear equations of motion. Joint torque necessary to maintain the initial configuration was generated by feedback gains of position, k_p, and velocity, k_v, with a delay, τ, and geometric scaling, $C = \left(\frac{S}{W}\right)^2$ (S is stance width, W is hip width). Nominal parameters for the model were selected based on average anthropometric values of height (1.8 m), mass (72 kg), and delay (100 ms). Further details of the model can be found in Appendix A.

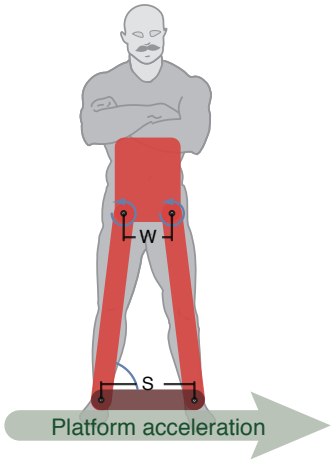

Figure 4.1: Application for a frontal-plane model of human mediolateral balance control. Frontal-plane motion of the body was modeled as a four-bar linkage. Two bars represented the legs, the third bar was the torso, and the fourth bar was the ground. Perturbations were applied as initial conditions in lieu of ground translations. Important parameters of the model were the hip width (W), stance width (S), and hip angle (q).

4.3.2 Analysis

The system ((4.22)) was first linearized about the symmetric equilibrium condition to generate a linear system of first order equations with states, $\mathbf{x} = [q\ \dot{q}]^T$.

$$\frac{d}{dt}\mathbf{x}(t) = \begin{bmatrix} 0 & 1 \\ \frac{G}{I} & 0 \end{bmatrix}\mathbf{x}(t) - C\begin{bmatrix} 0 & 0 \\ \frac{k_p}{I} & \frac{k_v}{I} \end{bmatrix}\mathbf{x}(t-\tau) \tag{4.23}$$

Next, using (4.6) the characteristic equation for the system was formed.

$$\det\left(\begin{bmatrix} 0 & 1 \\ \frac{G}{I} & 0 \end{bmatrix} - C\begin{bmatrix} 0 & 0 \\ \frac{k_p}{I} & \frac{k_v}{I} \end{bmatrix}e^{-\tau\lambda} - \lambda\begin{bmatrix} 1 & 0 \\ 0 & 1 \end{bmatrix}\right) \tag{4.24}$$

$$\det\left(\begin{bmatrix} -\lambda & 1 \\ \frac{G}{I} - C\frac{k_p}{I}e^{-\tau\lambda} & -\lambda - C\frac{k_v}{I}e^{-\tau\lambda} \end{bmatrix}\right) \tag{4.25}$$

$$\lambda^2 - \frac{G}{I} + C\left(\frac{k_p}{I} + \frac{k_v}{I}\lambda\right)e^{-\tau\lambda} = 0 \tag{4.26}$$

We explored the stability of the system at the nominal stance width ($S/W = 1$) by computing the dominant eigenvalues across all feasible pairs of delayed feedback gains. Previously identified stability boundaries were used to restrict feedback gains that produced unstable dynamics [7]. Across this region, we examined each stable gain pair in a 100×100 grid. First,

we verified stability by ensuring that none of the roots of the characteristic equation had a positive real part. A limited set of eigenvalues for each solution were then numerically determined using Cauchy's argument principle and a modification to the Lehmer polynomial root finding algorithm so that characteristic equations with delay could be solved[152, 68].

For representative cases, we computed the ϵ-pseudospectra to investigate the sensitivity of the dominant eigenvalues to perturbations. For each case, the magnitude of the resolvent was evaluated across a grid of complex values and these magnitudes were plotted as level sets to illustrate the pseudospectral variations across the level of perturbation ($1.0 \times 10^{-3} < \epsilon < 2.0$).

The stability radius (4.27) for each stable, delayed feedback gain pair was also calculated for each of 16 stance widths ranging from $S/W = 0.5$ to 2.0. Each stability radius result was solved using a bisection line search over the set of complex values along the imaginary axis to identify the minimum value of the argument.

$$r = \min_{\Re(z)=0} s_{min}\left(\begin{bmatrix} -z & 1 \\ \frac{G}{I} - C\frac{k_p}{I}e^{-\tau z} & -z - C\frac{k_v}{I}e^{-\tau z} \end{bmatrix}\right) \tag{4.27}$$

To compare the relative stability of feedback gain pairs within the same stance width the stability radius was compared across all feasible gain values at the nominal stance width ($S/W = 1$). A single pair of delayed feedback gains was selected that resulted in the maximum stability radius for the model at nominal stance width.

To compare the relative stability of feedback gain pairs across stance widths, k_p and k_v gains were found that resulted in the same stability radius across stance widths. Across the range of stance ratios the largest common stability radius was identified and for each stance width the associated delayed feedback gain pair was recorded.

Finally, to test the behaviors resulting from the selected feedback gains, we simulated the motions of the COM using the fully nonlinear equations of motion in both narrow and wide stances. An initial velocity disturbance was imposed (q_0 = [0 rad, 10 rad/s]) to the model at narrow ($S/W = 0.5$) and wide ($S/W = 2$) stance widths using the respective delayed feedback gain pairs associated with the same stability radius value.

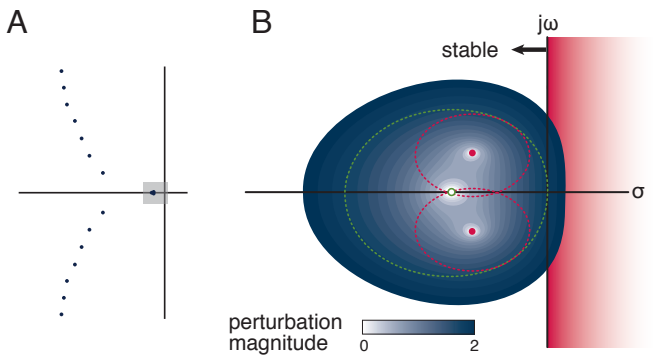

Figure 4.2: Eigenvalues and pseudospectra for a single feedback gain pair at the nominal stance width. (A) A subset of the infinite number of eigenvalues for the delayed four-bar linkage model (S/W = 2, k_p=243 N-m/rad, and k_v=57 N-m/rad/s). Shaded box is complex region surrounding the three dominant eigenvalues and enlarged in (B) The pseudospectra corresponding to a perturbation that caused the eigenvalues to go unstable is represented by dotted lines. The value of the smallest perturbation to cause any of the eigenvalues to go unstable was the stability radius for this system. For the neuromechanical system modeled here, the more negative eigenvalue (unfilled dot) went unstable at a lower level of perturbation than the dominant eigenvalues that were closer to the imaginary axis (filled dots).

4.4 Results

A pattern of three stable dominant eigenvalues was found for all stable feedback gains for the model at the nominal stance width (Fig. 4.2). The ϵ-pseudospectra of these eigenvalues as the perturbation ϵ increased from 0 to 0.8 demonstrated that the most positive eigenvalue was often least sensitive to parameter changes (Fig. 4.2). That is, an eigenvalue further from the imaginary axis (Figure 4.2B) was more sensitive to the imposed perturbation, crossing the imaginary axis first and rendering the system unstable.

Across all stable feedback gain pairs in the nominal stance width, the stability radius was found to be lowest at the boundaries and highest for mid-range gain values (Figure 4.3). The maximum stability radius (r = 0.92) at the nominal stance (S/W = 1.0) was found when k_p = 1540 N-m/rad and k_v = 405 N-m/rad/s. This stable feedback gain pair produced system behavior that was least sensitive to changes in system parameters.

Maximum stability radius was found to decrease as stance width increased. Maximum stability radius at narrow stance (r = 0.93 at S/W = 0.5) was associated with larger feedback gains (k_p = 7312 N-m/rad/s, k_v = 1982 N-m/rad) and stability radius at wide stance (r = 0.89 at S/W = 2.0) had smaller feedback gains (k_p = 323 N-m/rad/s, k_v = 79 N-m/rad) (dotted line

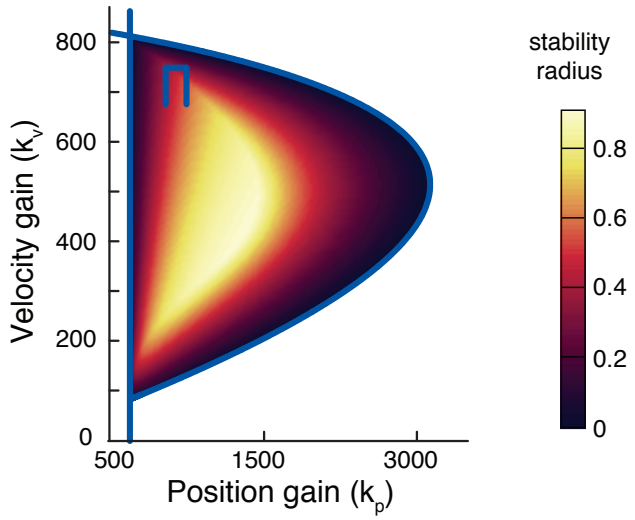

Figure 4.3: Stability radius across all stable feedback gains at the nominal stance width. The solid lines giving a D-shaped boundary encloses the range of all stable feedback gains at the nominal stance width ($S/W = 1.0$). Shaded intensity represents the value of the stability radius for each stable gain pair. Lighter values have greater stability radius and resulted in system behavior that was less sensitive to parameter variations.

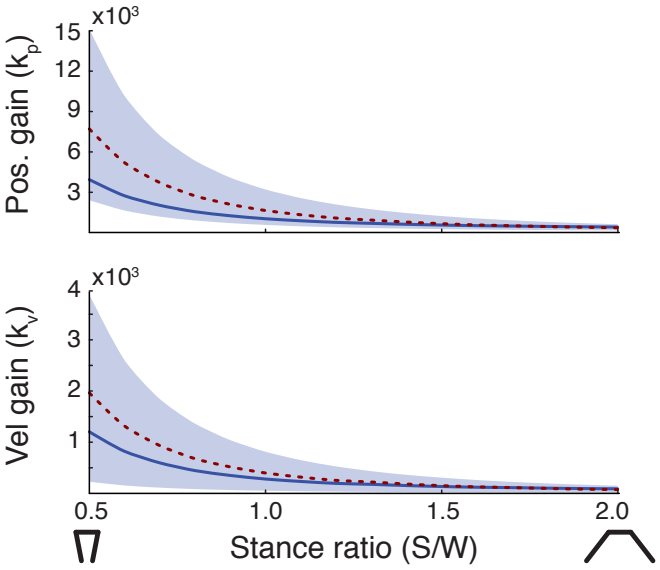

Figure 4.4: Stable feedback gains across stance width. The shaded regions defined all stable feedback gains across stance widths. The dotted line indicates the feedback gain pairs that produced maximum stability radius across stance widths. The solid line indicates the feedback gain values that produced the same stability radius ($r = 0.8$) across stance widths.

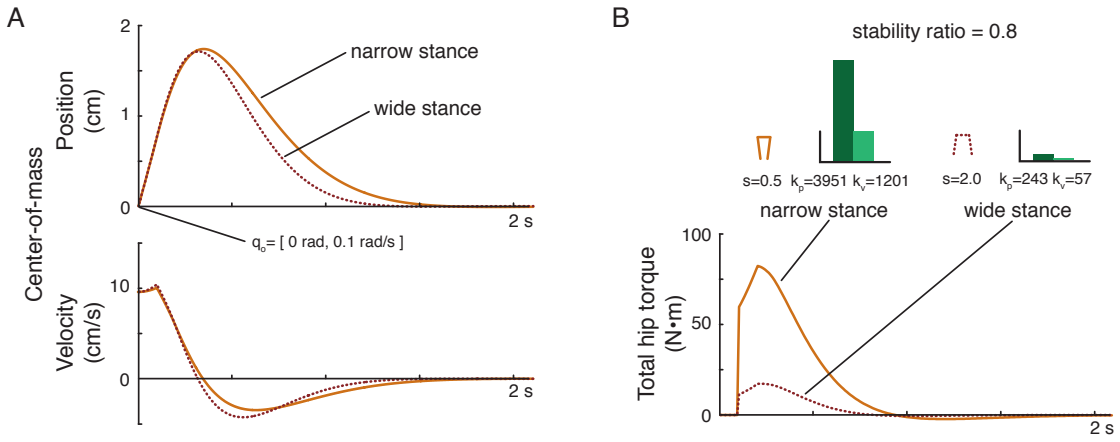

Figure 4.5: Simulated center-of-mass position across stance widths using feedback gains that produce the same stability radius. (A) Although feedback gain values differed substantially across stance widths, the resulting center-of-mass motion produced in response to a change in the initial state of the system was similar in narrow (solid) and wide (dotted) stance widths when feedback gains with the same stability radius were used. (B) The resulting torque necessary to generate the center-of-mass response was an order of magnitude smaller for the wide stance compared to the narrow stance

in Figure 4.4). Narrow stance was found to be less sensitive to parameter perturbations than wide stance.

The feedback gains k_p and k_v that maintained the same stability radius (r = 0.8) increased by over 16× from wide (k_p=243 N-m/rad and k_v=57 N-m/rad/s) to narrow (k_p=3951 N-m/rad and k_v=1201 N-m/rad/s) stance (solid line in Figure 4.4). This similar level of stability radius was found to be associated with gains that were within the mid-range of feasible feedback gains.

Simulations of the model at narrow and wide stance using feedback gains with the same stability radius (r=0.8) produced similar center-of-mass kinematics (Figure 4.5). Trajectories of the center-of-mass position were characterized by a near critically damped response in both cases.

4.5 Discussion

Here we demonstrated that stability radius is a useful metric for comparing behavior across neuromechanical conditions where both biomechanics (plant) and neural control (controller)

change during a task. Similar to previous applications of stability radius [41, 42] we identified the most robust neural feedback gains (controller parameters) for a given stance width (plant parameter). In addition, we used stability radius to quantify and predict how concurrent changes in neural control and biomechanical configuration affected system behavior. Using stability radius we identified the underlying delayed neural feedback gains associated with a stance width that produced similar center-of-mass behavior. Stability radius may provide insight into the neuromechanical interactions governing robust balance control by identifying the neural control parameters that yield the same stability radius across changes in biomechanical configuration. This type of analysis could be extended to understanding general principles of neuromotor control.

In contrast to typical stability analyses that explore tolerable delays, in our application the delay was a fixed parameter reflecting measured neural conduction and processing time. Standard delayed-system analyses pose a problem of finding the maximum delay for which the system is stable [117, 115] or the sensitivity of stability to delays [84]. In contrast, delays in neuromechanical systems are remarkably invariant to system changes [39, 38]. Thus, the problem is to identify how variations in system parameters, and not changes in delay, cause instability. Stability radius is particularly useful for delayed systems, because it is not necessary to explicitly compute any of the infinite number of eigenvalues associated with a delayed system.

The application of stability radius to a simple neuromechanical model of balance control with delayed neural feedback improved our ability to compare postural behaviors across biomechanical configurations. In our prior work using eigenvalue analysis, it was only possible to determine the set of feedback gains that produced stable behaviors at each stance width and to compare the relative stability of each solution within a stance width using the gain margin [7]. However, it was not possible to compare stability across stance widths without performing explicit forward simulations of the system using the different parameter values. This was because the gain margin is computed with respect to the boundary of stability, which was specific to each stance width. Thus, gain margin does not take into account the changes in stability due to changes in configuration, and provides only a relative measure of

stability within a stance width. In contrast, the stability radius is an absolute measurement of system behavior which allows comparisons of feedback gains across stance widths. For example, whereas the maximum gain margin was identical across stance widths, the stability radius demonstrated that narrow stance widths are actually more robust to parameter variations, consistent with our previous simulation results[7].

We show that changes in system behavior due to perturbations to the state variables of the model are described by the stability radius. Previously we demonstrated that precise tuning of delayed neural feedback gains were necessary to produce similar behaviors across stance widths, but we lacked a method to prospectively select the appropriate gains that generated a desired behavior [7]. We replicated the experimentally-observed similarity in center-of-mass kinematics across stance widths in response to imposed motion of the support surface by selecting feedback parameters with the same stability radii across stance widths. Thus, feedback gains and stance widths that reduced the sensitivity of the behavior to parameter variation were the same as those that led to similar responses to physical perturbations. Although the similarity in center-of-mass kinematics could be the result of the nervous system selecting robust feedback gains it is also possible that the nervous system selects the trajectory itself to produce robust behaviors.

Our results support the hypothesis that the nervous system may employ a neural strategy for selecting feedback gains and biomechanical configurations that reduces the sensitivity to parameter variation arising from sensory noise or imperfect control. The feedback gains in the model that produced maximum stability radius were in the mid-range of possible stable values, consistent with the feedback gain values identified by fitting the model to experimental data [7]. Similarly, research in upper-extremity control also suggests that motor strategies are selected that reduce sensitivity to parameter variation in dexterous tasks [122, 5].

Our results corroborate the idea that stability is maximized in unstable motor tasks, and stability radius could contribute to a better understanding of how increased stability is achieved. Previously, arm impedance has been shown to increase by muscle co-contraction when generating forces in an unstable environment [98, 46, 111]. However, limb impedance

can be altered by both muscle activity [64] as well as limb configuration [135]. Using stability radius, the contribution of muscle activity and limb configuration on stability could be dissociated. This may be useful for understanding modulation of feedback gains in a given context, as well as the selection of a particular configuration or strategy to achieve a desired behavior.

Our current formulation for stability radius assumes a conservative estimate of how parameters affect the stability of a neuromechanical system. Our perturbation to the system, E, assumed that the musculoskeletal and neural feedback gain parameters were equally variable. In this unstructured case, all parameters contributed equally to the stability radius, leading to a conservative estimate. It is possible to structure the parameter perturbations so that only specific parameters are affected [143, 42, 44]. Such a weighting may be useful in cases where some parameters are known to a greater accuracy and are unlikely to be perturbed, e.g. mass of the body, and could lead to a less conservative stability radius estimate. We also assumed that perturbations to parameters could be complex valued, which begs the question: When do real-world parameters have complex value? While the perturbations to system parameters are almost always real-valued, it is possible that imposing complex-valued perturbations could reveal how transient changes in parameters, e.g. oscillations from sensory noise, may further alter stability [43, 134]. In cases where it is reasonable to assume that parameter perturbations are only achieved through real values, such as uncertainty in knowing limb inertia, the perturbations can be restricted to only real values using a slightly more complicated minimization technique to identify the stability radius [41, 102].

To conclude, stability radius has many benefits over using eigenvalues alone for analysis of neuromechanical systems. Specifically, we were able to quantify the effect of both biomechanical and neural parameters on the stability of frontal-plane standing balance. Stability radius is generalizable and can be applied to a variety of complex systems that may be nonlinear and have delays. Thus, stability radius lends itself to additional applications that were not explored in the example presented in this paper. Stability radius can be used as a tool for bifurcation analysis to identify critical parameter values that cause large changes in system behavior [141]. Often the parameters in neuromechanical models are unknown,

using stability radius to determine the sensitivity of stability to these parameters can help to identify error bounds and simulation accuracy [1]. Determining muscle activation and musculoskeletal parameters that reproduce observed behaviors is often achieved through optimization[126, 104, 3]. However, simulations based on the optimized parameters are often unstable, which affects the ability to produce forward simulations over a long duration [89]. This affects the ability to perform dynamic optimization of parameters that rely on completion of a movement[137]. In contrast, selection of muscle activation patterns that produce a system with stable eigenvalues generate simulations that are stable and can be run for much longer simulation times [12, 14]. Further, parameters selected based on stability criteria result in responses to perturbations that are more similar to experimentally-measured responses than those found using minimum muscle stress criteria alone [12]. Stability radius could be used as an additional optimization criterion to identify parameters that generate stable behaviors, which would improve both optimization speed, as well as identifying parameters that could generate more physiologically-realistic behaviors. In short, stability radius offers a metric for quantifying the stability and dynamical responses of parameters within, and across, individuals, which offers a useful tool for the analysis of neuromechanical systems. In contrast to classical stability analyses from control theory, stability radius can concurrently evaluate the effect of active and passive mechanisms affecting system stability; this could be an important tool for the design of assistive and rehabilitative devices for improving motor function.

CHAPTER V

THE EFFECTS OF ALTERED BODY INERTIA ON NEURAL CONTROL

5.1 Introduction

A fundamental question of human movement is to what extent do the biomechanics, as opposed to neural control, influence movement? If you have ever stopped for a moment in a busy crowd and watched people walk by you were likely struck by the diversity of the human body yet the similarity in their movements. While similar, each gait is unique, so is it the differences in biomechanics that produce the subtle quirks that allow us to identify a friend based on his walk, or is it the underlying neural control? Conversely, there are times when apparently large changes in biomechanics are seemingly masked by the adaptability of neural control. Is it the highly trained nervous system of a trans-tibial amputee that makes it difficult to distinguish their gait from a healthy control, or is the amputation actually a relatively small disturbance to the biomechanics? Therefore, to understand whether the similarities and differences in movement between individuals is a result of the underlying biomechanics or due to neural control requires quantifying the separate contributions of each for a particular behavior.

In tasks that require balance, tightly regulated motion of the center-of-mass (CoM) has been observed across postures. Examples of this include standing under a variety of postures [39, 132] and perturbations [49] as well as in locomotion over different surface conditions [28]. Furthermore, the consistency in CoM motion produce simple dynamics that are remarkably well modeled by an inverted pendulum for both postural balance [150] and locomotion [119, 31]. The consistency of CoM motion may point to the CoM as task-level variable controlled by the nervous system despite varying biomechanical conditions [48]. Evidence

of neural control of the CoM has been presented for postural balance tasks, where muscle activity in response to support surface translations can be reconstructed based on the error of CoM kinematics from the desired upright state [107, 145, 69]. In addition, studies in low-gravity environments have observed regulation of posture with respect to CoM over veridical reference in low-gravity [61, 76]. Since the CoM motion is a consequence of both neural and biomechanical influences, separating their effects on CoM motion have not been achieved experimentally in a single paradigm. Here, our goal was to explicitly dissociate the effect of biomechanical and neural control on the CoM response to translational perturbations during frontal plane balance control.

Medial-lateral perturbation to standing balance in the frontal plane is a particularly well-suited paradigm for dissociating the interactions of biomechanics and neural control. The behavior and task are well defined; the CoM must be maintained over the base of support. Changes to the biomechanics can be controlled experimentally by altering the stance width [132, 39, 7, 34]. When a discrete perturbation of the support-surface is imposed there is an inherent neural feedback delay of 100 ms [48] that can be exploited to dissociate effect of *postural set* [49, 101] prior to the perturbation, biomechanics of the postural configuration, and active neural feedback. The initial CoM response is due to the combined effects of postural set and biomechanics and the later CoM motion is due to a combination of biomechanics, postural set, and delayed neural feedback response [48]. Using our previously developed frontal-plane model we can assess the separate contributions of biomechanics and neuromuscular state to the motion.

Observed similarity in the initial CoM response across stance widths suggests that the postural set is altered with changes in configuration; however, this has not been described. Evidence from healthy subjects shows little difference in initial CoM motion across stance widths [132, 39]. We showed that increasing stance width decreases the inertia of the body [7, 109], suggesting that there must be a concomitant change in postural set. However, the decrease in inertia as stance width increases also reduces the effective force of the perturbation on the CoM, which could account for the similarities in initial CoM across stance width without changes in postural set. Therefore, a consistent perturbation magnitude must

be matched across stance widths to have a similar effect on the CoM response. Moreover, our model shows that increasing stance width also increases the effective leverage of joint torques; the same postural state across stance widths will produce different effective torques about the CoM. Thus, the inertia of the body must be altered separately from the configuration to dissociate changes in CoM motion due to inertia or stance width. To address these issues in our current study, we included conditions with additional mass added to the torso and applied two levels of perturbation so that inertia and effective perturbation could be matched across stance widths.

Changes in neuromuscular responses with changes in configuration may be the result of altered neural feedback. Evidence from healthy subjects shows that, despite little change in peak CoM motion, muscle activation decreases in response to the same translational perturbation when standing with a wider stance [132, 39]. However, changes in feedback mechanisms were not possible to determine from the Henry experiments, since the separation of effects from postural set and neural feedback responses was not possible due to the minimal time (250 ms) between the acceleration and deceleration of the platform perturbation, obfuscating the feedback response that would have first become visible near the time of the deceleration. Therefore, we extended the length of the perturbation in order to separate the effect of passive biomechanics and delayed neural feedback on peak CoM excursion.

Previously, it has been shown that active neural feedback is the primary factor in corrective frontal-plane motion in the lower-body [36]. Similarly, we showed in a model that stable behavior across all stance widths could only be achieved if sensorimotor feedback gains decreased as stance increased [7], however these could be attributed to more peripheral sensory effects due to changes in leverage. It is possible that the sensory feedback change is due to configuration affecting the length and sensitivity of proprioceptive afferents. Therefore, changes to neuromuscular responses within the same stance width could be attributed to altered sensorimotor transformation and responses at different stance widths could be a combination of central and local effects. Thus, we altered body mass to produce different inertia within the same stance width to test central changes in the sensorimotor transformation and compared different stance widths where inertia was matched to test if additional

changes occurred due to peripheral effects.

Here, we hypothesized that changing stance width during standing balance control alters the neuromechanical interactions, necessitating adjustment of postural set and neural feedback gain to produce similar CoM motion. We used model predictions to test whether postural set changes across stance width we dissociated the effects of configuration and inertia by applying two levels of perturbation in weighted and unweighted conditions, such that inertia was matched across two stance widths. We predicted that changes in geometry would affect postural set differently than changes in inertia allowing for separate and quantifiable changes in the initial CoM response. We designed translational perturbations to lengthen the time between acceleration and deceleration to separate responses from postural set and neural feedback. We tested if changes in neural feedback were the result of changes in inertia or due to peripheral effects by comparing weighted and unweighted responses within and across stance widths. Finally, we predicted that this effect would be generalizable across perturbation magnitude and the CoM response would scale with the perturbation.

5.2 Methods

5.2.1 Frontal plane model of balance

In order to analyze frontal plane motion we used the extended version of our previously described four-bar linkage model that included non-delayed position and velocity feedback to model postural set and delayed position and velocity feedback for neural control (See Appendix A: Eq. A.16)[7]. Leg length, hip width and torso height of the model were scaled to each subject's anthropometric measurements and used with anthropometric tables to determine segment CoM and inertia [148]. Muscular force was modeled as a lumped term and applied with constant moment arms as torque about each hip joint. Hip torque was generated as non-delayed and delayed feedback of the hip joint angle with fixed gains on position and velocity. The delay was selected to be a single lumped value of 150 ms to account for neural transmission from sensation to actuation (100 ms) and mechanical actuation (50 ms) as observed from the automatic postural response [48]. The perturbation applied to the four-bar linkage was applied as an inertial acceleration of the ground recorded from the measured

platform acceleration. Numerical simulation of the equations of motion was performed in Matlab (Mathworks, Natick, MA). Integration was performed with the explicit trapezoidal rule with a step size of 1 ms, zero initial conditions, and zero-valued state history. Center-of-mass trajectories and ground reaction forces were recorded.

Model predictions were performed to identify the effects of specific parameters on the resulting simulated CoM trajectories. This was accomplished by setting the model to a nominal set of parameters associated with a subject of height 1.8 m, mass 70 kg and stance ratio (stance width / hip width) of 1.0. Non-delayed feedback gains were set to zero for the nominal condition. Delayed feedback gains were selected such that the simulated CoM trajectory matched average experimental results (k_p=600 N-m/rad, k_v=160 N-m/rad/s). Simulated perturbation was set to a gaussian acceleration pulse with a halfwidth of 80 ms and nominal amplitude of 0.2 g. Parameters were increased one at a time to observe changes to the initial slope, peak and settling time of the simulated CoM excursion and velocity. Mass was increased by 14 kg, stance ratio increased to 1.3, perturbation magnitude increased to 0.3 g, delayed and non-delayed stiffness increased by 100 N-m/rad and delayed and non-delayed damping increased by 50 N-m/rad/s.

Combined neuromechanical effects were simulated to predict CoM responses for possible neural control changes in response to changes in either configuration, body mass or body inertia. Following the experimental design to separate the effects of configuration and inertia, two matched inertia conditions (I_e = 55 kg-m^2, see Appendix A: Eq. A.7) were created by setting the model to a narrow stance ratio (S/W = 0.6) condition and a weighted, wide stance ratio (S/W = 1.4) condition with an additional 20% mass added to the torso. Next, three control policies of unchanged neural control, scaled delayed neural feedback, or scaled postural set were proposed to determine if neural feedback scaled with changes in configuration and body mass separately or with changes in body inertia. A nominal neural feedback control for the “unchanged” control policy scaled only with stance ratio and was set such that it maximized stability radius (see Chapter 4) at each of the stance ratios with only delayed feedback was set (Narrow: k_p = 3000 N-m/rad, k_v = 800 N-m/rad/s; Wide: k_p = 540 N-m/rad, k_v = 144 N-m/rad/s) and non-delayed feedback gain values were zeroed. For the weighted, wide

stance condition two additional control policies were simulated that increased feedback gain in proportion to the increase in mass or the change in inertia. The first modeled a scaling of the neural feedback control and increased the nominal delayed feedback gains by 20%. The second policy modeled changes in postural set by prescribing the non-delayed feedback gains to values that were 20% of the nominal delayed feedback gains.

5.2.2 Experimental design

Twelve young, healthy subjects (7 male, 5 female, 21.3±3.2 years of age) were recruited under protocols conforming to the Declaration of Helsinki and approved by the Georgia Tech and Emory University Institutional Review Boards.

Data were collected during perturbations of the support surface where the stance width, weight, and perturbation magnitude were varied. In each trial, subjects were instructed to stand upright and to maintain balance during perturbations. Each foot was located on an individual calibrated force plate (AMTI, Watertown, MA) that recorded all six reaction forces and moments. Perturbations were administered with a custom platform (Factory Automation Systems, Atlanta, GA) with position and acceleration of the platform recorded. Subject kinematics were captured with a custom 25-marker set that included head-arms-trunk, thigh, shank, and foot segments using a motion capture system (Vicon, Oxford, UK) utilizing 8 cameras. Motion capture was sampled at 120 Hz and platform kinematics at 1080 Hz. Platform kinematics were low-pass filtered at 30 Hz (third-order zero-lag Butterworth filter) and combined with motion capture kinematics to produce relative position, velocity and acceleration of the markers with respect to the platform. The relative motion of the markers and a proportional model of human mass were used to calculate center-of-mass position, velocity and acceleration for each subject [148].

To test the effects of varying stance width on CoM kinematics, each subject was tested at three different stance widths. Preferred (P) stance was identified as the stance width measured after instructing subjects to walk forward three steps and stop in a comfortable standing posture. Each subject was also asked to stand in a narrow (N) stance width of 10 cm and a wide (W) stance of 30 cm. These stance widths were fixed to allow for a range of ratios

of hip width to stance width caused by the natural variation in subjects' hip widths. Each stance width distance was measured between the centers of the heels and the lateral border of each foot was marked with masking tape to allow the subject to return to the specified stance width.

In order to produce conditions with similar inertia across stance widths, subjects were tested in weighted and unweighted conditions. The additional mass and its location was designed to produce matching inertia between unweighted-narrow and weighted-preferred conditions and between unweighted-preferred and weighted-wide conditions. The weighted condition consisted of an additional mass of 20% of the subject's total mass rounded to the nearest 5 lbs. Weight was applied with a small backpack filled with lead diving weights placed tight and flat across the upper back. To measure changes in CoM height, subjects were asked to lie on a horizontal platform and the ground-reaction force at one end was measured using the AMTI force plate. The COM height was then computed with respect to the soles of their feet using a static force balance [96, 6].

To match the effective force on the CoM across stance widths two levels of perturbation magnitude were used for each condition, low (L) and high (H), in the four cardinal directions. Translational ramp-and-hold platform perturbations were given in the anterior, posterior, left and right directions in random order. To maximize perturbation duration, all perturbations had a total movement distance of 24 cm, the largest possible on our device. Here we examined only responses to medial-lateral perturbations; anterior-posterior perturbation were not analyzed. In the medial-lateral directions, the low and high perturbation magnitudes differed across stance widths such that a constant CoM acceleration (0.2 g) due to the perturbation was achieved across stance widths in three conditions (N-H, P-L, W-L). Additionally, in three other conditions, a constant effective force was applied by the perturbation, resulting in a graded acceleration (0.1, 0.2, 0.3 g) across stance widths (N-L, P-H, W-H). Peak platform velocity and acceleration for low magnitude perturbations were specified as: 10 cm/s and 0.1 g for narrow; 15 cm/s and 0.2 g for preferred; and 15 cm/s and 0.2 g for wide. Similarly, high magnitude perturbations were specified as: 15 cm/s and 0.2 g for narrow; 20 cm/s and 0.2 g for preferred; and 30 cm/s and 0.3 g for wide.

To administer all combinations of weight, stance width and perturbation magnitude, trials were presented in blocks of unweighted and weighted trials, and sub-blocks of stance width, which were randomized. For each perturbation, subjects were instructed to stand upright with arms crossed and to maintain balance while looking straight ahead. For 8 subjects, the A group, only low perturbation magnitudes were administered in the rightward direction and only high perturbation magnitudes were administered in the leftward direction (8 repetitions x 4 directions x 1 magnitude each = 32 trials per subject). In these subjects we assumed the left and right responses were symmetrical and pooled all of these data for analyses. To ensure that these results were not biased due to the difference in perturbation magnitudes across direction, we tested an additional 4 subjects, the B group, in which both low and high perturbations were administered in both leftward and rightward direction (4 repetitions x 4 directions x 2 magnitudes each = 32 trials per subject). In each set of subjects we presented the unweighted conditions first for all but one subject. Within each block, sub-blocks were presented for each stance width of narrow, preferred and wide; the order of stance width was randomized within a block. Within each sub-block, 32 perturbation trials were randomly ordered. Inter-trial intervals were varied between 5-15 s to reduce predictability of perturbation onset. A total of 192 trials (2 weights x 3 stances x 32 perturbations = 192) were administered to each subject. In this study, a subset of 96 trials (2x3x16=96 trials) consisting of only the medial-lateral perturbations were analyzed for each subject.

5.2.3 Data analysis

To identify changes in CoM trajectories across conditions, we compared CoM excursion at time points associated with the response from postural set and the later response including neural feedback (Figure 5.1). The initial CoM excursion and velocity due to the passive properties of the musculoskeletal system was evaluated 100 ms after the peak in platform acceleration. Values of the CoM excursion for time points at 250 ms and 500 ms after the peak in platform acceleration were recorded to evaluate the later response that included neural feedback. CoM excursion was computed with respect to the feet and each data point was computed as the mean value over a 3 ms window centered at the selected time.

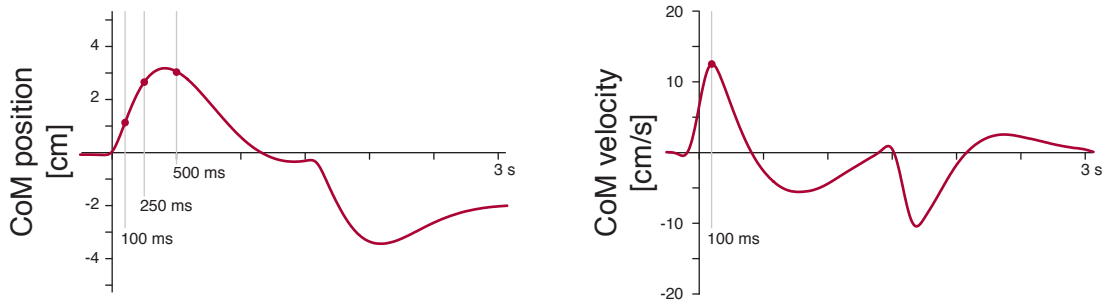

Figure 5.1: Location of CoM data points analyzed. Time zero marks the peak acceleration of the platform perturbation. Vertical lines delineate time points analyzed, which were referenced to the peak acceleration.

For the B group (4 subjects, 384 trials), we performed a five-way ANOVA to demonstrate the effects of subject, stance condition, weight condition, perturbation magnitude, and perturbation direction on CoM excursion. The ANOVA was modeled with all main effects and second-order interactions. The significance level used was α=0.05, adjusted with a Bonferroni correction for multiple comparisons (5 comparisons: α'=0.01).

We also performed two-way ANOVA tests at each time point using subsets of trials to evaluate the independent effect of each factor with significance set at α=0.05, adjusted with a Bonferroni correction for multiple comparisons (5 comparisons: α'=0.01). Each ANOVA had subject and either stance condition, weight condition, perturbation magnitude, or perturbation direction as factors. Significance of factor levels was determined with a Scheffe post hoc test at a significance level of α=0.05. The effect of perturbation magnitude was assessed for trials from the 4 subjects of B group in the unweighted condition at preferred stance width and perturbed leftward. The effect of perturbation direction was assessed for trials from the 4 subjects of B group in the unweighted condition at preferred stance width and perturbed at the low level. Across all subjects, the effect of increased stance width was assessed for trials having subjects in the unweighted condition and perturbed leftward at the constant level of acceleration. The effect of weight condition was assessed for trials having all subjects at preferred stance width and perturbed leftward at the low level. Finally, we compared CoM excursion in conditions where inertia was similar across stance widths by grouping trials by unweighted, narrow stance and weighted, preferred stance from all subjects.

5.3 Results

5.3.1 Model predictions

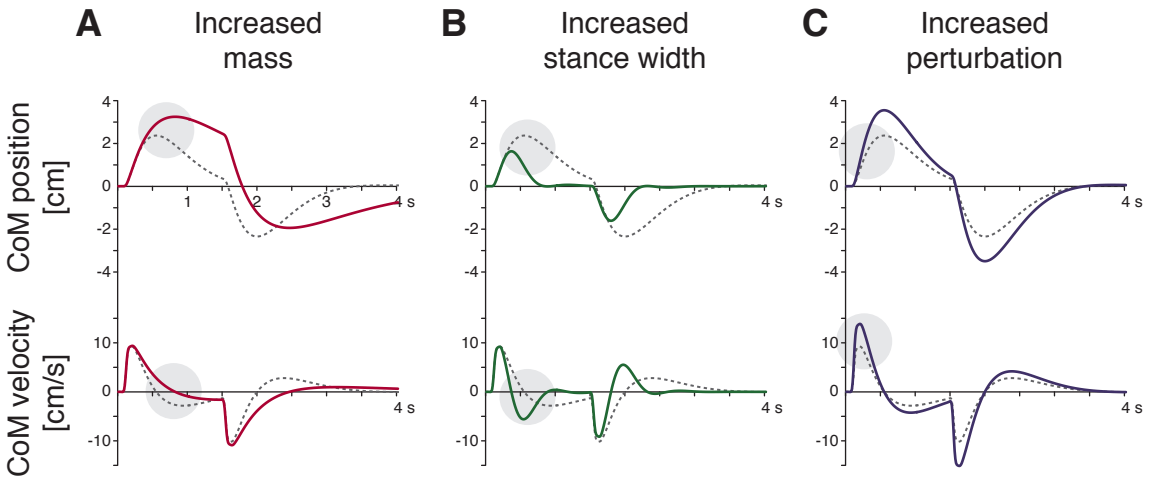

Figure 5.2: Changes to simulated CoM trajectories with changes in biomechanical parameters. Dotted trace is reference trajectory for nominal case. Shaded circles highlight important changes to CoM trajectories. A) Increased mass caused larger CoM position overshoot with lengthened response. B) Increased stance width decreased overshoot of position and increased oscillation of velocity. C) Increased perturbation caused increased position and velocity peak values.

Altering biomechanical parameters while holding all other model parameters constant had little effect on initial CoM motion, but affected the peak CoM excursion and later CoM kinematics. Increasing mass resulted in greater excursion of the CoM (Figure 5.2A). Conversely, increasing stance width decreased the excursion of the CoM. Increasing the stance width also effectively shortened the response time and generated larger oscillation in the velocity trace (Figure 5.2B). Increasing perturbation magnitude was the only parameter that increased the initial slope during the first 100 ms of CoM excursion and this also resulted in increased peak CoM excursion and increased peak velocity (Figure 5.2C). Increasing the perturbation magnitude was also the only parameter that did not affect the timing of the peak response; the peak occurred at the same time between the two perturbation magnitudes.

Altering the model neural feedback parameters, similar to biomechanical parameters, affected peak CoM response and later kinematics with minimal effect on the initial response.

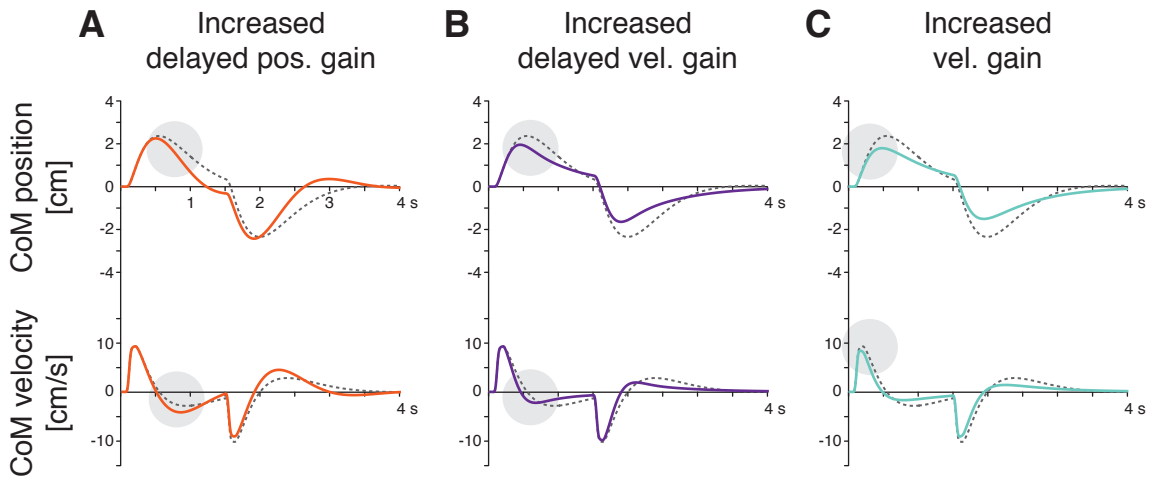

Figure 5.3: Changes to simulated CoM trajectories with changes in neural feedback parameters. Dotted trace is reference trajectory for nominal case. Shaded circles highlight important changes to CoM trajectories. A) Increased delayed position feedback gain resulted in a faster settling response. B) Increased delayed velocity feedback gain decreased the peak magnitude of the CoM position response. C) Increased non-delayed velocity feedback gain has very similar effects as the delayed velocity feedback gain, but was the only parameter that decreased the peak CoM velocity response.

Altering either delayed (Figure 5.3A) or non-delayed position feedback gain had very similar effects; however, increasing non-delayed position feedback gain had relatively minimal effect on the peak CoM excursion and mostly reduced settling time. Delayed stiffness also decreased settling time, but had even less of an effect on the peak excursion. Conversely, delayed velocity feedback, when increased, decreased the peak CoM excursion with less of an effect on the the settling time (Figure 5.3B). Therefore, combinations of delayed position feedback, which affect settling time, and delayed velocity feedback, which affect peak CoM excursion, could be combined to offset increases in mass or stance width. However, no biomechanical or delayed parameter was observed to significantly change the peak CoM velocity response.

Surprisingly, increasing model non-delayed velocity feedback was the only parameter that decreased the peak CoM velocity and was therefore the parameter that most affected the rise time of CoM excursion (Figure 5.3C). Therefore, differences in postural set from changes in non-delayed velocity feedback gain were observed in the model by observing the CoM velocity within the first 100 ms. Increasing non-delayed velocity feedback also reduced the peak CoM

excursion and affected settling time, similar to delayed velocity feedback.

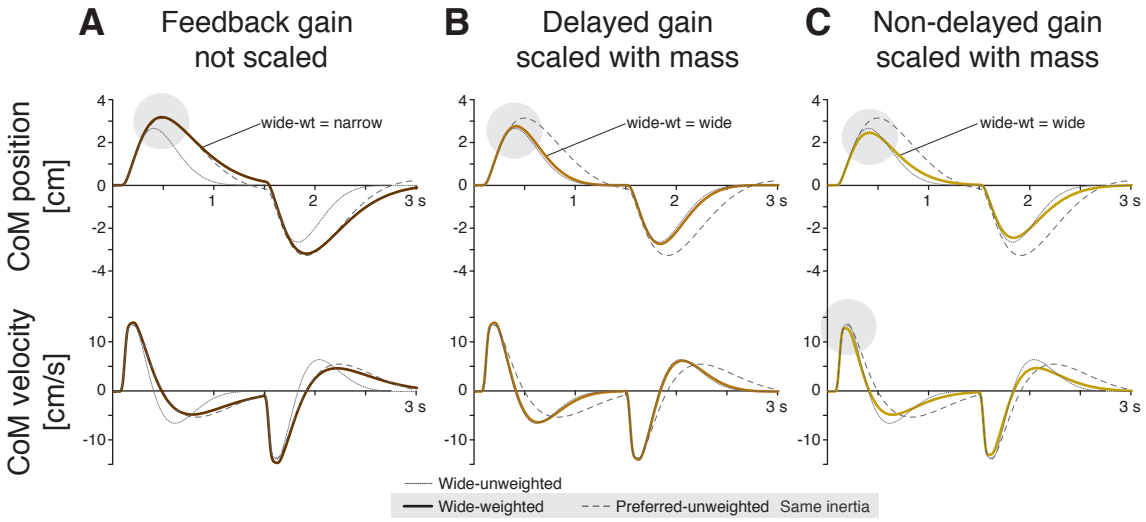

Figure 5.4: Predicted changes in CoM based on differences in feedback gain when inertia was matched. As reference, the dotted trace is for unweighted narrow stance width and the dashed trace is the unweighted wide stance width. The solid lines are the predicted weighted wide stance responses. Shaded circles highlight important features of the CoM trajectories. A) No additional scaling of feedback gain resulted in CoM traces that matched based on similar inertia, narrow-unweighted = wide-weighted. B) Scaling the delayed feedback gain in proportion to the change in mass resulted in CoM traces that matched based on similar stance width, wide-unweighted = wide-weighted. C) Scaling the non-delayed feedback gain in proportion to mass resulted in traces that matched based on similar stance width and also decreased the initial peak CoM velocity.

Predicted CoM responses for conditions where inertia was matched but stance was different resulted in three different behaviors depending on the form of neural feedback. The predicted scenarios for how neural control may change with differences in body inertia were: neural control does not change, delayed neural feedback is adjusted to account for changes in mass, or changes in postural set account for changes in mass (Table 5.1). In the condition that neural feedback was only scaled based on stance width, with no additional scaling based on differences in mass, CoM responses were matched between conditions of similar inertia; weighted, wide stance width had the same CoM response as unweighted, narrow stance (Figure 5.4A). Conversely, in the condition that delayed feedback gain was further scaled in proportion to increased mass, CoM responses were similar across stance width; weighted and unweighted wide stance had the same CoM response (Figure 5.4B). Finally, if non-delayed

Table 5.1: Three hypotheses of changes in neural control in response to increased body mass and their predicted effects on CoM kinematics

Neural control policy	Peak CoM excursion	Peak CoM velocity	Matched condition
Gain not scaled	↑ increased	= same	wide-wt = narrow
Delayed gain scaled	= same	= same	wide-wt = wide
Non-delayed gain scaled	= same	↓ decreased	wide-wt = wide

feedback was scaled in proportion to the increase in mass instead, CoM responses were similar across stance width as well; however, this had the distinct effect that peak CoM velocity was decreased unlike the other hypotheses (Figure 5.4C).

5.3.2 Anthropometrics and summary statistics of experimental groups

Anthropometric differences across all subjects were varied (height 176.3±12.7 cm and mass 70.4±12.1 kg), but CoM location was similar. Measured CoM location with respect to the subjects feet as a ratio of their height (CoM / height) was 0.58±0.01 for men and 0.56±0.01. The addition of 20% mass to the subjects' resulted in increasing the height of the CoM by approximately 4 cm, such that the CoM-to-height ratio increased to 0.60±0.01 for men and 0.60±0.01 for women. Subjects' preferred stance ratio was wider than hip width and men tended to have a relatively wider stance (S/W: men 1.54±0.33, women 1.15±0.13; stance: men 27.1±6.0 cm, women 20.4±0.9 cm). The effective body inertia between the two groups compared was similar (I_e: unweighted-narrow 58±15 kg-m^2, weighted-wide 58±14 kg-m^2). Finally, of the 12 subjects 11 subjects reported being right-handed with 10 of those subjects reporting right-leg dominance; only one subject reported both left-handedness with left-leg dominance.

Results of the five-way ANOVAs for the B group (n=4) demonstrated significant effects of subject, stance condition, perturbation magnitude, and perturbation direction and the insignificant effect of weight condition on CoM excursion. Across all time points the initial COM excursion and velocity for factors of subject, stance condition, and perturbation magnitude were found to be statistically significant (p<1e-3). Also, across all time points only stance condition and perturbation magnitude were found to have a significant interaction (p<1e-6). Finally, weight condition was only significant (p<1e-6) for the 500 ms time point

and not significant for all others (100 ms pos.: p=0.42, 100 ms vel.: p=0.47, 250 ms pos.: p=0.65). Perturbation direction was statistically significant for all times (p<1e-2) except the 100 ms position point (p=0.90).

Table 5.2: Average CoM excursion and velocity from the B group across all possible conditions.

Condition					100 Pos mm		250 Pos mm		500 Pos mm		100 Vel mm/s	
Stance	Mass	Mag	Dir		avg	std	avg	std	avg	std	avg	std
1	0	10	0		7.0	0.9	19.5	2.2	29.5	7.1	82.0	17.7
1	+20%	10	0		6.8	0.6	19.1	1.6	29.7	4.7	83.9	6.7
1	0	10	180		6.8	0.3	19.2	1.4	25.3	6.7	87.1	6.8
1	+20%	10	180		6.6	0.6	18.3	1.2	25.9	4.5	81.9	5.1
1	0	15	0		10.1	1.6	28.0	3.8	42.2	10.7	120.1	22.4
1	+20%	15	0		10.9	0.4	29.2	1.3	44.8	3.2	130.8	5.1
1	0	15	180		10.7	0.7	29.6	1.5	40.2	9.8	133.5	6.4
1	+20%	15	180		10.8	0.6	30.1	1.1	47.6	7.5	132.5	3.8
2	0	15	0		11.0	0.6	27.7	2.1	37.1	7.4	129.4	13.8
2	+20%	15	0		10.6	0.6	26.0	2.3	33.8	7.0	123.4	7.2
2	0	15	180		10.6	0.4	26.2	1.8	33.3	8.3	123.0	5.0
2	+20%	15	180		10.6	0.4	25.8	2.1	30.1	8.7	123.8	5.0
2	0	20	0		13.8	0.4	35.8	2.1	50.4	10.2	164.0	6.3
2	+20%	20	0		13.9	0.5	35.1	2.7	49.1	8.7	162.6	8.4
2	0	20	180		13.9	0.4	34.9	1.4	45.3	7.5	162.3	4.2
2	+20%	20	180		13.9	0.7	34.7	2.0	45.2	8.5	162.5	5.5
3	0	15	0		10.3	0.8	23.4	4.3	23.7	16.0	116.0	12.7
3	+20%	15	0		10.3	0.6	24.2	3.2	27.0	12.6	119.0	13.3
3	0	15	180		10.4	0.5	23.9	3.3	23.3	13.7	117.9	8.7
3	+20%	15	180		10.5	0.7	23.1	3.8	24.3	10.6	114.0	12.7
3	0	30	0		20.5	1.0	49.3	6.2	59.3	24.5	235.7	18.4
3	+20%	30	0		20.1	2.2	49.4	6.1	62.0	17.5	237.5	26.1
3	0	30	180		20.2	1.0	47.3	5.2	53.5	19.1	228.5	16.6
3	+20%	30	180		19.6	0.9	45.2	5.2	53.4	16.1	214.4	22.8

5.3.3 Changes in CoM kinematics were more similar within a stance width than across stance widths

Perturbation direction resulted in responses that suggested possible limb dominance. A modest effect of perturbation direction was observed in group B (n=4) for trials in the unweighted condition at preferred stance width and perturbed at the low level (Figure 5.5). During the initial response, non-significant differences (p=0.028) in excursion of the CoM at 100 ms

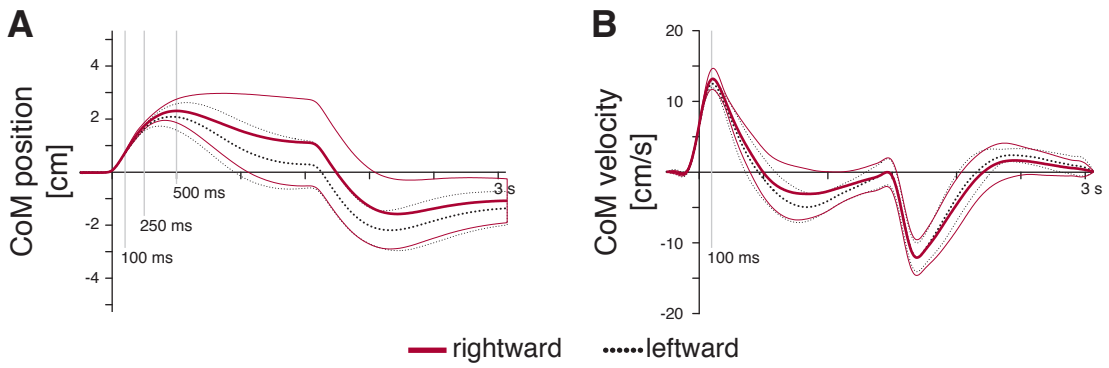

Figure 5.5: Perturbation direction resulted in responses that suggested possible limb dominance. Rightward trace flipped for comparison with leftward trace. Thicker lines are the average trials from B group subjects at preferred stance width, unweighted, and perturbed at the low level. Lighter bounding lines mark one standard deviation. Time zero marks the peak acceleration of the platform perturbation and the grey vertical lines mark time points used for quantification.

were observed between leftward perturbations, 10.6±0.4 mm, and rightward perturbations, 11.0±0.6 mm. There was a trend of increased CoM velocity in the rightward direction at 100 ms with magnitudes of 123.0±5.0 mm/s (leftward) and 129.4±13.8 mm/s (rightward) (p=0.070). The later response also showed differences in CoM excursion at both 250 ms (leftward: 26.2±1.8 mm, rightward: 27.7±2.1 mm, p=0.031) and 500 ms (leftward: 33.3±8.3 mm, rightward: 37.1±7.4 mm, p=0.080). The trend of increased rightward CoM excursion was observed in 3 of the 4 individual subject averages (all of these subjects reported right-leg dominance) and this trend was found to be consistent across all observed conditions (Table 5.2).

Increased perturbation magnitude caused increased CoM excursion across conditions. Similar to predicted CoM kinematics it was found that the magnitude of CoM excursion significantly increased with increased perturbation magnitude (Figure 5.6). During the initial response, excursion of the CoM at 100 ms in the unweighted condition at preferred stance width and perturbed leftward resulted in a magnitude of 10.6±0.4 mm for the low perturbation and 13.9±0.4 mm for the high perturbation (p<1e-6). Velocity of the CoM at 100 ms had magnitudes of 123.0±5.0 mm/s (low) and 162.3±4.2 mm/s (high) (p<1e-6). The later response also had an increase in CoM excursion at both 250 ms (low: 26.2±1.8 mm, high: 34.9±1.4

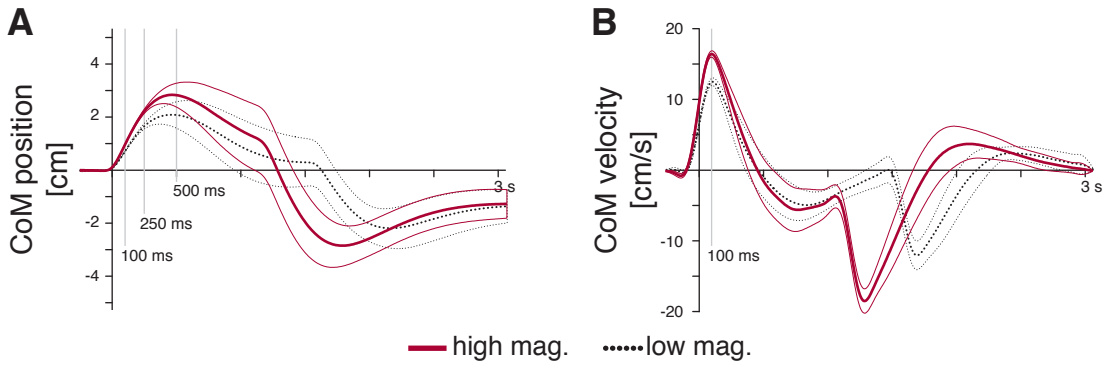

Figure 5.6: Increased perturbation magnitude caused increased CoM excursion across conditions. Thicker lines are the average trials from B group subjects at preferred stance width, unweighted and perturbed leftward. Lighter bounding lines mark one standard deviation. Time zero marks the peak acceleration of the platform perturbation and the grey vertical lines mark time points used for quantification.

mm, p<1e-6) and 500 ms (low: 33.3±8.3 mm, high: 45.3±7.5 mm, p<1e-6). This trend was also found to be consistent across all observed conditions (Table 5.2).

Table 5.3: Average CoM excursion and velocity from all subjects at selected time points of 100, 250 and 500 ms.

Condition					100 Pos mm		250 Pos mm		500 Pos mm		100 Vel mm/s	
Stance	Mass	Mag	Dir		avg	std	avg	std	avg	std	avg	std
1	0	15	180		10.8	0.5	29.0	1.8	40.3	6.7	130.6	5.9
1	+20%	15	180		10.6	0.8	28.4	2.2	42.7	7.7	127.7	7.4
2	0	15	180		10.6	0.5	25.8	1.6	29.8	6.5	123.0	5.0
2	+20%	15	180		10.6	0.6	25.9	2.1	31.5	7.1	122.9	6.6
3	0	15	180		10.4	0.4	23.0	2.6	19.7	10.4	115.8	6.1
3	+20%	15	180		10.3	0.4	23.4	2.8	23.3	9.1	115.5	8.6

Increased stance width resulted in decreased CoM excursion. Across all subjects (n=12), increased stance width was found to significantly (p<1e-6) decrease CoM excursion for trials in the unweighted condition and perturbed leftward at the constant level of acceleration (Figure 5.7). The initial response at 100 ms had a subtle, but significant decrease in CoM excursion from 10.8±0.5 mm (narrow), 10.6±0.5 mm (preferred), and 10.4±0.4 mm (wide). Velocity of the CoM at 100 ms had magnitudes of 130.6±5.9 mm/s (narrow), 123.0±5.0 mm/s (preferred), and 115.8±6.1 mm/s (wide). The later response also showed differences in CoM

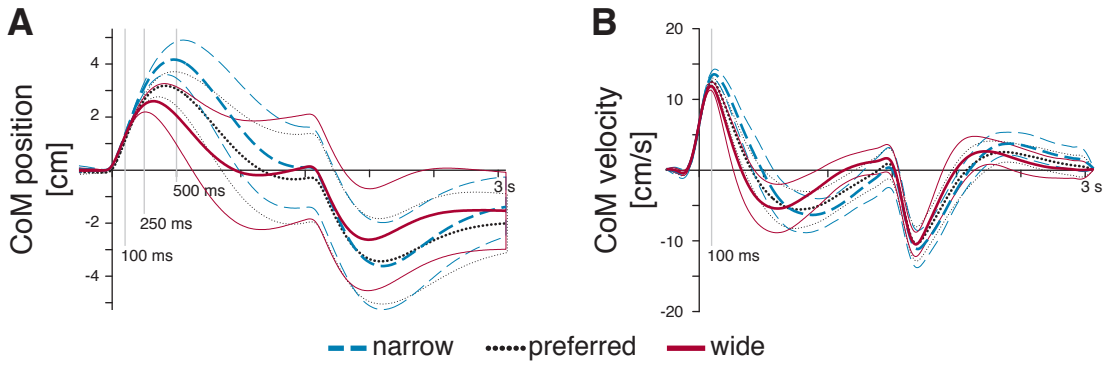

Figure 5.7: Increased stance width resulted in decreased CoM excursion. Thicker lines are the average trials from all subjects in the unweighted condition and perturbed leftward at the constant level of acceleration. Lighter bounding lines mark one standard deviation. Time zero marks the peak acceleration of the platform perturbation and the grey vertical lines mark time points used for quantification.

excursion at both 250 ms (narrow: 29.0±1.8 mm, preferred: 25.8±1.6 mm, wide: 23.0±2.6 mm) and 500 ms (narrow: 40.3±6.7 mm, preferred: 29.8±6.5 mm, wide: 19.7±10.4 mm). The trend of decreased CoM excursion as stance width increased was also found to be consistent across all observed conditions (Table 5.3).

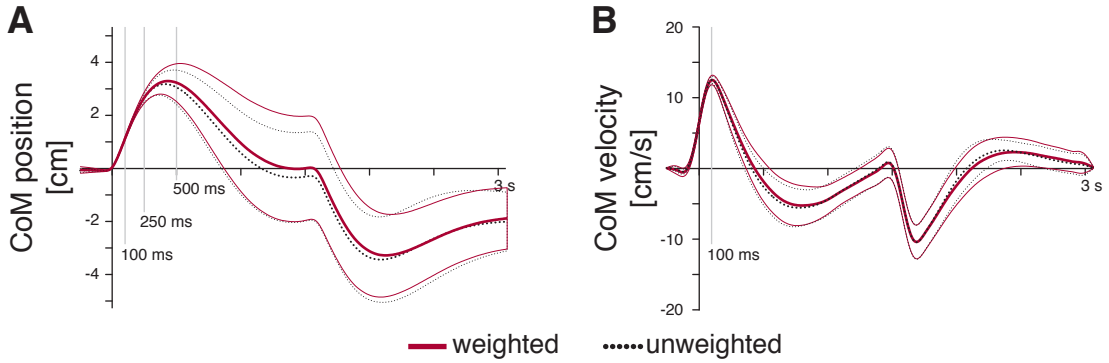

Figure 5.8: Increased mass did not significantly affect CoM excursion. Thicker lines are the average trials from all subjects at preferred stance width and perturbed leftward at the low level. Lighter bounding lines mark one standard deviation. Time zero marks the peak acceleration of the platform perturbation and the grey vertical lines mark time points used for quantification.

Consistent with the model predictions where neural feedback gain scaled with mass (Figure 5.3B and C), increased mass did not significantly affect CoM excursion. In trials having all subjects (n=12) at preferred stance width and perturbed leftward at the low level,

there was no significant difference between the unweighted and weighted conditions (Figure 5.8). The initial response at 100 ms had no significant change (p=0.884) in CoM excursion from 10.6±0.5 mm (unweighted) to 10.6±0.6 mm (weighted). Velocity of the CoM at 100 ms had magnitudes of 123.0±5.0 mm/s (unweighted), and 122.9±6.6 mm/s (weighted), (p=0.964). The later response also showed no statistical differences in CoM excursion at both 250 ms (unweighted: 25.8±1.6 mm, weighted: 25.9±2.1 mm, p=0.873) and 500 ms (unweighted: 29.8±6.5 mm, weighted: 31.5±7.1 mm, p=0.173). The trend of unchanged CoM excursion with increased torso mass was also found to be consistent across all observed conditions (Table 5.3).

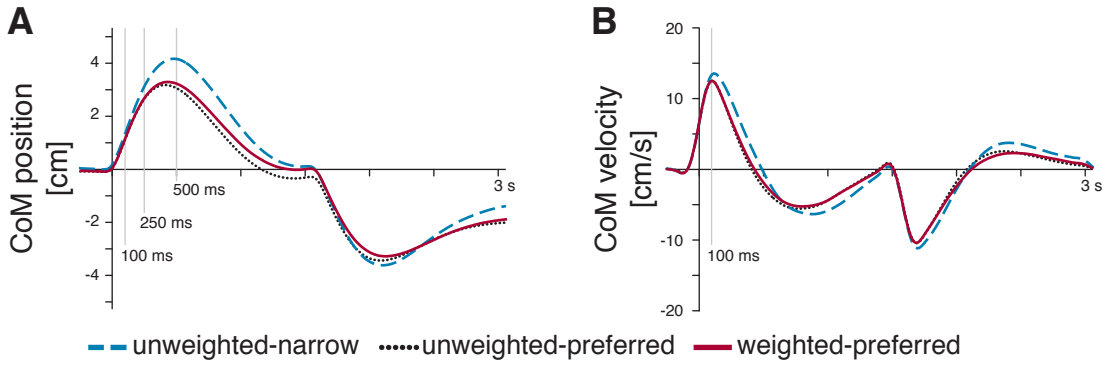

Figure 5.9: Responses from matched inertia scaled with stance width and not mass. Matched inertia conditions are the unweighted-narrow stance and weighted-wide stance. Lines are the average trials from all subjects grouped by unweighted-narrow stance, unweighted-preferred stance, and weighted-preferred stance for leftward perturbations at the constant level of acceleration. Standard deviation boundaries have been left off for clarity. Time zero marks the peak acceleration of the platform perturbation and the grey vertical lines mark time points used for quantification.

Changes in CoM excursion across different conditions of inertia were explained by changes in stance width and not mass; therefore, the model prediction that best explained the observed differences in the matched inertia conditions utilized a control policy that scaled delayed feedback gain with increased body mass (Figure 5.4B). CoM excursion in conditions where inertia was similar across stance widths by grouping trials by unweighted, narrow stance and weighted, preferred stance from all subjects had significantly different CoM responses (Figure 5.9). The initial CoM excursion response at 100 ms was the only time point that had no significant change (p=0.142) in motion from 10.8±0.5 mm (unweighted-narrow)

to 10.6±0.6 mm (weighted-preferred). Velocity of the CoM at 100 ms had statistically different (p<1e-6) magnitudes of 130.6±5.9 mm/s (unweighted-narrow), and 122.9±6.6 mm/s (weighted-preferred), (p=0.964). The later response also showed decreased (p<1e-6) CoM excursion at both 250 ms (unweighted-narrow: 29.0±1.8 mm, weighted-preferred: 25.9±2.1 mm) and 500 ms (unweighted-narrow: 40.3±6.7 mm, weighted-preferred: 31.5±7.1 mm).

5.4 Discussion

The results of this study are important because they suggest a definite change in neuromuscular control to account for altered configuration of the body. Perhaps the most distinguishing observations of the study are that increasing the mass of the torso, which significantly raised the height of the CoM, had little effect on the kinematic responses of the subjects' CoM; however, increasing stance width had a consistent effect of decreasing the motion of the CoM. Our simple model best predicted these experimental results based on a control policy that changed postural set in response to changes in stance width and updated delayed neural feedback with changes in both body mass and stance width. These results provide evidence of possible neural strategies, such as maintaining similar stability, that trigger changes in the sensorimotor transformation that affects the neural control of standing balance.

We showed that, unlike previous reports [132, 39], "similar" CoM motion does not necessarily mean the "same" CoM motion. In platform translation perturbations, if the deceleration follows too soon after the acceleration there is the possibility of forcing the CoM to its initial position before the subject can actively respond. By maximizing the time of the constant velocity phase of the platform, our perturbations were designed to remove the effect of the deceleration on the subjects' active response to the perturbation. This revealed that CoM responses were not actually identical across stance widths. Rather, only the initial response was found to appear to be nearly identical and responses 300 ms after the perturbation onset were found to decrease as stance width increased.

The initial CoM position response is dominated by inertial effects of the perturbation on the body, but the initial CoM velocity may be modulated by postural set. Model predictions suggest that the changes to the initial response in CoM position is nearly immutable under

physiological ranges in stance width and added body mass (Figure 5.2) as well as changes in postural set (Figure 5.3). This is likely because the inertial effects of the perturbation vastly outweigh any torque developed at the joints of the subject. Further evidence of this is that only increased perturbation magnitude was capable of causing noticeable changes in the initial response (Figure 5.2C). However, while changes in the CoM position may be non-existent, changes in initial CoM velocity are detectable and statistically significant as stance width changes (Figure 5.7B). Model predictions suggest that these differences are due to changes in postural set, specifically changes in non-delayed velocity feedback gain, or damping, that affect the initial peak CoM velocity (Figure 5.3C). A changes to postural set from altered stance width seems intuitive. The change in geometry likely affects the lengths of muscle groups, which in turn affect muscle properties. These biomechanical changes alone may account for the differences in the initial response, but additional feedforward changes may also occur to account for the less obvious effects the initial kinematic state may have on the later CoM response.

The later response from 300 ms to the platform deceleration are similar, but not exactly the same across stance widths and may be the result of delayed feedback gains that are selected based on similar levels of stability. Previously we have shown that delayed feedback gain must decrease as stance width increases in order to produce stable responses [7]. We also predicted that selecting the delayed feedback gains with similar stability, as suggested in chapter 4, would produce slightly decreased CoM excursion as stance width increased in order to produce similar performance. The observed experimental responses certainly follow the trend of decreased CoM excursion as stance width increases, but the more interesting point is that the responses follow a characteristically critically damped response that matches the predicted consistent level of stability across stance widths (Figure 5.7). Producing a similar level of stability across different conditions can also be interpreted as the neural control placing the neuromechanical system in a state that is most robust to possible disturbances and motor errors. In this context there is a considerable amount of evidence that suggests that the sensorimotor system operates in regimes that minimize uncertainty and variation caused from internal motor noise [5], precision of timing [18] or posture [135].

We were also able to show that delayed neural feedback is likely sensitive to changes in body mass and that similarity in the CoM motion cannot be explained based on biomechanical factors alone. Remarkably, CoM responses were most similar between unweighted and weighted conditions (Figure 5.8). Across all combinations of perturbation magnitude and stance width the responses of the CoM kinematics were not statistically different between the unweighted and weighted conditions (Tables 5.2 and 5.3). This may seem surprising, as the additional mass was non-trivial; 20% of body mass is on the order of having four *Principles of Neural Science* [56] books in a book-bag.

Furthermore, our model predicted that increasing body mass by this amount without changing neural feedback would have a significant increase in CoM motion (Figure 5.2). These observations are not necessarily unique to this experimental paradigm as similarity in motor responses between conditions with different inertial properties has also been reported in lean-and-release tasks between healthy and obese subjects [78] and identical whole-body reaching responses in conditions of altered body inertia [105]. In order to reproduce this phenomenon, our model predicted that either delayed feedback gains (Figure 5.4B) or postural set (Figure 5.4C) must scale with the increase in mass. Postural set was removed as a possible hypothesis since scaling the postural set also affected the initial CoM velocity response contrary to the experimental observation that the initial velocity was unchanged with the increase in mass (Figure 5.8B). Therefore, the model predicted that similarity in the CoM responses was the result of delayed neural feedback that scaled with increased body mass.

We also showed that changes in delayed feedback caused by changes in stance width were likely the result of changes in body geometry and body mass, but not directly changes in inertia. Since changing stance width affects both body geometry and inertia we designed experimental conditions where the inertia was matched across two different stance widths. If delayed neural feedback was scaled with inertia our model predicted that CoM responses should be identical when inertia was matched (Figure 5.4A). However, experimental results showed that when inertia was matched the CoM response behaved like the matched stance width instead (Figure 5.9). Therefore, delayed neural feedback was predicted to scale with the increase in mass and not actually the change in inertia (Figure 5.4B). This is a subtle but

important addition to the result described in the previous paragraph. An increase in body mass within a stance width is also an increase in inertia; to determine if the neural feedback scaled with body mass or inertia required comparing behavior across stance widths. That the changes in neural control appear to change with body mass and not inertia may corroborate previous reports that gravitational forces, or weight, affect running behavior [17] or object manipulation [157] differently than inertial effects.

Changes in neural feedback in response to altered configuration and body mass may be driven by sensory cues of ground reaction force. A remarkable feature of the hypothesized neural changes in this study is the rapidity of their change. While anecdotal, no noticeable differences were found between the first and last trials within a stance width. Also, postural adaptation of a slight forward lean appeared to occur immediately upon adding the additional mass. Certainly it could be possible that these changes are the result of updating an internal model of the body. However, studies that suggest changes in internal models of body dynamics report a lengthy adaptation period, which has been presented in conditions where limb inertia was altered [91] or in reaching environments where endpoint inertia is altered [114, 67]. Therefore, the apparently sudden changes in neural control and their impact on CoM kinematics may be driven by signals associated with changes in ground reaction forces. An update of an internal model may not be necessary for these conditions as ground reaction forces are immediately affected by changes in body mass and stance width even during static conditions; ground reaction force could directly regulate neural feedback gains. While the role of ground reaction forces was not addressed in this study, previous research points to the importance of load receptors on appropriate muscle responses in standing balance [22] and the coordination of contralateral limb motion [45]. Furthermore, this would predict that changes in body inertia that cannot be statically sensed would result in motor errors until an internal model was updated. This appears to be the case in reaching tasks based on observed systematic movement errors corresponding to differences in arm inertia [37].

The implications of this work may be important for understanding changes in balance for populations where stance and weight are affected. In obese populations both mass and stance

width are increased [106] and it is reported that falls are twice as common over healthy individuals [29]. Our work would suggest that these biomechanical changes necessarily cause changes in the neural control in order to maintain balance. Specifically, it would be expected that delayed neural feedback would need to increase to compensate for increased mass, but still be decreased to maintain stability at the widened stance. From our previous work, increased delayed feedback at wide stance may be destabilizing [7]; therefore, the increase in stance width and accompanied increase in mass may pose a dual threat to the stability of these individuals. Furthermore, since neural control is likely altered it may be important to consider possible residual neural control patterns that may persist as individuals exercise and lose weight, which may affect their balance. In cases of rapid weight loss, such as immediately after pregnancy, it has been reported that there is decreased balance stability, which may be due to neural strategies that have not compensated for the sudden change in body mass [54].

This study suggests that changes in body mass affect neural feedback, which may have critical implications for rehabilitation strategies that implement reduced body weight. Weight support devices used in gait rehabilitation have the advantage of providing support for individuals who may not have the strength or motor coordination necessary to stand. However, this may have an unintended consequence that balance may not be being trained and even possibly maladjusted through inappropriate ground reaction cues. This may be one reason that weight supported rehabilitation devices have had poor results when rehabilitating subjects who suffer from spinal cord injury [147], stroke [63], or multiple sclerosis [140]. Therefore, rehabilitation of these individuals may be significantly improved if rehabilitation is done in two parts, one focusing on strength training that may utilize body support and a second part that focuses on balance in a condition with realistic ground reaction forces, such that both muscles and neural control are appropriately trained.

In conclusion, we showed evidence that changing stance width during standing balance control alters neuromechanical interactions, necessitating adjustment of postural set and neural feedback gain to produce similar CoM motion. We showed that changes in geometry affect both postural set and neural feedback, while changes in body mass only affect delayed

neural feedback. We also found that changes in neural feedback are not cued to changes in inertia for the conditions we studied. Finally, we showed that these phenomena were observed across different perturbation magnitudes, stance widths and mass conditions. We believe that these data provide important insights into how sensorimotor feedback is changed to account for alterations in biomechanics and show the importance of neuromechanical interactions for stable balance. Thus, stability of movement may be the reason behavior is similar, however the subtle differences that make our movements unique are likely due to a little bit of biomechanics and a little bit of neural control.

CHAPTER VI

CONCLUSION

6.1 Stable covariation of biomechanical and neural factors are necessary for healthy standing balance

This thesis argued that for stable behavior both neural control and biomechanical configuration must covary in a stable manner. A conclusion that is often made by those who study biomechanics is the apparent dictum of form following function. Studying the curvature of articular surfaces, the muscle physiology and even the microstructure of bone all relate to a functional purpose for efficient movement. Evidence of the importance of biomechanics in motor behavior is exemplified by passive dynamic walkers [79], resonance of feeding apparatus in aplysia [154] and multi-leg interaction in cockroaches running over rough terrain [118]. Therefore, form of the biomechanics is expected to have significant effects on neural control [136]. Certainly the converse is also true, without neural input driving musculature even simple movement would not be possible.

I first showed that simple changes in configuration, such as stance width drive changes in neural control to maintain stability. My model demonstrated that the increase in stance width allows for mechanical leverage at the hip to increase, allowing greater torque generation about the center of mass. A wider stance thus lessens the muscular effort required for balance control, which may allow a subject to resist larger perturbations. However, my results demonstrated that this increase in functional stability was only possible when accompanied by appropriately scaled delayed neural feedback. The same mechanical effects that allowed for reduced effort and larger responses to perturbations in wide stance also increased the inherent instability of the musculoskeletal system and limited the set of feasible stable feedback gains at wide stance. This was important, because it showed that the perception

of increased stability at wide stance is not simply due to changes in the biomechanics of the body, but predicated on the requisite flexibility and appropriate response of the neural system.

I also used our model to show the extent that neural control can compensate for changes in biomechanics and, conversely, how configuration can compensate for changes in neural control. I showed that time to peak torque can be increased through many model parameters: lengthened neural delay, narrowed stance width, increased position feedback, or decreased velocity feedback. The increase in time to peak torque from one parameter could then be compensated by commensurate changes in others. I showed that for the case where neural feedback delay was increased changes in time to peak torque could be compensated by either increasing velocity feedback without changing stance width, or narrowing stance width without changing feedback gains.

Using an experimental paradigm I provided evidence of changes in neuromuscular control to account for altered configuration of the body. These observations showed that increasing the mass of the torso and altering the location of the CoM had little effect on the kinematic responses of the subjects' CoM. Using our model to interpret these results we found that postural set is likely updated in response to changes in stance width while delayed neural feedback is updated with changes in both body mass and stance width. Furthermore, our results showed that the similar responses in different biomechanical contexts could be explained by changes in neural control that complemented changes in biomechanics to result in a consistent level of system stability. This confirmed previous work showing that changes in arm impedance occur in unstable environments [98, 46, 111] and those changes can be achieved through muscle activity [64] as well as limb configuration [135]. In short, stable behavior requires neural and biomechanical systems to stably interact and deficiencies in one may be compensated through changes in the other.

6.2 Clinical relevance

This work was scientifically motivated to determine how changes in either neural or biomechanical configuration might affect the behavior of standing balance. However, the results

show a promising direction for improving clinical diagnosis and rehabilitation for a variety of balance disorders from both the biomechanical and neurological side. First, the model fits and stability radius technique provide a way to quantitatively measure balance stability and separate out possible differences in either biomechanics or neural control that may be contributing to a balance deficiency. There are many subjective measures to quantify balance performance (Berg Balance Scale, Brunel Balance Assessment, etc) and a handful of quantitative models [93, 94], but these tests do not separate biomechanical effects from neural effects on balance deficiency. The ability to have tools that can predict these differences in balance stability is an important addition to previous work to identify different sources of sensorimotor deficiency [88, 99].

This thesis shows that changes in stance width can significantly impact stability of standing balance and affects how neural control responds to perturbation. Since stance width is a conceivably simple behavior to alter, understanding the optimal stance width for improving stability for a patient could have significant consequences. Changes in neural gain are reported for many neurological populations [52, 9, 23], and it may be conceivable to offset some of these effects by adopting a different posture. For example, damage to the basal ganglia in Parkinson's disease may impair the ability to modify postural muscle responses in response to changing postural configurations. Parkinson subjects are unable to modulate the muscle activity evoked during standing balance perturbation across different stance widths [24]. Parkinson's subjects can maintain balance to postural perturbation when standing, but persist in activating leg muscle when subsequently seated [50]. Moreover, Parkinson subjects have characteristically stiff joint responses to perturbations [47]. These observations can be interpreted as an inability to adjust feedback gains associated with changing biomechanical constraints [60]. Stiffening may be the result of increased feedback gains, which our model suggests are less stable in wide stance. Thus, patients with Parkinson's disease may select narrow stance to compensate for inflexible high gains. Also, it has been observed that stance width decreases as people age [80, 124]. Sensorimotor delay has been reported to lengthen with aging [151] and the four-bar model predicts that this should result in decreased feedback gains [2] due to smaller feasible feedback gains for maintaining stability. Therefore, it

may be advisable for subjects with known balance deficits to monitor their stance width to help improve their stability in the context of reduced neural flexibility. Further, o Another possible compensation to increased delay may be to decrease stance width, which has been observed in elderly populations [80, 124].

In a similar vein, changes in mass may also have consequences on neural feedback and stability. In the obese, both mass and stance width are increased [106] and the increase in stance width with increased feedback gains necessary to accommodate increase in mass may pose a threat to the stability of these individuals. Therefore, since neural control is likely altered it may be important to consider possible residual neural control patterns that may persist as individuals exercise and lose weight, which may affect their balance. This may be most important if long-term adaptation of neural feedback to changes is slow compared to biomechanical changes in postural configuration, such as in during pregnancy and postpartum. Reports of decreased stability in balance postpartum have been reported. During pregnancy, stance width increases gradually and frontal plane sway remains consistent. However, shortly after delivery, preferred stance width returns to pre-pregnancy width and frontal plane sway increases [54]. The decrease in stability postpartum may be due to using low feedback gains appropriate for wide stance at the preferred stance width, generating a transient aftereffect [112] of instability while the neural gains must re-adapt to the preferred configuration. In cases of rapid weight loss, it may be important to enforce a slow return of posture to accommodate adaptation of neural feedback gains to appropriately matched levels.

Finally, this study suggests that changes in body mass affect neural feedback, which may have critical implications for rehabilitation strategies that implement reduced body weight. Gait rehabilitation strategies that utilize weight support devices have the advantage of providing support for individuals with reduced strength and motor coordination. Unfortunately, the reduced body weight removes cues from ground reaction forces that may be important for balance. This may be one reason for poor outcomes when rehabilitating subjects with weight support devices who suffer from spinal cord injury [147], stroke [63], or multiple sclerosis [140]. Therefore, rehabilitation of these individuals may be significantly improved if rehabilitation is done such that both muscles and neural control are appropriately trained. This

might be achieved by first focusing on strength training that may utilize body support and a then training balance in conditions with realistic ground reaction forces.

6.3 Future work

All future work that I pursue stemming from this thesis will be influenced by the research philosophy learned here about the power of combining modeling, experimentation and analysis. The simple analytic model of frontal plane standing balance provides a spring board for a wide array of possible experiments to test neuromechanical interactions and their effect on behavior. I have also developed stability radius as a quantitative tool that promises an useful technique for analyzing and comparing the stability of different neuromechanical systems and conditions. Opportunities exist for extending this work both depth-wise and breadth-wise.

Many questions remain from chapter 3 about delayed responses due to aging. Behavioral responses were explored in the context of joint torque, but an equally important question would be to perform the same analysis and examine the effects on the observed CoM kinematics. Furthermore, a question raised by this investigation that seems critically relevant is whether the observed decrease in stance width with the increase in age actually corresponded to a change in the stability of the individual. An obvious change would be to repeat the experiments with the subjects restricted to specified stance widths. Using the techniques from chapter 2 feedback gains could be determined based on the CoM response and using stability radius from chapter 4 to compare the stability of the individuals.

There is still a considerable amount left to develop for the stability radius as a method. While not immediately useful for postural tasks, an obvious extension would be to extend stability radius to describe locomotor tasks that may have limit cycles. This would require formulating the problem in terms of Floquet analysis. Furthermore, the stability radius technique as it was presented in chapter 4 considers the most conservative case, where any perturbation could possibly lead to instability. Obvious extensions of this would be to restrict the set of possible perturbations to external environmental forces or specific model parameters. Work on structured perturbations has already been done for non-delayed systems [42],

so extending this may be straightforward.

Changes in neural control elicited from altered stance width and inertia likely have significant consequences on stability. The data from chapter 5 is ripe for fitting the model as in chapter 2 and using stability radius from chapter 4 to determine the relative changes in stability across the different conditions. Preliminary work towards this goal has been shown that this is feasible in appendix B. Furthermore, it would be interesting to see if differences in anthropometrics and preferred stance width relate to any differences in stability between the subjects. Simply, did subjects prefer their most stable posture?

A glaring hole in all of these studies is the lack of analysis of electromyographic (EMG) data. All of the studies that were analyzed in this thesis have corresponding muscle activity recorded; however, none of the results made it into the thesis because they were too preliminary. A significant amount of analysis remains to examine how changes in muscle activity relate to changes in predicted feedback gain and postural set. This data may help to answer questions about whether variability in muscle activity is constrained by feasible feedback gains as is suggested in chapter 2. It may also highlight whether neural delay or neural feedback is most affected with increased age as was brought up in chapter 3. Finally, questions of changes in postural set and neural feedback raised in chapter 5 may be better answered by looking at muscle activity before and during the response to the postural perturbation.

Further depth-wise investigation includes anchoring the template four-bar linkage model into a more realistic and detailed musculoskeletal model [31]. The four-bar model's most obvious deficiency is an inability to take a step. Some work to correct this has been started [13]. In addition, a fully articulated model would allow predictive simulations to test differences in stability if control were local (joint based), task level (CoM based), or hierarchical (both joint and CoM based).

Breadth-wise extension is also obvious; these methods are directly applicable to pathological populations. The experimental studies in this thesis focused on healthy populations; however, the true benefit of studying postural stability will surely come from those populations where stability is reduced. This also has two distinct directions: the first, populations with biomechanical deficiencies and the second, those with neurological deficiencies. It may

be possible to predict changes in stability due to factors affecting neural control that are accompanied with aging and neuropathies such as stroke and Parkinson's disease. Conversely, the four-bar model can be used to predict changes in postural stability due to altered strength and configuration, which could be used to explore how biomechanical pathologies such as ligament deficiency, arthritis, and amputation affect postural stability.

In general, the framework of modeling, experimentation and analysis is a powerful method for understanding complex systems holistically. With a simple model and relative stability metric a vast array of experimental questions pertaining to neuromechanical principles may be interpreted that span from understanding evolutionary principles of form and function to developing better control for robotic devices. There is much work left to be done, so while this document must end, really it is just the beginning.

APPENDIX A

FOUR-BAR LINKAGE MODEL

A.1 Symbols

COM	center-of-mass
k_p	delayed position feedback gain
k_v	delayed velocity feedback gain
g	earth's gravitational acceleration
S	stance width
W	hip width
L	leg length
L_{COM}	length from ankle to center-of-mass of leg
H_{COM}	vertical distance from hip center to center-of-mass of torso segment
t	time
τ	delay parameter
q_A	ankle angle
I	non-linear model inertia
Q	non-linear model centripetal and coriolis terms
T	non-linear model joint torques
P	non-linear model perturbation terms
G	non-linear model gravitational terms
C_P	non-linear model configuration dependent coefficient for perturbation
I_e	linearized model inertia
G_e	linearized model gravitational terms
${}^iC$	linearized model configuration dependent coefficient for feedback

A.2 Parameters

Table A.1: Anthropometric data for four-bar linkage model of human standing

Description	Symbol	Value	Unit
Nominal human mass	M	70	kg
Nominal human height	H	1.8	m
Leg mass	m_{leg}	$0.161M$	kg
Leg length	L_{leg}	$0.630H$	m
Leg CoM w.r.t. ankle	$L_{C_{leg}}$	$0.293H$	m
Leg inertia w.r.t. CoM	I_{leg}	$0.030MH^2$	$kg \cdot m^2$
Trunk mass	m_{trunk}	$0.678M$	kg
Trunk CoM w.r.t. hip joint	$L_{C_{trunk}}$	$0.108H$	m
Trunk inertia w.r.t. CoM	I_{trunk}	$0.020MH^2$	$kg \cdot m^2$
Width between hip joints	W	$0.134H$	m

A.3 Model

The four-bar linkage model was a single degree-of-freedom system with the ankle angle, q_A , selected as the generalized coordinate. The form of the equation-of-motion was separated into configuration dependent inertia terms, I, centripetal and coriolis terms, V, and gravitational terms, G.

$$I(q_A(t))\ddot{q}_A(t) + Q(q_A(t), \dot{q}_A(t)) + G(q_A(t)) = T(q_A(t-\tau), \dot{q}_A(t-\tau)) + P(q_A(t), t) \tag{A.1}$$

Generalized forces applied to the model were divided into joint torques, T, and perturbations, P. The joint torque was dependent on delayed position and velocity values of the feedback signal, where the delay was signified by τ. The platform perturbation, (A.2), was applied as a generalized force with a configuration dependent inertia term, C_p, and an acceleration profile, a. When experimentally measured accelerations were unavailable the acceleration term consisted of two Gaussian pulses with opposite direction. The pulses were 40 ms wide (ρ), spaced 500 ms apart ($t_f - t_o$) and had amplitudes ranging from 0.1-0.5 g (A).

$$P(q_A(t), t) = C_p(q_A(t))\, a(t) = C_p(q_A(t))\, A \left(e^{-\frac{(t-t_o)^2}{2\rho^2}} - e^{-\frac{(t-t_f)^2}{2\rho^2}} \right) \tag{A.2}$$

A.4 Linearization

For the stability analysis and sensitivity of parameters the equations-of-motion with perturbation forces removed, (A.1), were linearized by taking the first order Taylor series expansion about an equilibrium. The equilibrium angle of the ankle was defined with (A.3), where W was the hip width, S was the stance width and L was the leg length.

$$q_{A_o} = \arccos\left(\frac{S-W}{2L}\right) \tag{A.3}$$

The equations-of-motion were then expressed as linear relations, (A.4), with respect to the generalized coordinate states and their delayed counterparts. Linearized inertial, I_e, and gravitational, G_e, terms were then expressed as constant coefficients for a specified configuration and the coriolis terms, Q, vanished.

$$I_e \ddot{q}_A(t) - G_e q_A(t) = T_i \tag{A.4}$$

The linearized inertia, (A.7), was represented as a single lumped value dependent on stance width (S) and the subject specific leg and trunk masses (m_{leg}, m_{trunk}), inertias (I_{leg}, I_{trunk}) and geometry (W, L, L_{COM}, H_{COM}).

$$\delta = S - W \tag{A.5}$$

$$\eta = \frac{1}{2}\sqrt{4L^2 - \delta^2} \tag{A.6}$$

$$I_e = 2\left(m_{leg}L_{COM}^2 + I_{leg}\right) + \frac{1}{W^2}\left[m_{trunk}\left(H_{COM}\delta - W\eta\right)^2 + I_{trunk}\delta^2\right] \tag{A.7}$$

Similarly, the linearized gravitational stiffness, (A.8), was dependent on subject specific mass and geometry as well as stance width.

$$G_e = \left(\frac{m_{trunk}\left(H_{COM}\delta^2\right)}{W^2} - \frac{\left(2L_{COM}m_{leg} + L m_{trunk}\right)\left(\delta\eta^2 - L^2 S\right)}{L W \eta}\right) g \tag{A.8}$$

The linearized expression for the generalized torque, (A.9), was written in terms of the feedback law and a configuration dependent term, ${}^iC$, that was specific to each type of feedback signal. For the following equations the superscript i is a substitute for either hip or COM feedback signals.

$$T = -{}^iC\frac{S}{W}\left({}^ik_p q_A(t-\tau) + {}^ik_v \dot{q}_A(t-\tau)\right) \tag{A.9}$$

Two types of feedback signals were used, when hip angular position and velocity was used, the configuration dependent coefficient, ${}^{hip}C$, was dependent only on the width of stance and distance between the hips, (A.10).

$$ {}^{hip}C = \frac{S}{W} \tag{A.10} $$

When the center-of-mass excursion was used as a feedback signal the expression for the configuration dependent coefficient, ${}^{com}C$, was more complex and was related to the height of the center-of-mass, (A.11).

$$ {}^{com}C = \frac{H_{COM} L\, m_{trunk}\, \delta - W \left(L\, m_{trunk} + 2 L_{COM}\, m_{leg}\right) \eta}{L W \left(2 m_{leg} + m_{trunk}\right)} \tag{A.11} $$

A.5 Stability boundaries

The closed-loop stability of the delayed feedback system was accomplished by analyzing the system about equilibrium, (A.3), and assuming exponential solutions to the differential equation. This resulted in the development of the following characteristic equation, (A.12).

$$ I_e \lambda^2 - G_e + {}^{i}C \left(\frac{S}{W}\right) \left[k_p e^{-\lambda\tau} + k_v \lambda e^{-\lambda\tau}\right] = 0 \tag{A.12} $$

The solutions to the characteristic equation become unstable when the real part transitions from negative to positive. Stability was then determined by finding solutions, values of $\lambda = r + j\omega$, to the characteristic equation that had strictly zero real part, $r = 0$. These solutions therefore were described as curves parameterized by the magnitude of the imaginary part, ω.

The left-hand boundary, (A.13), represented a lower limit on delayed position feedback gain, k_p, described by a fold bifurcation. The functional consequence of this limit corresponded to feedback stiffness, k_p, of the delayed position feedback gain being unable to counteract the destabilizing gravitational stiffness, G_e.

$$ LHB \equiv \begin{cases} {}^{i}k_p = & \frac{1}{{}^{i}C} \frac{W}{S} G_e \\ {}^{i}k_v = & \mathbb{R} \end{cases} \tag{A.13} $$

The right-hand boundary, (A.14), restricted both position and velocity feedback gains and was described by a Hopf bifurcation. This upper boundary was a consequence of the feedback

delay and functionally represented an instability due to over-correction.

$$RHB \equiv \begin{cases} {}^{i}k_p = & \frac{1}{{}^{i}C}\left(I_e\omega^2 + G_e\right)\frac{W\cos(\tau\omega)}{S} \\ {}^{i}k_v = & \frac{1}{{}^{i}C}\left(I_e\omega^2 + G_e\right)\frac{W\sin(\tau\omega)}{\omega S} \end{cases} \tag{A.14}$$

Finally, an upper limit on the length of delay was found for which there were no feedback gain values that were stable, (A.15). This occurred when the right-hand boundary was reduced to a single point.

$$\tau_{max} = \sqrt{\frac{2I_e}{G_e}} \tag{A.15}$$

A.6 Non-delayed feedback

The four-bar linkage with delayed feedback may be extended to include non-delayed feedback terms. This modification includes additional torque components associated with passive stiffness, k, and damping, b, and the linearized equations of motion take on the form below.

$$I_e\ddot{q}_A(t) - G_e q_A(t) = -{}^{i}C\frac{S}{W}\left({}^{i}k_p q_A(t-\tau) + {}^{i}k_v\dot{q}_A(t-\tau)\right) - \frac{S^2}{W^2}\left(k q_A(t) + b\dot{q}_A(t)\right) \tag{A.16}$$

The stability boundaries in terms of the delayed feedback gains are therefore found to have the following form.

$$LHB_{passive} \equiv \begin{cases} {}^{i}k_p = & \frac{1}{{}^{i}C}\left[\frac{W}{S}G_e - \frac{S}{W}k\right] \\ {}^{i}k_v = & \mathbb{R} \end{cases} \tag{A.17}$$

$$RHB_{passive} \equiv \begin{cases} {}^{i}k_p = & \frac{1}{{}^{i}C}\left[\left(I_e\omega^2 + G_e\right)\frac{W\cos(\tau\omega)}{S} - \frac{S}{W}\left(k\cos(\tau\omega) - b\omega\sin(\tau\omega)\right)\right] \\ {}^{i}k_v = & \frac{1}{{}^{i}C}\left[\left(I_e\omega^2 + G_e\right)\frac{W\sin(\tau\omega)}{\omega S} - \frac{1}{\omega}\frac{S}{W}\left(k\sin(\tau\omega) + b\omega\cos(\tau\omega)\right)\right] \end{cases} \tag{A.18}$$

APPENDIX B

MODEL FITS TO EXPERIMENTAL DATA AND PRELIMINARY STABILITY RADIUS RESULTS

B.1 Summary

Co-variation of biomechanical and neural parameters are likely required in order to achieve stability for a particular behavior. Changes in stability may be driven by changes in posture, such as standing with a wider stance on a moving train or adjusting arm angles when reaching in unstable environments [135]. Changes in stability may also be driven by muscle co-contractions, which have been observed to affect arm impedance within the same arm configuration when generating forces in an unstable environment [98, 46, 111]. Changes in neural control and biomechanical configuration is also observed to occur concomitantly. For example, in the case of translational perturbations increased stance width is accompanied by decreased muscle activity [39], which, based on our previous model [7], may be a necessary condition for maintaining stability. Further evidence of stability driving simultaneous changes in neural and biomechanical parameters has been reported by research in upper-extremity control where both muscle activity and arm configuration is altered in a way to reduce sensitivity to parameter variation in dexterous tasks [122, 5]. It has previously been difficult to quantify how these changes might affect stability, as stability reflects the dynamical behavior of the body, such as limb impedance, which can be altered by both muscle activity [64] as well as limb configuration [135]. Therefore, to quantify the importance of neuromechanical interactions on stable behavior this appendix provides evidence of how a particular pairing of biomechanical context and neural control state would result in greater or less stability for the task of standing balance.

This appendix serves as an addendum to chapter 5 with the purpose of providing preliminary analysis of those data using the model fitting procedures of chapter 2 and the stability comparison metric of chapter 4. The principle goal was to show whether changes in stance width, which have been shown to be accompanied with changes in feedback gains (chapter 2), result in changes in stability. The central hypothesis was that changes in biomechanical context (different stance widths or mass) would be matched by changes in feedback gain that result in similar levels of stability across conditions.

The results of the preliminary analysis showed that across stance widths there was a similar level of stability, but there was a trend of greater robustness at wider stance. However, increased mass, while accompanied with changes in feedback gains, showed a marked decrease in relative stability within the same stance width. Finally, when conditions were set such that inertia was matched but weight and stance width were different, the wide-weighted condition was less stable than the narrow-unweighted condition. When subjects were analyzed separately it appeared that these trends still held even though the relative stability between subjects was observed to vary considerably.

B.2 Methods

B.2.1 Data analyzed

A subset of the data acquired in chapter 5 was used that consisted of trials from all subjects (n=12) from perturbations in the leftward direction with magnitude of 24 cm, 15 cm/s and 0.15 g. This included three stance widths of narrow (10 cm), preferred, and wide (30 cm) as well as unweighted and weighted (20% additional mass) conditions. Trials that had stepping responses and fits with a cost of greater than 15 were removed. Each condition had at least 4 repeats with some conditions having more, thus the paired down subset spanned all conditions with 389 trials (12 x 3 x 2 x 4 = 288).

B.2.2 Model fitting

The extended version of our previously described four-bar linkage model that included non-delayed position and velocity feedback to model postural set and delayed position and velocity

feedback for neural control was used to fit to experimental data to identify changes in feedback parameters across subjects and conditions (See Appendix A: Eq. A.16)[7]. Leg length, hip width and torso height of the model were scaled to each subject's anthropometric measurements and used with anthropometric tables to determine segment CoM and inertia [148]. Muscular force was modeled as a lumped term and applied with constant moment arms as torque about each hip joint. Hip torque was generated as non-delayed and delayed feedback of the hip joint angle with fixed gains on position and velocity. The delay was selected to be a single lumped value of 120 ms to account for neural transmission from sensation to actuation and mechanical actuation. Numerical simulation of the equations of motion was performed in Matlab (Mathworks, Natick, MA). Integration was performed with the explicit trapezoidal rule with a step size of 1 ms, zero initial conditions, and zero-valued state history. Center-of-mass trajectories and ground reaction forces were recorded.

The model was fit to experimental data to identify changes in feedback parameters across subjects and conditions. To determine non-delayed and delayed model feedback parameters, simulated CoM position and velocity trajectories were fit to each experimental trial through optimization with the perturbation applied to the four-bar linkage as an inertial acceleration of the ground recorded from the measured platform acceleration. A cost function (Eq. B.1c) was defined using error between simulated and experimental center-of-mass trajectories with penalties on absolute (weight of 1) and sum-squared error (weight of 10); error in position was weighted twice the error in velocity; and the errors summed.

$$e_k = sim_k - exp_k \tag{B.1a}$$

$$J_i = 10\left(\sum e_k\right)^2 + \max(|e_k|) \tag{B.1b}$$

$$J = 2J_{pos} + J_{vel} \tag{B.1c}$$

To produce unique feedback gain values, optimization was performed in two steps. The first optimization kept non-delayed feedback gains fixed at zero-value and used only the delayed feedback gains to fit 2.5 s of simulation. To identify non-delayed feedback gains, the second optimization kept delayed feedback gains fixed to the values found in the first optimization and used the delayed feedback gains to improve the fit. Optimization was achieved

by using a grid-search with bounds set on delayed gains within the feasible range and non-delayed gains to be positive and less than the found delayed feedback gains.

B.2.3 Feedback gain and stability analysis

Relative stability was calculated using the stability radius method described in chapter 4. Linearized equations of motion (Appendix A: Eq. A.16) were used to formulate system matrices (Eq. B.2) from the anthropometric properties and found feedback gains discovered from the fit procedure described above. Using a grid search the minimization for equation 4.21 was solved to determine the stability radius for each fit trial. The bounds for the grid search were restricted to be strictly positive imaginary values with an upper bound (UB=1000) heuristically set to two orders of magnitude larger than the largest imaginary value observed from the first 10 eigenvalues.

$$\frac{d}{dt}\mathbf{x}(t) = \frac{1}{I_e}\begin{bmatrix} 0 & I_e \\ G_e - k\left(\frac{S}{W}\right)^2 & -b\left(\frac{S}{W}\right)^2 \end{bmatrix}\mathbf{x}(t) - \frac{1}{I_e}\left(\frac{S}{W}\right)^2\begin{bmatrix} 0 & 0 \\ k_p & k_v \end{bmatrix}\mathbf{x}(t-\tau) \qquad \text{(B.2)}$$

Three experimental conditions were analyzed for changes in non-delayed feedback gain, delayed feedback gain and stability radius. Across subjects, the effect of increased stance width was assessed for trials having subjects in the unweighted condition, statistical tests were performed between the narrow and wide stance width. The effect of weight condition was assessed for trials having all subjects at preferred stance width. Finally, we compared CoM excursion in conditions where inertia was similar across stance widths by grouping trials by unweighted, narrow stance and weighted, preferred stance. For each variable of interest statistical significance was determined using a Students' t-test (α=0.05) to reject the null hypothesis that the two means within a group were not from the same distribution.

B.3 Results

No statistical difference in stability radius was observed between narrow and wide unweighted conditions (p=0.19). However, wide stance had a trend of slightly greater stability radius compared to narrow stance. Increased mass significantly decreased (p<1e-5) the relative stability between the weighted and unweighted condition at preferred stance (Figure B.1). Stability

Table B.1: Average feedback gain and stability results from fitting the fourbar model to experimental trials of narrow (N), preferred (P), and wide (W) for unweighted (U) and weighted (W) conditions.

Cond.	k N-m/rad	b N-m/rad/s	k_p N-m/rad	k_v N-m/rad/s	stab. rad.
NU	82.0 ± 133.5	144.5 ± 123.2	3133.2 ± 1548.3	613.2 ± 294.8	0.52 ± 0.12
PU	83.3 ± 85.9	74.0 ± 60.1	702.2 ± 338.7	112.7 ± 57.4	0.53 ± 0.15
PW	75.8 ± 109.8	75.4 ± 74.1	730.7 ± 412.9	130.2 ± 73.6	0.39 ± 0.17
WU	68.3 ± 58.5	37.8 ± 21.7	373.4 ± 139.7	67.4 ± 42.3	0.57 ± 0.24

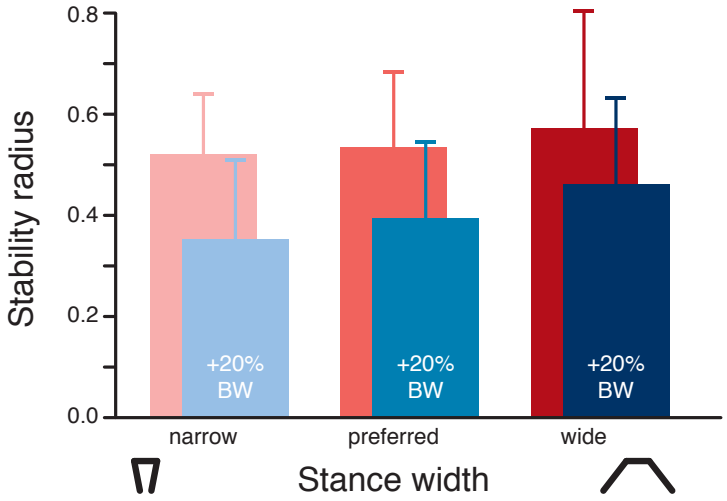

Figure B.1: Stability radius predicts decreased stability with increased body mass across stance widths.

was also reduced (p<1e-4) in the wide, weighted condition compared to the inertia matched condition of narrow, unweighted. A representative subject had similar trends in stability radius across the conditions (NU: 0.50±0.03, PU: 0.53±0.10, PW: 0.33±0.17, WU: 0.67±0.04). Stability radius at the preferred stance width in the unweighted condition varied from 0.25-0.70 across subjects (Figure B.2).

The fitted non-delayed feedback gains appeared to be insensitive to changes in mass and slightly affected by changes in stance width. Non-delayed position feedback did not significantly change across any of the conditions (p>0.47). Non-delayed velocity feedback was sensitive to changes in stance width and decreased significantly from narrow to wide stance width (p<1e-6). However, non-delayed velocity feedback did not significantly change with increased mass (p=0.91). Non-delayed position feedback gains were found to be an order of

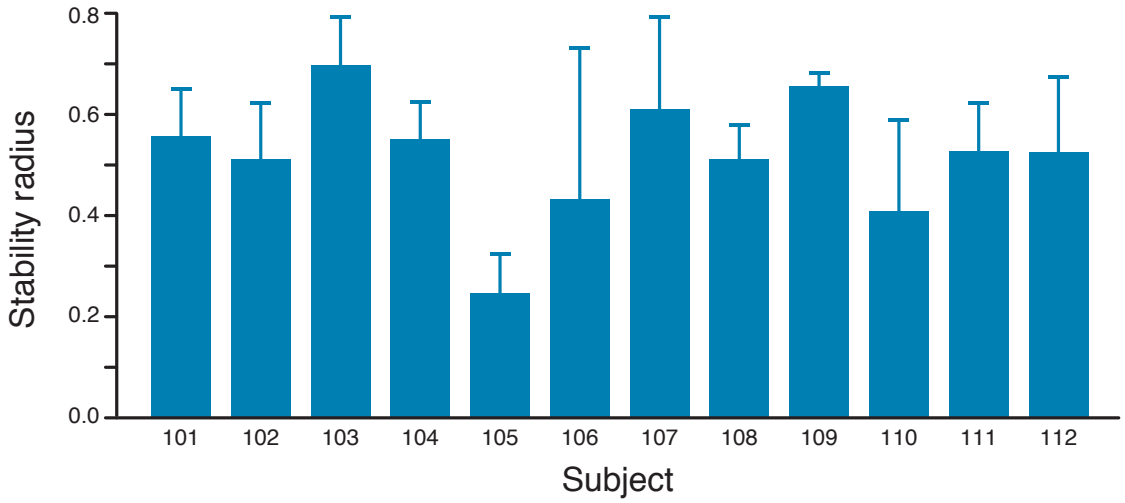

Figure B.2: Stability radius varies across subjects. Shown for the preferred stance width the median stability radius across all trials within the low-level, leftward perturbations shows different levels of stability and variance across subjects.

magnitude smaller than the delayed position feedback gains, suggesting only minimal effects on behavioral response. Conversely, non-delayed velocity feedback were of a similar order of magnitude to the delayed velocity feedback gains, suggesting relatively higher importance on their effect on behavior.

Delayed feedback gains fitted to the experimental data increased as stance width decreased and mass increased. There was a statistically significant increase in feedback gain between wide and narrow stance in both delayed position ($p<1e-6$) and velocity ($p<1e-6$) feedback gains. While not statistically significant, delayed position ($p=0.67$) and velocity ($p=0.14$) increased slightly with the increase in body mass.

REFERENCES

[1] ACKLAND, D. C., LIN, Y.-C., and PANDY, M. G., "Sensitivity of model predictions of muscle function to changes in moment arms and muscle-tendon properties: a Monte-Carlo analysis.," *Journal of biomechanics*, vol. 45, pp. 1463–71, May 2012.

[2] ALLUM, J. H. J., CARPENTER, M. G., HONEGGER, F., ADKIN, A. L., and BLOEM, B. R., "Age-dependent variations in the directional sensitivity of balance corrections and compensatory arm movements in man," *The Journal of Physiology*, vol. 542, pp. 643–663, May 2002.

[3] ANDERSON, F. C. and PANDY, M. G., "Static and dynamic optimization solutions for gait are practically equivalent.," *Journal of biomechanics*, vol. 34, pp. 153–61, Feb. 2001.

[4] BAKKER, M., ALLUM, J. H. J., VISSER, J. E., GRÜNEBERG, C., VAN DE WARRENBURG, B. P., KREMER, B. H. P., and BLOEM, B. R., "Postural responses to multidirectional stance perturbations in cerebellar ataxia.," *Experimental Neurology*, vol. 202, pp. 21–35, Nov. 2006.

[5] BAYS, P. M. and WOLPERT, D. M., "Computational principles of sensorimotor control that minimize uncertainty and variability.," *The Journal of physiology*, vol. 578, pp. 387–96, Jan. 2007.

[6] BERNSTEIN, N., *The co-ordination and regulation of movements*. London: Pergamon Press Ltd., 1967.

[7] BINGHAM, J. T., CHOI, J. T., and TING, L. H., "Stability in a frontal plane model of balance requires coupled changes to postural configuration and neural feedback control," *J Neurophysiol*, vol. 106, pp. 437–448, July 2011.

[8] BLACK, H. S., "Stabilized Feed-Back Amplifiers," *Transactions of the American Institute of Electrical Engineers*, vol. 53, pp. 114–120, Jan. 1934.

[9] BLOOD, A. J., "New hypotheses about postural control support the notion that all dystonias are manifestations of excessive brain postural function," *Bioscience Hypotheses*, vol. 1, no. 1, pp. 14–25, 2008.

[10] BOLING, M. C., PADUA, D. A., and ALEXANDER CREIGHTON, R., "Concentric and eccentric torque of the hip musculature in individuals with and without patellofemoral pain.," *Journal of athletic training*, vol. 44, no. 1, pp. 7–13, 2009.

[11] BOSCO, G. and POPPELE, R. E., "Representation of multiple kinematic parameters of the cat hindlimb in spinocerebellar activity," *Journal of Neurophysiology*, vol. 78, no. 3, pp. 1421–1432, 1997.

[12] BUNDERSON, N. E., MCKAY, J. L., TING, L. H., and BURKHOLDER, T. J., "Directional constraint of endpoint force emerges from hindlimb anatomy," *J Exp Biol*, vol. 213, no. Pt 12, pp. 2131–2141, 2010.

[13] BUNDERSON, N. E., BINGHAM, J. T., SOHN, M. H., TING, L. H., and BURKHOLDER, T. J., "Neuromechanic: A computational platform for simulation and analysis of the neural control of movement.," *International journal for numerical methods in biomedical engineering*, vol. 28, pp. 1015–27, Oct. 2012.

[14] BUNDERSON, N. E., BURKHOLDER, T. J., and TING, L. H., "Reduction of neuromuscular redundancy for postural force generation using an intrinsic stability criterion.," *Journal of biomechanics*, vol. 41, pp. 1537–44, Jan. 2008.

[15] CDC, "Injury Prevention & Control: Data & Statistics (WISQARS)," 2012.

[16] CENCIARINI, M., LOUGHLIN, P. J., SPARTO, P. J., and REDFERN, M. S., "Stiffness and damping in postural control increase with age.," *IEEE transactions on bio-medical engineering*, vol. 57, pp. 267–75, Feb. 2010.

[17] CHANG, Y. H., HUANG, H. W., HAMERSKI, C. M., and KRAM, R., "The independent effects of gravity and inertia on running mechanics," *J Exp Biol*, vol. 203, no. Pt 2, pp. 229–238, 2000.

[18] COHEN, R. G. and STERNAD, D., "State space analysis of timing: exploiting task redundancy to reduce sensitivity to timing.," *Journal of neurophysiology*, vol. 107, pp. 618–27, Jan. 2012.

[19] CUTHBERT, S. C. and GOODHEART, G. J., "On the reliability and validity of manual muscle testing: a literature review.," *Chiropractic & osteopathy*, vol. 15, p. 4, Jan. 2007.

[20] DE FREITAS, P. B., KNIGHT, C. A., and BARELA, J. A., "Postural reactions following forward platform perturbation in young, middle-age, and old adults.," *Journal of electromyography and kinesiology : official journal of the International Society of Electrophysiological Kinesiology*, vol. 20, pp. 693–700, Aug. 2010.

[21] DELIAGINA, T. G., ZELENIN, P. V., BELOOZEROVA, I. N., and ORLOVSKY, G. N., "Nervous mechanisms controlling body posture," *Physiology & Behavior*, vol. 92, no. 1-2, pp. 148–154, 2007.

[22] DIETZ, V., GOLLHOFER, A., KLEIBER, M., and TRIPPEL, M., "Regulation of bipedal stance: dependency on load receptors," *Experimental Brain Research*, vol. 89, pp. 229–231, Apr. 1992.

[23] DIETZ, V. and SINKJAER, T., "Spastic movement disorder: impaired reflex function and altered muscle mechanics," *The Lancet Neurology*, vol. 6, no. 8, pp. 725–733, 2007.

[24] DIMITROVA, D., HORAK, F. B., and NUTT, J. G., "Postural muscle responses to multidirectional translations in patients with Parkinson's disease.," *Journal of Neurophysiology*, vol. 91, no. 1, pp. 489–501, 2004.

[25] DINGWELL, J. B. and CUSUMANO, J. P., "Nonlinear time series analysis of normal and pathological human walking," *Chaos*, vol. 10, no. 4, pp. 848–863, 2000.

[26] DORF, R. C. and BISHOP, R. H., *Modern Control Systems*. Upper Saddle River, NJ: Prentice-Hall, 9th ed., 2000.

[27] ENGELBORGHS, K., LUZYANINA, T., and ROOSE, D., "Numerical bifurcation analysis of delay differential equations using DDE-BIFTOOL," *ACM Transactions on Mathematical Software*, vol. 28, no. 1, pp. 1–21, 2002.

[28] FERRIS, D. P., LOUIE, M., and FARLEY, C. T., "Running in the real world: adjusting leg stiffness for different surfaces.," *Proceedings. Biological sciences / The Royal Society*, vol. 265, pp. 989–94, June 1998.

[29] FJELDSTAD, C., FJELDSTAD, A. S., ACREE, L. S., NICKEL, K. J., and GARDNER, A. W., "The influence of obesity on falls and quality of life.," *Dynamic medicine : DM*, vol. 7, p. 4, Jan. 2008.

[30] FRANKLIN, D. W., OSU, R., BURDET, E., KAWATO, M., and MILNER, T. E., "Adaptation to Stable and Unstable Dynamics Achieved By Combined Impedance Control and Inverse Dynamics Model," *Journal of Neurophysiology*, vol. 90, no. 5, pp. 3270 –3282, 2003.

[31] FULL, R. J. and KODITSCHEK, D. E., "Templates and anchors: neuromechanical hypotheses of legged locomotion on land.," *The Journal of Experimental Biology*, vol. 202, pp. 3325–32, Dec. 1999.

[32] GENESIO, R., TARTAGLIA, M., and VICINO, A., "On the estimation of asymptotic stability regions: State of the art and new proposals," *IEEE Transactions on Automatic Control*, vol. 30, pp. 747–755, Aug. 1985.

[33] GIESL, P. and WENDLAND, H., "Numerical determination of the basin of attraction for exponentially asymptotically autonomous dynamical systems," *Nonlinear Analysis: Theory, Methods & Applications*, vol. 74, pp. 3191–3203, July 2011.

[34] GOODWORTH, A., CHANDAN, A., CHASE, H., FOSTER, E., FRANCOEUR, H., MICHAUD, J., and TERRY, K., "Stance width influences frontal plane balance responses to centripetal accelerations.," *Gait & posture*, vol. 37, pp. 98–102, Jan. 2013.

[35] GOODWORTH, A. D. and PETERKA, R. J., "Sensorimotor integration for multisegmental frontal plane balance control in humans.," *Journal of neurophysiology*, vol. 107, pp. 12–28, Jan. 2012.

[36] GOODWORTH, A. D. and PETERKA, R. J., "Influence of Stance Width on Frontal Plane Postural Dynamics and Coordination in Human Balance Control.," *Journal of Neurophysiology*, Apr. 2010.

[37] GORDON, J., GHILARDI, M. F., COOPER, S. E., and GHEZ, C., "Accuracy of planar reaching movements. II. Systematic extent errors resulting from inertial anisotropy.," *Experimental brain research. Experimentelle Hirnforschung. Expérimentation cérébrale*, vol. 99, pp. 112–30, Jan. 1994.

[38] HENRY, S. M., FUNG, J., and HORAK, F. B., "EMG responses to maintain stance during multidirectional surface translations.," *Journal of Neurophysiology*, vol. 80, no. 4, pp. 1939–1950, 1998.

[39] HENRY, S. M., FUNG, J., and HORAK, F. B., "Effect of stance width on multidirectional postural responses.," *Journal of neurophysiology*, vol. 85, pp. 559–70, Feb. 2001.

[40] HILL, A. V., "The Heat of Shortening and the Dynamic Constants of Muscle," *Proceedings of the Royal Society of London*, vol. 126, B, no. 843, pp. 136–195, 1938.

[41] HINRICHSEN, D. and PRITCHARD, A., "Stability radii of linear systems," *Systems & Control Letters*, vol. 7, pp. 1–10, Feb. 1986.

[42] HINRICHSEN, D. and PRITCHARD, A., "Stability radius for structured perturbations and the algebraic Riccati equation," *Systems & Control Letters*, vol. 8, pp. 105–113, Dec. 1986.

[43] HINRICHSEN, D. and PRITCHARD, A., "A note on some differences between real and complex stability radii," *Systems & Control Letters*, vol. 14, pp. 401–408, June 1990.

[44] HINRICHSEN, D. and PRITCHARD, A., *Mathematical Systems Theory I: Modelling State Space Analysis, Stability and Robustness*. Berlin, Heidelberg: Springer Verlag, 2nd ed., 2005.

[45] HOCHMAN, S., HAYES, H. B., SPEIGEL, I., and CHANG, Y.-H., "Force-sensitive afferents recruited during stance encode sensory depression in the contralateral swinging limb during locomotion.," *Annals of the New York Academy of Sciences*, vol. 1279, pp. 103–13, Apr. 2013.

[46] HOGAN, N., "The mechanics of multi-joint posture and movement control," *Biological Cybernetics*, vol. 52, no. 5, pp. 315–331, 1985.

[47] HORAK, F. B., DIMITROVA, D., and NUTT, J. G., "Direction-specific postural instability in subjects with Parkinson's disease.," *Experimental Neurology*, vol. 193, no. 2, pp. 504–21, 2005.

[48] HORAK, F. B. and MACPHERSON, J. M., "Postural orientation and equilibrium," in *Handbook of Physiology*, ch. Section 12, pp. 255–292, New York: American Physiological Society, 1996.

[49] HORAK, F. B. and NASHNER, L. M., "Central programming of postural movements: adaptation to altered support-surface configurations.," *Journal of Neurophysiology*, vol. 55, pp. 1369–81, June 1986.

[50] HORAK, F. B., NUTT, J. G., and NASHNER, L. M., "Postural inflexibility in parkinsonian subjects," *Journal of the Neurological Sciences*, vol. 111, no. 1, pp. 46–58, 1992.

[51] HUXLEY, A. F. and SIMMONS, R. M., "Proposed mechanism of force generation in striated muscle," *Nature*, vol. 233, no. 5321, pp. 533–538, 1971.

[52] HYNGSTROM, A. S., JOHNSON, M. D., MILLER, J. F., and HECKMAN, C. J., "Intrinsic electrical properties of spinal motoneurons vary with joint angle," *Nature Neuroscience*, vol. 10, no. 3, pp. 363–369, 2007.

[53] JACOBS, J. V. and HORAK, F. B., "Cortical control of postural responses," *Journal of Neural Transmission*, vol. 114, no. 10, pp. 1339–1348, 2007.

[54] JANG, J., HSIAO, K. T., and HSIAO-WECKSLER, E. T., "Balance (perceived and actual) and preferred stance width during pregnancy," *Clinical Biomechanics (Bristol, Avon)*, vol. 23, no. 4, pp. 468–476, 2008.

[55] KAMINSKI, T. W., PERRIN, D. H., and GANSNEDER, B. M., "Eversion strength analysis of uninjured and functionally unstable ankles.," *Journal of athletic training*, vol. 34, pp. 239–45, July 1999.

[56] KANDEL, E. R., SCHWARTZ, J. H., and JESSELL, T. M., *Principles of neural science*. Columbus, OH: McGraw-Hill, 4th ed., 2000.

[57] KANE, T. R. and LEVINSON, D. A., *Dynamics: Theory and Applications*. Mcgraw-Hill College, 1985.

[58] KHALIL, H. K., *Nonlinear Systems*. Upper Saddle River, NJ: Prentice-Hall, 3rd ed., 2002.

[59] KIM, S., ATKESON, C. G., and PARK, S., "Perturbation-dependent selection of postural feedback gain and its scaling.," *Journal of biomechanics*, vol. 45, pp. 1379–86, May 2012.

[60] KIM, S., HORAK, F. B., CARLSON-KUHTA, P., and PARK, S., "Postural feedback scaling deficits in Parkinson's disease.," *Journal of neurophysiology*, vol. 102, pp. 2910–20, Nov. 2009.

[61] KINGMA, I., TOUSSAINT, H. M., COMMISSARIS, D. A., and SAVELSBERGH, G. J., "Adaptation of center of mass control under microgravity in a whole-body lifting task.," *Experimental brain research. Experimentelle Hirnforschung. Expérimentation cérébrale*, vol. 125, pp. 35–42, Mar. 1999.

[62] KONRADSEN, L., PEURA, G., BEYNNON, B., and RENSTRÖM, P., "Ankle eversion torque response to sudden ankle inversion Torque response in unbraced, braced, and pre-activated situations.," *Journal of orthopaedic research : official publication of the Orthopaedic Research Society*, vol. 23, pp. 315–21, Mar. 2005.

[63] KRISHNAN, C., KOTSAPOUIKIS, D., DHAHER, Y. Y., and RYMER, W. Z., "Reducing Robotic Guidance During Robot-Assisted Gait Training Improves Gait Function: A Case Report on a Stroke Survivor.," *Archives of physical medicine and rehabilitation*, Nov. 2012.

[64] KRUTKY, M. A., RAVICHANDRAN, V. J., TRUMBOWER, R. D., and PERREAULT, E. J., "Interactions between limb and environmental mechanics influence stretch reflex sensitivity in the human arm.," *Journal of neurophysiology*, vol. 103, pp. 429–40, Jan. 2010.

[65] KUO, A. D., "An optimal control model for analyzing human postural balance.," *IEEE Transactions on Bio-medical Engineering*, vol. 42, pp. 87–101, Jan. 1995.

[66] KUO, A. D. and ZAJAC, F., "Human standing posture: multi-joint movement strategies based on biomechanical constraints," *Progress in Brain Research*, vol. 97, pp. 349–358, 1993.

[67] LACKNER, J. R. and DIZIO, P., "Motor control and learning in altered dynamic environments.," *Current opinion in neurobiology*, vol. 15, pp. 653–9, Dec. 2005.

[68] LEHMER, D. H., "A Machine Method for Solving Polynomial Equations," *Journal of the ACM*, vol. 8, pp. 151–162, Apr. 1961.

[69] LOCKHART, D. B. and TING, L. H., "Optimal sensorimotor transformations for balance.," *Nature Neuroscience*, vol. 10, pp. 1329–36, Oct. 2007.

[70] LORAM, I. D. and LAKIE, M., "Direct measurement of human ankle stiffness during quiet standing: the intrinsic mechanical stiffness is insufficient for stability," *The Journal of Physiology*, vol. 545, pp. 1041–1053, Nov. 2002.

[71] MACPHERSON, J. M., FUNG, J., and JACOBS, R., "Postural orientation, equilibrium, and the spinal cord," *Advanced Neurology*, vol. 72, pp. 227–232, 1997.

[72] MAKI, B. E., EDMONDSTONE, M. A., and MCILROY, W. E., "Age-related differences in laterally directed compensatory stepping behavior.," *The Journals of Gerontology. Series A, Biological Sciences and Medical Sciences*, vol. 55, pp. M270–7, May 2000.

[73] MARK, T., MANCHESTER, I., and TEDRAKE, R., "Invariant Funnels Around Trajectories Using Sum-Of-Squares Programming," in *Proceedings of the 18th IFAC World Congress* (SERGIO, B., ed.), no. 1, pp. 9218–9223, Aug. 2011.

[74] MARTIN, J., "State-space measures for stability robustness," *IEEE Transactions on Automatic Control*, vol. 32, pp. 509–512, June 1987.

[75] MASANI, K., VETTE, A. H., KAWASHIMA, N., and POPOVIC, M. R., "Neuromusculoskeletal torque-generation process has a large destabilizing effect on the control mechanism of quiet standing.," *Journal of Neurophysiology*, vol. 100, pp. 1465–75, Sept. 2008.

[76] MASSION, J., POPOV, K., FABRE, J. C., RAGE, P., and GURFINKEL, V., "Is the erect posture in microgravity based on the control of trunk orientation or center of mass position?," *Experimental brain research. Experimentelle Hirnforschung. Expérimentation cérébrale*, vol. 114, pp. 384–9, Apr. 1997.

[77] MATALLANA, L. G., BLANCO, A. M., and BANDONI, J. A., "Estimation of domains of attraction: A global optimization approach," *Mathematical and Computer Modelling*, vol. 52, pp. 574–585, Aug. 2010.

[78] MATRANGOLA, S. L. and MADIGAN, M. L., "The effects of obesity on balance recovery using an ankle strategy.," *Human movement science*, vol. 30, pp. 584–95, June 2011.

[79] MCGEER, T., "Passive Dynamic Walking," *The International Journal of Robotics Research*, vol. 9, pp. 62–82, Apr. 1990.

[80] MCILROY, W. E. and MAKI, B. E., "Preferred placement of the feet during quiet stance: development of a standardized foot placement for balance testing.," *Clinical Biomechanics (Bristol, Avon)*, vol. 12, pp. 66–70, Jan. 1997.

[81] MELZER, I., KURZ, I., and ODDSSON, L. I. E., "A retrospective analysis of balance control parameters in elderly fallers and non-fallers.," *Clinical biomechanics (Bristol, Avon)*, vol. 25, pp. 984–8, Dec. 2010.

[82] MERGNER, T., "A neurological view on reactive human stance control," *Annual Reviews in Control*, vol. 34, pp. 177–198, Dec. 2010.

[83] MERGNER, T., MAURER, C., and PETERKA, R. J., "A multisensory posture control model of human upright stance," *Progress in Brain Research*, vol. 142, pp. 189–201, 2003.

[84] MICHIELS, W., FRIDMAN, E., and NICULESCU, S.-I., "Robustness assessment via stability radii in delay parameters," *International Journal of Robust and Nonlinear Control*, vol. 19, pp. 1405–1426, Sept. 2009.

[85] MICHIELS, W., GREEN, K., WAGENKNECHT, T., and NICULESCU, S.-I., "Pseudospectra and stability radii for analytic matrix functions with application to time-delay systems," *Linear Algebra and its Applications*, vol. 418, pp. 315–335, Oct. 2006.

[86] MICHIELS, W. and NICULESCU, S.-I., *Stability and Stabilization of Time-Delay Systems: An Eigenvalue Approach*. Philidelphia, PA: SIAM, 2007.

[87] MILTON, J. G., CABRERA, J. L., and OHIRA, T., "Unstable dynamical systems: Delays, noise and control," *EPL (Europhysics Letters)*, vol. 83, p. 48001, Aug. 2008.

[88] NASHNER, L. M., BLACK, F. O., and WALL, C., "Adaptation to altered support and visual conditions during stance: patients with vestibular deficits.," *The Journal of neuroscience : the official journal of the Society for Neuroscience*, vol. 2, pp. 536–44, May 1982.

[89] NEPTUNE, R. R., "Optimization algorithm performance in determining optimal controls in human movement analyses.," *Journal of biomechanical engineering*, vol. 121, pp. 249–52, Apr. 1999.

[90] NICHOLS, T. R. and HOUK, J. C., "Improvement in linearity and regulation of stiffness that results from actions of stretch reflex.," *Journal of neurophysiology*, vol. 39, pp. 119–42, Jan. 1976.

[91] NOBLE, J. W. and PRENTICE, S. D., "Adaptation to unilateral change in lower limb mechanical properties during human walking.," *Experimental brain research. Experimentelle Hirnforschung. Expérimentation cérébrale*, vol. 169, pp. 482–95, Mar. 2006.

[92] NORTON, R. L., *Design of Machinery: An introduction to the synthesis and analysis of mechanisms and machines*. New York: McGraw-Hill, 2nd ed., 2001.

[93] PAI, Y.-C., MAKI, B. E., IQBAL, K., MCILROY, W. E., and PERRY, S. D., "Thresholds for step initiation induced by support-surface translation: a dynamic center-of-mass model provides much better prediction than a static model.," *Journal of Biomechanics*, vol. 33, pp. 387–92, Mar. 2000.

[94] PAI, Y.-C. and PATTON, J. L., "Center of mass velocity-position predictions for balance control.," *Journal of Biomechanics*, vol. 30, pp. 347–54, Apr. 1997.

[95] PARK, S., HORAK, F. B., and KUO, A. D., "Postural feedback responses scale with biomechanical constraints in human standing.," *Experimental Brain Research*, vol. 154, pp. 417–27, Feb. 2004.

[96] PATAKY, T. C., ZATSIORSKY, V. M., and CHALLIS, J. H., "A simple method to determine body segment masses in vivo: reliability, accuracy and sensitivity analysis," *Clinical Biomechanics*, vol. 18, pp. 364–368, May 2003.

[97] PATTON, J. L., LEE, W. A., and PAI, Y.-C., "Relative stability improves with experience in a dynamic standing task," *Experimental Brain Research*, vol. 135, pp. 117–126, Oct. 2000.

[98] PERREAULT, E. J., KIRSCH, R. F., and CRAGO, P. E., "Multijoint dynamics and postural stability of the human arm.," *Experimental brain research. Experimentelle Hirnforschung. Expérimentation cérébrale*, vol. 157, pp. 507–17, Aug. 2004.

[99] PETERKA, R. J., "Sensorimotor integration in human postural control.," *Journal of neurophysiology*, vol. 88, pp. 1097–118, Sept. 2002.

[100] PETERKA, R. J., "Comparison of human and humanoid robot control of upright stance.," *Journal of Physiology, Paris*, vol. 103, no. 3-5, pp. 149–58, 2009.

[101] PROCHAZKA, A., "Sensorimotor gain control: a basic strategy of motor systems?," *Prog Neurobiol*, vol. 33, no. 4, pp. 281–307, 1989.

[102] QIU, L., BERNHARDSSON, B., RANTZER, A., DAVISON, E., YOUNG, P., and DOYLE, J., "A formula for computation of the real stability radius," *Automatica*, vol. 31, pp. 879–890, June 1995.

[103] RANCOURT, D. and HOGAN, N., "Stability in force-production tasks.," *Journal of motor behavior*, vol. 33, pp. 193–204, June 2001.

[104] REMY, C. D. and THELEN, D. G., "Optimal estimation of dynamically consistent kinematics and kinetics for forward dynamic simulation of gait.," *Journal of biomechanical engineering*, vol. 131, p. 031005, Mar. 2009.

[105] ROBERT, G., BLOUIN, J., RUGET, H., and MOUCHNINO, L., "Coordination between postural and movement controls: effect of changes in body mass distribution on postural and focal component characteristics.," *Experimental brain research. Experimentelle Hirnforschung. Expérimentation cérébrale*, vol. 181, pp. 159–71, July 2007.

[106] RUNHAAR, J., KOES, B. W., CLOCKAERTS, S., and BIERMA-ZEINSTRA, S. M. A., "A systematic review on changed biomechanics of lower extremities in obese individuals: a possible role in development of osteoarthritis.," *Obesity reviews : an official journal of the International Association for the Study of Obesity*, vol. 12, pp. 1071–82, Dec. 2011.

[107] SAFAVYNIA, S. A. and TING, L. H., "Task-level feedback can explain temporal recruitment of spatially-fixed muscle synergies throughout postural perturbations," *J Neurophysiol*, vol. 107, no. 1, pp. 159–177, 2012.

[108] SCHEYS, L., VAN CAMPENHOUT, A., SPAEPEN, A., SUETENS, P., and JONKERS, I., "Personalized MR-based musculoskeletal models compared to rescaled generic models in the presence of increased femoral anteversion: effect on hip moment arm lengths.," *Gait & posture*, vol. 28, pp. 358–65, Oct. 2008.

[109] SCRIVENS, J. E., DEWEERTH, S. P., and TING, L. H., "A robotic device for understanding neuromechanical interactions during standing balance control.," *Bioinspiration & Biomimetics*, vol. 3, p. 026002, June 2008.

[110] SEIDEL, G., MARCHINDA, D., DIJKERS, M., and SOUTAS-LITTLE, R., "Hip joint center location from palpable bony landmarks - A cadaver study," *Journal of Biomechanics*, vol. 28, no. 8, pp. 995–998, 1995.

[111] SELEN, L. P., FRANKLIN, D. W., and WOLPERT, D. M., "Impedance control reduces instability that arises from motor noise," *Journal of Neuroscience*, vol. 29, no. 40, pp. 12606–12616, 2009.

[112] SHADMEHR, R. and MUSSA-IVALDI, F. A., "Adaptive representation of dynamics during learning of a motor task," *Journal of Neuroscience*, vol. 14, no. 5b, pp. 3208–3224, 1994.

[113] SHADMEHR, R. and KRAKAUER, J. W., "A computational neuroanatomy for motor control.," *Experimental brain research. Experimentelle Hirnforschung. Expérimentation cérébrale*, vol. 185, pp. 359–81, Mar. 2008.

[114] SHADMEHR, R., SMITH, M. A., and KRAKAUER, J. W., "Error correction, sensory prediction, and adaptation in motor control.," *Annual review of neuroscience*, vol. 33, pp. 89–108, Jan. 2010.

[115] SIEBER, J. and KRAUSKOPF, B., "Extending the permissible control loop latency for the controlled inverted pendulum," *Dynamical Systems*, vol. 20, pp. 189–199, June 2005.

[116] SIEBER, J. and KRAUSKOPF, B., "Bifurcation analysis of an inverted pendulum with delayed feedback control near a triple-zero eigenvalue singularity," *Nonlinearity*, vol. 17, no. 1, pp. 85–103, 2004.

[117] SIPAHI, R., NICULESCU, S., ABDALLAH, C. T., and MICHIELS, W., "Stability and Stabilization of Systems with Time Delay," *IEEE Control Systems*, vol. 31, pp. 38–65, Feb. 2011.

[118] SPONBERG, S. and FULL, R. J., "Neuromechanical response of musculo-skeletal structures in cockroaches during rapid running on rough terrain.," *The Journal of Experimental Biology*, vol. 211, pp. 433–46, Mar. 2008.

[119] SRINIVASAN, M. and RUINA, A., "Computer optimization of a minimal biped model discovers walking and running.," *Nature*, vol. 439, pp. 72–5, Jan. 2006.

[120] STEPAN, G. and KOLLAR, L., "Balancing with reflex delay," *Mathematical and Computer Modelling*, vol. 31, pp. 199–205, Feb. 2000.

[121] STERGIOU, N., JENSEN, J. L., BATES, B. T., SCHOLTEN, S. D., and TZETZIS, G., "A dynamical systems investigation of lower extremity coordination during running over obstacles.," *Clinical biomechanics (Bristol, Avon)*, vol. 16, pp. 213–21, Mar. 2001.

[122] STERNAD, D., ABE, M. O., HU, X., and MÜLLER, H., "Neuromotor noise, error tolerance and velocity-dependent costs in skilled performance.," *PLoS computational biology*, vol. 7, p. e1002159, Oct. 2011.

[123] STRANG, G., *Introduction to Applied Mathematics*. Wellesley, MA: Wellesley-Cambridge Press, 1986.

[124] SWANENBURG, J., DE BRUIN, E. D., UEBELHART, D., and MULDER, T., "Falls prediction in elderly people: a 1-year prospective study.," *Gait & posture*, vol. 31, pp. 317–21, Mar. 2010.

[125] TAN, W. and PACKARD, A., "Stability Region Analysis Using Polynomial and Composite Polynomial Lyapunov Functions and Sum-of-Squares Programming," *IEEE Transactions on Automatic Control*, vol. 53, pp. 565–571, Mar. 2008.

[126] THELEN, D. G. and ANDERSON, F. C., "Using computed muscle control to generate forward dynamic simulations of human walking from experimental data," *Journal of Biomechanics*, vol. 39, pp. 1107–1115, Jan. 2006.

[127] TING, L. H. and MCKAY, J. L., "Neuromechanics of muscle synergies for posture and movement.," *Current opinion in neurobiology*, vol. 17, pp. 622–8, Dec. 2007.

[128] TING, L. H., VAN ANTWERP, K. W., SCRIVENS, J. E., MCKAY, J. L., WELCH, T. D. J., BINGHAM, J. T., and DEWEERTH, S. P., "Neuromechanical tuning of nonlinear postural control dynamics," *Chaos (Woodbury, N.Y.)*, vol. 19, p. 026111, June 2009.

[129] TODOROV, E., "Direct cortical control of muscle activation in voluntary arm movements: a model," *Nature Neuroscience*, vol. 3, no. 4, pp. 391–398, 2000.

[130] TODOROV, E. and GHAHRAMANI, Z., "Unsupervised learning of sensory-motor primitives," *Proceedings of the 25th Annual International Conference of the IEEE Engineering in Medicine and Biology Society (IEEE Cat. No.03CH37439)*, pp. 1750–1753, 2003.

[131] TODOROV, E. and JORDAN, M. I., "Optimal feedback control as a theory of motor coordination," *Nature Neuroscience*, vol. 5, no. 11, pp. 1226–1235, 2002.

[132] TORRES-OVIEDO, G. and TING, L. H., "Subject-specific muscle synergies in human balance control are consistent across different biomechanical contexts," *Journal of Neurophysiology*, vol. 103, no. 6, pp. 3084–3098, 2010.

[133] TORRES-OVIEDO, G., MACPHERSON, J. M., and TING, L. H., "Muscle synergy organization is robust across a variety of postural perturbations.," *Journal of neurophysiology*, vol. 96, pp. 1530–46, Sept. 2006.

[134] TREFETHEN, L. N. and EMBREE, M., *Spectra and Pseudospectra: The Behavior of Nonnormal Matrices and Operators*. Princeton, NJ: Princeton University Press, 2005.

[135] TRUMBOWER, R. D., KRUTKY, M. A., YANG, B.-S., and PERREAULT, E. J., "Use of self-selected postures to regulate multi-joint stiffness during unconstrained tasks.," *PloS One*, vol. 4, no. 5, p. e5411, 2009.

[136] TYTELL, E. D., HOLMES, P., and COHEN, A. H., "Spikes alone do not behavior make: why neuroscience needs biomechanics.," *Current opinion in neurobiology*, vol. 21, pp. 816–22, Oct. 2011.

[137] VAN DEN BOGERT, A. J., BLANA, D., and HEINRICH, D., "Implicit methods for efficient musculoskeletal simulation and optimal control.," *Procedia IUTAM*, vol. 2, pp. 297–316, Jan. 2011.

[138] VAN DER KOOIJ, H., JACOBS, R., KOOPMAN, B., and VAN DER HELM, F., "An adaptive model of sensory integration in a dynamic environment applied to human stance control.," *Biological cybernetics*, vol. 84, pp. 103–15, Feb. 2001.

[139] VAN DER KOOIJ, H., VAN ASSELDONK, E., and VAN DER HELM, F. C. T., "Comparison of different methods to identify and quantify balance control.," *Journal of neuroscience methods*, vol. 145, pp. 175–203, June 2005.

[140] VANEY, C., GATTLEN, B., LUGON-MOULIN, V., MEICHTRY, A., HAUSAMMANN, R., FOINANT, D., ANCHISI-BELLWALD, AM PALACI, C., and HILFIKER, R., "Robotic-assisted step training (lokomat) not superior to equal intensity of over-ground rehabilitation in patients with multiple sclerosis," *Neurorehabilitation and neural repair*, vol. 26, no. 13, pp. 212–21, 2012.

[141] VERDAASDONK, B. W., KOOPMAN, H. F. J. M., VAN GILS, S. A., and VAN DER HELM, F. C. T., "Bifurcation and stability analysis in musculoskeletal systems: a study in human stance.," *Biological cybernetics*, vol. 91, pp. 48–62, July 2004.

[142] VERRIEST, S.-I. N. E. I. and DUGARD, L., "Stability and Robust Stability of Time-Delay Systems : A Guided Tour," in *Stability and Control of Time-delay Systems*, pp. 1–71, Springer, 1998.

[143] WAGENKNECHT, T., MICHIELS, W., and GREEN, K., "Structured pseudospectra for nonlinear eigenvalue problems," *Journal of Computational and Applied Mathematics*, vol. 212, pp. 245–259, Mar. 2008.

[144] WEISS, P. L., HUNTER, I. W., and KEARNEY, R. E., "Human ankle joint stiffness over the full range of muscle activation levels.," *Journal of biomechanics*, vol. 21, pp. 539–44, Jan. 1988.

[145] WELCH, T. D. J. and TING, L. H., "A feedback model reproduces muscle activity during human postural responses to support-surface translations.," *Journal of Neurophysiology*, vol. 99, pp. 1032–8, Feb. 2008.

[146] WELCH, T. D. J. and TING, L. H., "A feedback model explains the differential scaling of human postural responses to perturbation acceleration and velocity.," *Journal of Neurophysiology*, vol. 101, pp. 3294–309, June 2009.

[147] WESSELS, M., LUCAS, C., ERIKS, I., and DE GROOT, S., "Body weight-supported gait training for restoration of walking in people with an incomplete spinal cord injury: a systematic review.," *Journal of rehabilitation medicine : official journal of the UEMS European Board of Physical and Rehabilitation Medicine*, vol. 42, pp. 513–9, June 2010.

[148] WINTER, D. A., *Biomechanics and motor control of human movement*. New York: Wiley Press, 3rd ed. ed., 1995.

[149] WINTER, D. A., "Human balance and posture control during standing and walking," *Gait & Posture*, vol. 3, no. 4, pp. 193–214, 1995.

[150] WINTER, D. A., PATLA, A., PRINCE, F., ISHAC, M., and GIELO-PERCZAK, K., "Stiffness control of balance in quiet standing," *Journal of Neurophysiology*, vol. 80, no. 3, p. 1211, 1998.

[151] WOOLLACOTT, M., INGLIN, B., and MANCHESTER, D., "Response preparation and posture control. Neuromuscular changes in the older adult.," *Annals of the New York Academy of Sciences*, vol. 515, pp. 42–53, Jan. 1988.

[152] WU, Z. and MICHIELS, W., "Reliably computing all characteristic roots of delay differential equations in a given right half plane using a spectral method," *Journal of Computational and Applied Mathematics*, vol. 236, pp. 2499–2514, Mar. 2012.

[153] YAVUZ, S. U., SENDEMIR-URKMEZ, A., and TÜRKER, K. S., "Effect of gender, age, fatigue and contraction level on electromechanical delay.," *Clinical neurophysiology : official journal of the International Federation of Clinical Neurophysiology*, vol. 121, pp. 1700–6, Oct. 2010.

[154] YE, H., MORTON, D. W., and CHIEL, H. J., "Neuromechanics of coordination during swallowing in Aplysia californica," *Journal of Neuroscience*, vol. 26, no. 5, pp. 1470–1485, 2006.

[155] YOUNG, R. P., SCOTT, S. H., and LOEB, G. E., "An intrinsic mechanism to stabilize posture - joint-angle-dependent moment arms of the feline ankle muscles," *Neuroscience Letters*, vol. 145, pp. 137–140, 1992.

[156] ZAJAC, F. E., "Muscle and tendon: properties, models, scaling, and application to biomechanics and motor control," *Crit Rev Biomed Eng*, vol. 17, no. 4, pp. 359–411, 1989.

[157] ZATSIORSKY, V. M., GAO, F., and LATASH, M. L., "Motor control goes beyond physics: differential effects of gravity and inertia on finger forces during manipulation of hand-held objects.," *Experimental brain research. Experimentelle Hirnforschung. Expérimentation cérébrale*, vol. 162, pp. 300–8, May 2005.